REPORT NO.
UCB/EERC-85/04
FEBRUARY 1985

EARTHQUAKE ENGINEERING RESEARCH CENTER

DEVELOPMENT 0F SUBSTRUCTURING TECHNIQUES FOR ON-LINE COMPUTER CONTROLLED SEISMIC PERFORMANCE TESTING

by

S. N. DERMITZAKIS
S. A. MAHIN

Report to the National Science Foundation

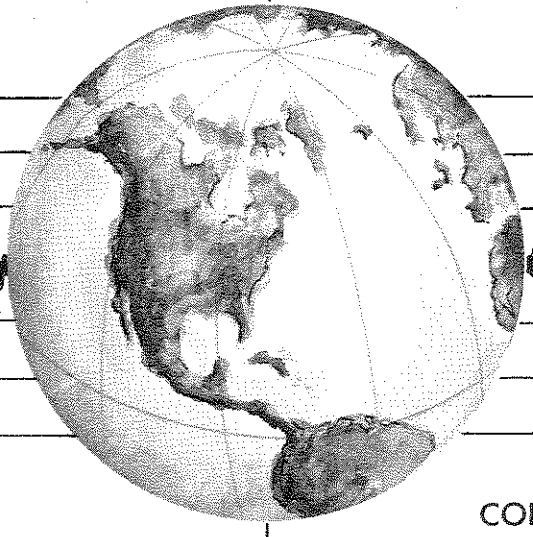

COLLEGE OF ENGINEERING

UNIVERSITY OF CALIFORNIA · Berkeley, California

DEVELOPMENT OF SUBSTRUCTURING TECHNIQUES FOR ON-LINE COMPUTER CONTROLLED SEISMIC PERFORMANCE TESTING

by

Stavros N. Dermitzakis

and

Stephen A. Mahin

A Report to Sponsor
National Science Foundation

Report No. UCB/EERC-85/04
Earthquake Engineering Research Center
College of Engineering
University of California
Berkeley, California

February 1985

ABSTRACT

Application of substructuring concepts to on-line computer controlled (pseudodynamic) testing is developed so that analytical subassemblages can be combined with a physical test assemblage to simulate the seismic response of the complete system. Numerical algorithms are developed to carry out analytical substructuring. Their reliability is investigated by means of pseudodynamic tests of several specimens. The results of these tests are presented and discussed and their correlation with analytical simulations is evaluated.

The pseudodynamic method is a relatively new experimental technique which has been used for the evaluation of the performance of complete structural systems subjected to seismic excitations. During such a test, conventional integration methods are used to calculate displacements which are imposed on a test specimen. The restoring force characteristics are obtained experimentally from the test structure. By considering these analytical and experimental procedures, it is possible to simulate in the laboratory the dynamic response of a structure to severe earthquake excitations.

For economic or other reasons, it may be desirable to pseudodynamically test only a portion of a complete structure and model the remaining part analytically. The theoretical background of these "substructuring" techniques is formulated herein and the characteristics of the integration methods involved in the substructuring algorithms are presented and discussed. It is shown that, according to the type of test structure considered, numerical stability criteria may govern the selection of the integration method. Propagation of experimental feedback errors in the substructuring algorithms is also investigated.

Pseudodynamic tests of several multiple-degree-of-freedom systems were performed to verify the substructuring techniques. A two-degree-of-freedom steel specimen was tested pseudodynamically as a complete system and, subsequently, the same system was tested with its top half being modeled analytically. Good correlation has been achieved between the two

tests. By means of substructuring techniques, it is also possible to test equipment mounted on structures without the need to construct the supporting structure. The numerical algorithms for such equipment tests are developed and discussed, and results from verification tests are presented. The applications of substructuring concepts are further extended by considering subassemblages that behave nonlinearly. The results of the pseudodynamic verification tests using nonlinear hysteretic elements are presented and compared to analytical simulations.

All these studies indicate that substructuring techniques can be used reliably to combine analytical subassemblages with pseudodynamic test specimens. Conclusions regarding the reliability of the method are offered. Needs for further research and development are identified.

ACKNOWLEDGEMENTS

This research investigation was financially supported by the National Science Foundation. The authors are grateful for this support. Any opinions, findings and conclusions or recommendations expressed in this report, however, are those of the authors and do not necessarily reflect the views of the National Science Foundation.

The significant contribution of P.B. Shing, C. Thewalt and A. Gilani in the pseudo-dynamic project is acknowledged. Special thanks are also owed to David Steere and Albert Lawrence for their assistance in the laboratory. The work of Richard Steele in preparing some of the figures in this report is also appreciated.

Table of Contents

CHAPTER 1

INTRODUCTION

1.1 The Pseudodynamic Test Method

In seismically active regions, buildings are usually designed to deform inelastically during rare and unusually severe earthquakes. By providing a structure with a good energy dissipation capacity, it should be able to survive such excitations without collapse. However, the inelastic performance of structural systems depends on many factors, including the characteristics of the excitation, configuration of the structural system, type of foundation system used, intensity of gravity loads, etc. A particularly crucial role is played by the details used for the critical structural components since these directly relate to energy dissipation capacity. Currently, analytical methods are unable to fully predict the complex inelastic behavior exhibited by most structural systems and components under seismic loading conditions. Therefore, we must depend on results of experimental testing to improve our ability to design seismic-resistant structures.

There are several experimental methods available for evaluating the inelastic seismic performance of a particular structure. The most realistic simulations of seismic response are shaking table tests. However, shaking tables are scarce and expensive to construct. They also have significant limitations on the size,weight and strength of specimens that can be tested. Because of these limitations, quasi-static tests tests are often used to impose prescribed histories of load (or displacement) on a specimen. These tests are more economical to perform and utilize conventional laboratory loading equipment and instrumentation. Although quasi-static tests are more versatile, the prescribed loading histories on the test structure may not be

representative of earthquake loading conditions. Thus, questions arise as to whether the specimen is over- or under-tested.

Recently, a new experimental method has been developed which attempts to combine the economy and flexibility of quasi-static tests with the realism of shaking table tests [1,4,8,9,16,24]. In this method, a computer is used on-line to determine the displacement history to be imposed on a test specimen. Conventional step-by-step integration methods are used to calculate these displacements based on the equations of motion formulated for the specimen. The inertial and damping characteristics of the test structure as well as the earthquake accelerogram are numerically prescribed by the user at the outset of a test. The structure's restoring force characteristics are likely to vary significantly during a test due to damage. Consequently, these are measured experimentally from the deformed specimen at each step in the test.

Since the algorithms used in these on-line tests explicitly account for dynamic effects, the computed displacements can be quasi-statically imposed on the test structure using electro-hydraulic actuators. Because of the relatively slow rate at which the displacements are imposed, it is possible to observe the behavior of the specimen in detail during testing as well as to use conventional data recording equipment.

Previous studies [1,5,9,15,24] have shown that this "so called" *pseudodynamic method* can be very reliable if appropriate test equipment and techniques are used. The numerical procedures which are used in the pseudodynamic method are derived from well-established methods used in nonlinear finite element analyses. However, the method may not be suitable for certain types of structures. Since lumped mass structural models are most convenient to formulate and test, it may be difficult to apply the method to structures with significant distributed masses. Due to the quasi-static manner of displacement application it may not be possible to test structures constructed from materials which have properties that are highly sensitive to loading rate. Because damping characteristics are numerically idealized, structures in which viscous damping is likely to have a significant effect on response may not be

appropriate for this method.

1.2 Review of Previous Research

Research studies to verify and implement the pseudodynamic method have been carried out since the early 1970's. Japanese researchers have developed pseudodynamic numerical algorithms and have been involved in experimental testing of single degree-of-freedom and multiple degree-of-freedom steel and concrete specimens [1,3,4,5,6,7,26]. Experimental facilities have been developed at the University of Tokyo and the Building Research Institute (BRI) of Japan. The BRI experimental facilities [6,28] permit testing of multistory structures at full-scale. Good correlation has been reported of pseudodynamic test results with shaking table tests and analytical predictions [4]. A full-scale seven story reinforced concrete building and a six story structural steel building have been successfully tested at the BRI facility as part of the U.S.-Japan Cooperative Earthquake Research Program [6,7,17,26].

Work on the method has also been carried out in the U.S., notably at the University of California, Berkeley and the University of Michigan, Ann Arbor. Several tests have been completed [9,24]. Research at the University of Michigan, Ann Arbor has focused on evaluating and improving pseudodynamic test control algorithms. In addition, special attention has been given to developing optimum actuator control systems [8,15,16].

Research efforts at the University of California, Berkeley have thus far been concentrated in two main areas : (i) evaluation of numerical integration methods with particular attention to their sensitivity to experimental errors and (ii) verifying the validity and the reliability of the method by simple experimental applications. Numerical studies have been performed by Shing and Mahin [9,24] to evaluate the accuracy of numerical integration methods which can be used to control a pseudodynamic test. The Newmark explicit and the central difference integration methods have been investigated, and their stability and accuracy criteria have been established. In addition, the propagation of experimental errors in

pseudodynamic tests have been studied by Williams and Mahin [29], and Shing and Mahin [9,24]. The sources of experimental errors have been identified, and the effects of various types of experimental errors on the response of a test structure have been analyzed. Improved numerical methods have been developed to mitigate these effects. Correlation of shaking table and pseudodynamic test results and with analytical results for several specimens indicate that good accuracy is possible with the method. It was concluded from these studies that reliable pseudodynamic test results can be obtained, provided good instrumentation and experimental techniques are used in conjunction with appropriate numerical techniques.

1.3 Substructuring Concepts in Pseudodynamic Testing

While the pseudodynamic method can realistically simulate the seismic response of a structural model in the laboratory, current applications have been limited to tests of complete structural systems. Tests of complete full-scale models are not only expensive, but require special large scale and high capacity test facilities as well. Tests of reduced-scale models may allow use of more moderate facilities, but can introduce dynamic and material similitude problems. Where detailed information on the local behavior of critical regions is required, reduced scale tests may not produce meaningful results. In addition, the lateral load resistance of many structures is contributed mainly by certain critical components which suffer the most severe inelastic deformations during a strong earthquake. In such cases, it may be inefficient, uneconomical and unnecessary to test the entire structure. Thus, it would be desirable to extend the pseudodynamic method to testing of large subassemblages.

There are several other related applications where one would want to test only a portion of a dynamically excited structure. For example, most structural specimens which have been tested in the past did not include the flexibility effects of the supporting soil and foundation. It is difficult to realistically simulate such effects in laboratory tests even though soil-structure interaction can significantly affect the response of certain structures. Pseudodynamic methods

to account for such flexible boundary conditions would be useful. In addition, one may be interested in the dynamic response of components or equipment mounted on structures which are subjected to ground excitation. However, since the ground motion is not directly applied to the base of the equipment, the supporting structure has to be accounted for in such tests. This leads to a costly and inefficient test setup or significant simplifications that may reduce the accuracy of the results.

One approach to overcoming these difficulties with the pseudodynamic method is by application of substructuring concepts used in conventional dynamic analyses. In such analyses, different portions of a structure are grouped into substructures which are treated separately, for convenience in formulating the data as well for computational economy. In a pseudodynamic test it may be possible to use similar methods, except that certain substructures may be analytically formulated and others are subassemblages that are physically tested. By means of substructuring techniques the displacements which are imposed on the test structure would be obtained by solving the equations of motion of the "combined" system, where the restoring force characteristics of the portion which is not subjected to experimental testing are provided by mathematical models.

1.4 Conventional Substructure Techniques

The concepts which were described in the previous section are related to substructure techniques which have originated from the static and dynamic analysis of structural systems. Significant research efforts have been devoted to developing techniques which can offer flexibility in the structural description and reduce computational efforts in the analysis [25]. The advantages of these methods over conventional linear and nonlinear analyses are : (i) repeated structural modules can be used to reduce the effort to define the entire structural assemblage, (ii) the analysis problems are partitioned into subproblems of manageable size, and (iii) in some cases a reduction in computational effort can be achieved [25].

A brief description of conventional analytical substructuring methods is given below : Substructures can be assembled from groups of elements. By means of static condensation, each substructure's stiffness and loads can be expressed in terms of the degrees-of-freedom at the external connection nodes. Subsequently, the complete structure can be assembled by connecting all the substructures. After the global response of the complete structure has been solved, the internal displacements of the individual substructures can be recovered by back substitution procedures.

Although similar in concept, the substructuring techniques which are developed in this report differ from usual analytical substructure methods in the following two aspects : (i) there are both analytical and experimental substructures considered in the partitioning of the complete structure, and (ii) non-boundary degrees-of-freedom are not condensed out for the test subassemblage.

1.5 Objectives and Scope

The main objectives of this work are to develop and evaluate techniques for pseudodynamic testing in which a portion of a structure is represented by a mathematically modeled subassemblage and the remainder of it is tested experimentally. For convenience this technique will be referred to as *substructuring*. The numerical algorithms which are used for this approach are developed and guidelines for their proper use are given. A series of verification tests are performed to demonstrate the reliability of the developed methods.

In Chapter 2, some basic substructuring applications are identified and general categories are developed for later solution. The limitations of substructuring concepts are also described.

In Chapter 3, numerical methods which are used in pseudodynamic tests with substructuring are developed and their stability criteria are summarized. Special requirements for numerical methods for implementing substructuring in pseudodynamic tests are pointed out.

The experimental error propagation characteristics of these numerical methods are briefly examined.

Several experimental tests have been performed to evaluate the reliability of the method. Chapters 4 and 5 present the results of an experimental program with a two-degree-of-freedom steel specimen. Chapter 4 describes the pseudodynamic test of the complete specimen. In Chapter 5, the substructuring methods used to re-test the specimen are described. Substructuring test results are compared with "benchmark" analytical simulations as well as with experimental results from Chapter 4.

In Chapter 6, the procedure for testing components mounted on structures by the pseudodynamic method is outlined. The response of a one-degree-of-freedom equipment specimen mounted on a steel frame is compared with analytic results.

Chapter 7 presents the results of a pseudodynamic test of a three-story frame. A single member of this structure was tested, while inelastic analytical subassemblages were used to simulate the remainder of the frame.

Finally, conclusions and recommendations are offered in Chapter 8 related to the reliability and practicability of substructuring concepts in pseudodynamic testing. Future research areas are also suggested.

CHAPTER 2

APPLICATION OF SUBSTRUCTURING IN PSEUDODYNAMIC TESTING

2.1 Applications

As stated in the introduction, substructuring techniques may permit the combination of analytical subassemblages with physical subassemblages in pseudodynamic tests. This may permit the testing of subassemblages and components using the pseudodynamic test method. In order to demonstrate the desirability of substructuring methods in pseudodynamic testing, a number of useful applications are described in this section. These applications are for convenience based on planar frames subject to horizontal excitation.

Structural Subassemblages

(i) *Reduction in Plan :* A simple shear wall system is shown in Fig. 2.1 . A shear wall usually interacts with the adjacent moment frames resulting in complicated behavior. However, most of the initial stiffness and resistance is provided by the shear wall and the focus of a test is usually on the behavior of the wall. Because of the flexibility of the frames, framing members are likely to suffer less damage initially (or even remain elastic) than the stiffer walls. Also, analytical models for framing members are much more advanced and reliable than for walls. Consequently, it may be acceptable to analytically model the frame and to test only the wall. Using substructuring methods, the wall can be tested, and its interaction with the remainder of the structure can be taken into account.

A similar approach might be used for testing a structure which consists of ductile moment-resisting frames and the concentrically braced bent shown in Fig. 2.2 . The behavior of braces in the post-buckling range is more critical and complex than the post-yielding behavior of the moment-resisting frames. However, the interaction of the frame and braced bent must be taken into account for realistic simulation. Thus, the behavior of this structure might be investigated by testing only the braced portion while the adjacent moment-resisting frames are modeled analytically.

(ii) *Reduction in Elevation* : In some structures, damage may tend to concentrate at certain floor levels and it would be uneconomical to test the levels that remain elastic. In other structures, construction details and damage may be more or less uniform from level to level and not much new data would be obtained by testing more than a few levels. Figure 2.3 illustrates the reduction of a four-story building to a two degree-of-freedom specimen by means of substructuring concepts ; the top two stories are modeled analytically and the bottom two stories are tested experimentally.

(iii) *Combinations of* (i) *and* (ii) : Inelastic deformations may concentrate in certain regions of a structure. For example, one might expect the lower two or three stories of the wall system in Fig. 2.1 to suffer the most damage. While it is important to include the effects of the upper stories in the experiment in order to apply the correct wall moment and shear, it is uneconomical to do this experimentally. In this case, only the lower portion of the wall need to be tested and remainder of the structure might be modeled analytically. Thus, using substructuring it may be possible to test only the components expected to be heavily damaged.

Internal Equipment in Structures

Substructuring techniques also provide very efficient means to test contained equipment pseudodynamically. Consider, for example, a typical structure-equipment assemblage shown in Fig. 2.4 , where only the single degree-of-freedom equipment needs to be tested. The supporting frame can be modeled analytically. If the support of the equipment specimen is assumed rigid, the experimentally imposed displacements are equal to the relative displacements of the equipment with respect to the floor. Even if the structure is subjected to only horizontal seismic excitations the base of the equipment may move vertically and rotate due to the flexibility of the supporting beam. A more detailed discussion of equipment testing is presented in Chapter 6.

Soil-Structure Interaction

Flexible foundation conditions can alter the response of a structure as well as change the distribution of internal deformations. There are many analytical techniques by which one can model soil-structure interaction. Including this interaction in pseudodynamic testing can be achieved by analytically modeling the soil media and incorporating it along with the superstructure, which is tested pseudodynamically. As illustrated in Fig 2.5, there are several means to analytically idealize the ground flexibility. Linear and rotational springs are examples of commonly used simple models. If a more detailed modeling of the soil media is required, finite element meshes can be assembled.

2.2 Classification of Test Structures

In pseudodynamic testing, a test structure is idealized as a discrete-parameter system. When substructuring methods are used, the analytically prescribed subassemblages have a

finite number of degrees-of-freedom. The number of degrees-of-freedom that can be considered in these are only limited by the size of the operations that the computer can perform during the desired real time step interval. On the other hand, appropriate idealizations must be made in the substructure to be tested so that an practical experimental setup is obtained. Therefore, it is preferable to have a small number of degrees-of-freedom associated with a test specimen and care must be taken so that the selected degrees-of-freedom can accurately represent the dynamic behavior of the test system.

In order to achieve the proper boundary conditions for the physical specimen, different degrees-of-freedom than those used in a test of the entire structure, may be necessary. It is useful to group the specimens which can be tested using substructuring concepts into two categories :

(i) The first category includes test structures for which the degrees-of-freedom used to compute the dynamic response remain the same as if the entire structure were tested. As an example, consider the simple four story structure pictured in Fig. 2.3. By substructuring the upper two stories, two lateral degrees-of-freedom are considered for the experimental specimen and the remaining two are included in the analytical model. The degrees-of-freedom used to control the the lower two stories of the experimental substructure are the same as if the entire prototype structure were tested.

(ii) The second category includes test structures which possess different experimental degrees-of-freedom when compared to the equivalent parts in complete prototype specimens. The complexity of the interface between the test specimen and the analytical substructure determines whether new experimental degrees-of-freedom need to be controlled. Consider, for example, the five story frame illustrated in Fig. 2.6. Assuming that the beams are axially rigid, there are five lateral degrees-of-freedom which must be controlled during a pseudo-dynamic test of the prototype frame subjected to horizontal base excitations. If the upper four stories are analytically substructured, there is only one lateral degree-of-freedom to be controlled. However, to obtain realistic boundary conditions between the first and second

stories, two rotational and two vertical translational degrees-of-freedom must be introduced (Fig. 2.6).

Based on the interface between the analytically substructured subassemblages and the test specimen, the total number of the experimental degrees-of-freedom can be smaller, equal or bigger than the corresponding number in the prototype structure. For example, if the complete eccentrically braced frame pictured in Fig. 2.7 is tested pseudodynamically, the story displacements can be controlled by three actuators. When substructuring is used to model analytically the top two stories, more actuators are required since two rotational and five translational degrees-of-freedom must be considered at the first level.

2.3 Limitations

Substructuring techniques offer substantial versatility to the application of the pseudodynamic test method. However, in addition to the limitations related to the basic principles of the pseudodynamic method, the approximations which are introduced by the substructuring techniques must be thoroughly understood. In particular, the reliability of the pseudodynamic test results is directly related to the realism of the analytically modeled substructure. Consequently, to obtain meaningful test results, one must select realistic analytical models. Clearly, if the analytically modeled components are expected to undergo large inelastic deformations under a given earthquake excitation, it is insufficient to model these components with linear elastic elements or with simple nonlinear models. If an approximation is used, the response of the experimental specimen may not be realistic.

In some cases, the number of degrees of freedom to be controlled during a pseudodynamic test when using substructuring techniques, may be more than the number of original degrees of freedom. Control of these additional degrees of freedom may render the experiment impractical and difficult to implement. Therefore, tests involving a large number of degrees of freedom at the interface of the test specimen and the modeled substructure may be

difficult to perform.

The numerical algorithms for pseudodynamic testing with the substructuring concept will be formulated and examined in Chapter 3. It will be shown that additional degrees of freedom in a test specimen may introduce numerical stability problems in the integration algorithms. Methods to overcome these problems will also be presented.

CHAPTER 3

NUMERICAL IMPLEMENTATION OF SUBSTRUCTURING CONCEPTS

3.1 Integration Methods for Pseudodynamic Application

In pseudodynamic testing, a test structure is idealized as a discrete parameter system having a finite number of degrees of freedom. This discretization procedure approximates lower modes and truncates the higher modes of a continuous test specimen. However, since the lower frequencies of a structure usually dominate its overall response during an earthquake excitation, no significant loss of accuracy results from the discrete parameter idealization in most practical cases. In conventional structural analysis, mass is usually considered lumped at each floor (node) of the model. Lateral displacements at each node are the experimental degrees of freedom. Therefore, relatively few degrees-of-freedom of the structure need be considered to obtain realistic results; and the test can accurately represent the structure's performance during a seismic event [24].

The equations of motion for a linear elastic system with n degrees of freedom can be represented in matrix form as

$$\mathbf{m}\mathbf{a} + \mathbf{c}\mathbf{v} + \mathbf{k}\mathbf{d} = \mathbf{f} \tag{3.1}$$

where

$\mathbf{m}$ = mass matrix (nxn)

$\mathbf{c}$ = damping matrix (nxn)

$\mathbf{k}$ = stiffness matrix (nxn)

$\mathbf{a}$ = acceleration vector (nx1)

$\mathbf{v}$ = velocity vector (nx1)

$\mathbf{d}$ = displacement vector (nx1)

$\mathbf{f}$ = external force excitation vector (nx1)

In a pseudodynamic test, the restoring forces are measured experimentally from the deformed specimen. Therefore, the product of the stiffness matrix and the displacement vector, ($\mathbf{k}$ $\mathbf{d}$), is replaced by the restoring force vector $\mathbf{r}$ in the equations of motion. The mass and damping matrices, and the external force excitation vector are analytically prescribed.

For a given ground excitation, the equations of motion of a nonlinear structural system can be numerically solved by a step-by-step integration method, where the duration T for which the response of a structure is to be evaluated is divided into a number of equal time intervals, Δt. The response at each time step is calculated based on the response of the previous step or steps. For a total duration T, there are N time steps to be considered ($N = \frac{T}{\Delta t}$). The integration methods which have been recommended for pseudodynamic applications are briefly described in the following :

(i) *The Explicit Newmark Method.*

The Newmark explicit algorithm assumes that at time $(i+1)\Delta t$, where $i = 1,...,N$,

$$\mathbf{d}_{i+1} = \mathbf{d}_i + \frac{\Delta t}{2}\mathbf{v}_i + \frac{\Delta t^2}{2}\mathbf{a}_i \tag{3.2}$$

$$\mathbf{v}_{i+1} = \mathbf{v}_i + \frac{\Delta t}{2}(\mathbf{a}_i + \mathbf{a}_{i+1}) \tag{3.3}$$

and

$$\mathbf{m}\mathbf{a}_{i+1} + \mathbf{c}\mathbf{v}_{i+1} + \mathbf{r}_{i+1} = \mathbf{f}_{i+1} \tag{3.4}$$

Therefore, at every step, the displacement vector is computed by using Eq. (3.2); the restoring force vector $\mathbf{r}_{i+1}$ is measured from the specimen ; and the acceleration and velocity vectors are computed based on the Eqs. (3.4) and (3.3) [24].

Furthermore,a modified Newmark algorithm having numerical dissipation properties has been proposed by Shing and Mahin [24] to suppress the spurious growth of higher frequency responses caused by experimental errors.

The modified Newmark algorithm is expressed by the following equations :

$$\mathbf{m}\,\mathbf{a}_{i+1} + \left[\,(1+\alpha)\,\mathbf{k} + \frac{\rho}{\Delta t^2}\,\mathbf{m}\,\right]\mathbf{d}_{i+1} = \mathbf{f}_{i+1} + \left[\,\alpha\,\mathbf{k} + \frac{\rho}{\Delta t^2}\,\mathbf{m}\,\right]\mathbf{d}_i \tag{3.5}$$

$$\mathbf{d}_{i+1} = \mathbf{d}_i + \Delta t\,\mathbf{v}_i + \frac{\Delta t^2}{2}\,\mathbf{a}_i \tag{3.6}$$

$$\mathbf{v}_{i+1} = \mathbf{v}_i + \frac{\Delta t}{2}\,(\,\mathbf{a}_i + \mathbf{a}_{i+1}\,) \tag{3.7}$$

where, α and ρ are numerical damping parameters.

(ii) *The Central Difference Method.*

The central difference method has been applied to pseudodynamic testing by Japanese researchers [1]. The numerical algorithm consists of the following equations :

$$\mathbf{m}\,\mathbf{a}_{i+1} + \mathbf{c}\,\mathbf{v}_{i+1} + \mathbf{r}_{i+1} = \mathbf{f}_{i+1} \tag{3.8}$$

$$\mathbf{a}_i = \frac{\mathbf{d}_{i+1} - 2\,\mathbf{d}_i + \mathbf{d}_{i-1}}{\Delta t^2} \tag{3.9}$$

$$\mathbf{v}_i = \frac{\mathbf{d}_{i+1} - \mathbf{d}_{i-1}}{2\,\Delta t} \tag{3.10}$$

The numerical characteristics of the above algorithms have been investigated by Shing and Mahin [9,24]. The modified Newmark explicit algorithm has been recommended by Shing and Mahin [9,24] to compensate for experimental error propagation effects.

3.2 Algorithms for Substructuring Applications.

3.2.1 Introduction

By means of substructuring techniques , a test structure can be considered as an assembly of two distinct parts : (i) a physical subassemblage which is experimentally tested using load applying actuators ; and (ii) an analytical subassemblage consisting of mathematical models of structural elements. If nonlinear models are used in the formation of the analytical substructure, their stiffness must be updated when the models enter new states. Linear elastic elements retain the same stiffness characteristics throughout the integration process and do not need to be updated.

The numerical implementation of substructuring concepts can be demonstrated by an illustrative example. Consider the m story tall, linear elastic shear building shown in Fig. 3.1 subjected to horizontal excitations. If the entire structure is tested pseudodynamically, m hydraulic actuators are required to impose the calculated displacements to each story. The governing equations of motion can be written as,

$$\mathbf{M}\,\mathbf{a} + \mathbf{C}\,\mathbf{v} + \mathbf{R} = \mathbf{F} \tag{3.11}$$

where $\mathbf{M}$ and $\mathbf{C}$ are analytically prescribed mass and damping (mxm) matrices, and $\mathbf{a}$ and $\mathbf{v}$ are the computed acceleration and velocity vectors (mx1). The vector $\mathbf{R}$ contains the restoring force values measured by the load transducers. The external force excitation vector is represented by $\mathbf{F}$.

Consider now a typical substructuring application using the same structural system. For convenience the structure will be assumed to remain elastic. The upper $m-n$ stories are modeled analytically and the lower n stories are tested pseudodynamically. Hydraulic actuators are only attached to the lower n stories and the stiffness of the upper $m-n$ stories is analytically prescribed. The restoring forces for the substructured stories are analytically computed as the product of the predefined stiffness matrix and the displacement vector. In this case, the equations of motion take the following form :

$$\mathbf{M}\,\mathbf{a} + \mathbf{C}\,\mathbf{v} + \mathbf{R}' + \mathbf{R}^* = \mathbf{F} \tag{3.12}$$

where,

$\mathbf{R}'$ contains the restoring force vector of the analytical subassemblage and is for linear elastic systems expressed as $\mathbf{R}' = \mathbf{K}^* \mathbf{d}$

$\mathbf{d}$ is the displacement vector representing all the degrees-of-freedom (mx1),

$\mathbf{K}^*$ is the stiffness matrix of the substructured subassemblage, and is expressed as ,

$$K^* = \begin{bmatrix} & & n & n+1 & \\ & 0 & & & 0 \\ & & & & \\ & 0 & K'_{n,n} & k_{n,n+1} & \\ & 0 & k_{n+1,n} & k_{n+1,n+1} & \\ & 0 & & & k_{m-1,m} \\ & & & k_{m,m-1} & k_{m,m} \end{bmatrix}$$

where $K'_{n,n}$ is the contribution to the interface degree of freedom from the analytical part of the model, and $\mathbf{R}^*$ contains the restoring force vector of the physical specimen, and is expressed as ,

$$\mathbf{R}^* = \begin{bmatrix} R_1^* \\ R_2^* \\ \cdot \\ \cdot \\ \cdot \\ R_n^* \\ 0 \\ \cdot \\ \cdot \\ 0 \end{bmatrix}$$

The stiffness matrix terms corresponding to the degrees-of-freedom of the experimental specimen which are not at the interface with the analytical substructure are all zero. However, the interface degree-of-freedom has non-zero stiffness terms, which are provided by the part of the analytical subassemblage that is connected to it. On the other hand, the measured restoring force vector contains zero values for all the substructured degrees-of-freedom. Comparing equations (3.11) and (3.12) , we can also observe that, in general, for the interface degree-of-freedom n, $\mathbf{R}_n^*$ is not equal to $\mathbf{R}_n$. This occurs because the restoring force for the interface degree-of-freedom is partly provided by the test specimen and partly by the stiffness of the substructure. The above example illustrates how the basic equations of motion are modified to incorporate an analytical subassemblage to a pseudodynamically tested specimen. The integration algorithms which can be used to solve Equations (3.12) are described in the following sections.

3.2.2 The Explicit Newmark Algorithms

The solution of Equations (3.12) by means of the explicit Newmark method is similar to the general one considered in Section 3.1. The only difference comes from the addition of the restoring forces resulted from the analytically modeled components into the equations of motion. The flow diagram in Fig. 3.2 illustrates the solution procedure. If the substructured subassemblages are modeled with elastic elements, the stiffness matrix $\mathbf{K}^*$ is assembled at the beginning of the computation and is not changed throughout the test. If nonlinear members are used for the substructured components, a state determination for every nonlinear element is required at every integration step to determine whether the element has changed stiffness properties. If an element has changed stiffness, the corresponding terms in the stiffness matrix $\mathbf{K}^*$ must be updated. The new restoring force vector for the substructured subassemblage is then computed according to the following equation :

$$\mathbf{R}_{i+1}^* = \mathbf{R}_i^* + \mathbf{K}_{i+1}^* \, \Delta \mathbf{d}_{i+1} \tag{3.13}$$

where

$$\Delta \mathbf{d}_{i+1} = \mathbf{d}_{i+1} - \mathbf{d}_i \tag{3.14}$$

where $\mathbf{k}^*_{i+1}$ is the tangent stiffness of the analytical portion.

The modified Newmark algorithm suggested by Shing and Mahin [9,24] is also applicable to substructuring problems, and when there are multiple experimental degrees of freedom, the algorithm is very useful for numerically dissipating the spurious growth of higher frequency responses induced by experimental errors. Fig. 3.3 illustrates the flow diagram of the algorithm for substructuring problems.

To obtain bounded solutions , we must satisfy the stability criteria for the explicit Newmark algorithms. Therefore, for any multiple-degree-of-freedom systems, the stability condition for the explicit Newmark method is ,

$$0 \leq \omega_n \, \Delta t \leq 2 \tag{3.15}$$

where ω_n is the highest angular frequency of the entire structural system and Δt is the time step used in the integration [9,24]. The stability of the modified Newmark algorithm is governed by the following condition [9,24] :

$$\sqrt{\frac{\rho}{\alpha}} \leq \omega_n \, \Delta t \leq \frac{1 + \sqrt{1 - (1 + \alpha)\rho}}{1 + \alpha} \tag{3.16}$$

To obtain reliable solutions, appropriate damping parameters (α and ρ) must be selected to represent realistic damping characteristics of the complete system.

In pseudodynamic testing with displacement control, explicit integration algorithms are especially useful since the imposed displacements are computed based on parameters of the previous time step only. In addition, explicit methods are computationally very efficient. However, for a given time interval Δt , stability requirements limit the types of systems that can be tested according to their natural frequencies. On the other hand, a decrease in the time interval Δt results in an increase in the total number of test steps needed to produce a given duration of earthquake response.

3.2.3 The Implicit-Explicit Integration Algorithm

As we have already seen, explicit integration methods are only conditionally stable. Unconditional stability can only be achieved by implicit methods. Implicit methods assume that the displacement solution is a function of the previous and current solutions. Due to this assumption, implicit methods cannot be directly applied to pseudodynamic testing. This can be seen by considering the general Newmark family of implicit algorithms, where,

$$\mathbf{M}\ \mathbf{a}_{i+1} + \mathbf{C}\ \mathbf{v}_{i+1} + \mathbf{K}\ \mathbf{d}_{i+1} = \mathbf{F}_{i+1} \tag{3.17}$$

$$\mathbf{d}_{i+1} = \mathbf{d}_i + \Delta t\ \mathbf{v}_i + \Delta t^2 \left[\left(\frac{1}{2} - \beta\right) \mathbf{a}_i + \beta\ \mathbf{a}_{i+1} \right] \tag{3.18}$$

$$\mathbf{v}_{i+1} = \mathbf{v}_i + \left[(1-\gamma)\ \mathbf{a}_i + \gamma\ \mathbf{a}_{i+1} \right] \tag{3.19}$$

for $\beta \neq 0$. To obtain the value of the product $\mathbf{K}\ \mathbf{d}_{i+1}$ ($= \mathbf{R}_{i+1}$) from the experimental specimen, we must know the value of the imposed displacement ($\mathbf{d}_{i+1}$) *a priori*. Therefore, equations (3.17)-(3.19) have four unknowns, ($\mathbf{a}_{i+1}$, $\mathbf{v}_{i+1}$, $\mathbf{d}_{i+1}$, $\mathbf{K}$ at step $(i+1)$) , and they cannot be solved simultaneously. If the stiffness characteristics of a part of the test structure are known, then, for that part, there are only three unknown quantities at each step and an implicit algorithm can be successfully used. This shows that when substructuring is considered for subassemblages of a structural system, the equations of motion for the substructured components can be solved by means of an implicit method. Since an explicit scheme is necessary to compute the displacement solution of the physical specimen, the combination of implicit and explicit integration methods is very useful to substructuring applications.

An implicit-explicit integration algorithm has been proposed by Hughes and Liu [19,20] for finite element analyses of systems such as fluid-structure assemblies . The algorithm assumes that the elements of a system are divided into two groups : the implicit group and the explicit group. The interface conditions are automatically accounted for by the assembly procedure of the stiffness terms. The implementation of the implicit-explicit algorithm to pseudodynamic testing with substructured subassemblages is evaluated here and compared to

the algorithms which are currently used.

In the following equations, superscript I denotes the implicit group (substructured group) and superscript E denotes the explicit group (experimental specimen). The governing equations are as follows :

$$\mathbf{M}\ \mathbf{a}_{i+1} + \mathbf{C}^I\ \mathbf{v}_{i+1} + \mathbf{C}^E\ \bar{\mathbf{v}}_{i+1} + \mathbf{K}^I\ \mathbf{d}_{i+1} + \mathbf{R}^*_{i+1} = \mathbf{F}_{i+1} \tag{3.20}$$

where,

$$\mathbf{M} = \mathbf{M}^I + \mathbf{M}^E \tag{3.21}$$

$$\bar{\mathbf{d}}_{i+1} = \mathbf{d}_i + \Delta t\ \mathbf{v}_i + \frac{\Delta t^2}{2}(1 - 2\beta)\ \mathbf{a}_i \tag{3.22}$$

$$\bar{\mathbf{v}}_{i+1} = \mathbf{v}_i + \Delta t\ (1 - \gamma)\ \mathbf{a}_i \tag{3.23}$$

$$\mathbf{d}_{i+1} = \bar{\mathbf{d}}_{i+1} + \Delta t^2\ \beta\ \mathbf{a}_{i+1} \tag{3.24}$$

$$\mathbf{v}_{i+1} = \bar{\mathbf{v}}_{i+1} + \Delta t\ \gamma\ \mathbf{a}_{i+1} \tag{3.25}$$

The flow diagram of the algorithm when applied to pseudodynamic testing with substructuring is illustrated in Fig. 3.4 . During each integration time step the following operations are performed :

(i) Explicit displacements $\bar{\mathbf{d}}_{i+1}$ are calculated for the degrees-of-freedom which are attached to the experimental specimen , based on the corrected displacements from the previous step (Eq. 3.22).

(ii) Incremental displacements are imposed on the experimental specimen, relative to the explicit displacements from the previous step, and forces ($\mathbf{R}^*_{i+1}$) are measured by the load transducers.

(iii) Explicit velocities are computed for the degrees-of-freedom which are attached to the test specimen using (Eq. 3.23).

(iv) The "generalized" stiffness matrix $\mathbf{K}^*$ is assembled according to the respective equation in the flow diagram. If the substructured components undergo inelastic deformations , the stiffness matrix $\mathbf{K}^I$ for the implicit group must be updated. If linear subassemblages are considered , then $\mathbf{K}^I$ remains constant throughout the integration. In this case , matrix $\mathbf{K}^*$ is only assembled at the beginning of the integration and this step is passed.

(v) The "generalized" force vector $\mathbf{F}^*_{i+1}$ is formed based on the respective equation in the flow diagram.

(vi) The solution of the simultaneous equations $\mathbf{K}^* \mathbf{d}_{i+1} = \mathbf{F}^*_{i+1}$ gives the corrected displacement vector for all the degrees-of-freedom in the complete system.

(vii) The acceleration and the velocity of all the degrees-of-freedom are computed using Equations (3.24) and (3.25).

A discussion of the characteristics and the advantages of the implicit-explicit method is presented in the next section.

3.2.4 Characteristics of the Implicit-Explicit Algorithm

From the description of the algorithm , we can observe that the restoring forces of the test specimen are measured after "explicit" displacements are imposed on the experimental degrees-of-freedom. In general, these displacements are not equal to the displacements obtained after the solution of the equations $\mathbf{K}^* \mathbf{d}_{i+1} = \mathbf{F}^*_{i+1}$. Consequently, the experimental restoring forces are measured at a "predictor" point. Although this phenomenon introduces a numerical error in the solution of the equations of motion , the error propagation effects appear to be negligible in the displacement solution. This can be readily seen in correlations of analytical simulations with experimental results from tests described in Chapter 4.

The solution of the generalized equations of motion $\mathbf{K}^* \mathbf{d}_{i+1} = \mathbf{F}^*_{i+1}$ at every integration step is computationally less efficient than the matrix multiplication performed in the explicit Newmark algorithms. However, in the explicit Newmark method , massless degrees-of-

freedom, such as rotations , must be eliminated because (i) when damping is not considered , the inversion of matrix [$\mathbf{M} + \mathbf{C}\Delta t$] brings about infinite terms , and (ii) the angular frequencies associated with massless degrees-of-freedom are infinitely large and the numerical stability criteria cannot be satisfied.

The stability criteria for the implicit-explicit algorithm are less severe than those for the explicit Newmark scheme [20]. In the case of the implicit group , if

$$\gamma \geq 0.5 \tag{3.26}$$

$$\beta = \frac{(\gamma + 0.5)^2}{4} \tag{3.27}$$

then unconditional stability is achieved. Furthermore, the numerical stability for the explicit group is governed by the condition ,

$$\omega \Delta t < \left(\left(\xi^2 + 2\gamma \right)^{\frac{1}{2}} - \xi \right) / \gamma \tag{3.28}$$

where , ξ is the viscous damping coefficient. Equation (3.28) must be satisfied for every frequency ω of the explicit element group. However, Hughes and Liu [20] recommend to select a time step according to the more stringent condition :

$$\omega \Delta t < \frac{2(1 - \xi)}{(\gamma + 0.5)} \tag{3.29}$$

For the undamped case , where $\gamma = 0.5$, Equation (3.29) is identical to the stability condition for the explicit Newmark method (Eq. 3.15). Therefore, by an appropriate selection of β and γ values, we can achieve unconditional stability for the implicit group even if the implicit elements have zero mass. If rotations need to be controlled in experimental specimens to realistically represent the boundary conditions, rotational masses need to be specified, since these degrees of freedom will be solved explicitly. The values of the rotational masses must be determined considering Equation (3.29) in order to attain numerical stability.

3.3 Computational Aspects of Substructuring Algorithms

For structural systems with a large number of degrees-of-freedom, numerical operations in each integration step may considerably slow the experimental process. In the implicit-explicit algorithm, the longest computational task is the solution of the equations

$$\mathbf{K}^{*} \quad \mathbf{d}_{i+1} = \mathbf{F}^{*}_{i+1} \tag{3.30}$$

If the stiffness matrices of the analytically modeled substructured components of a structural system remain constant throughout the integration, significant savings in computational time can be achieved by by means of static condensation.

We may rewrite Equ. (3.30) in the following partitioned form,

$$\begin{bmatrix} \mathbf{K}^{*}_{EE} & \mathbf{K}^{*}_{EI} \\ \mathbf{K}^{*}_{IE} & \mathbf{K}^{*}_{II} \end{bmatrix} \quad \begin{bmatrix} \mathbf{d}^{E}_{i+1} \\ \mathbf{d}^{I}_{i+1} \end{bmatrix} = \begin{bmatrix} \mathbf{F}^{*}_{E_{i+1}} \\ \mathbf{F}^{*}_{I_{i+1}} \end{bmatrix} \tag{3.31}$$

where , superscripts E and I denote the experimental and the substructured degrees-of-freedom respectively. It should be noted that the interface degrees-of-freedom are considered experimental since they are attached to hydraulic actuators. If the analytically modeled portion remains linear elastic , static condensation can be applied to reduce the amount of computation required. Hence , Equation (3.31) can be rewritten in terms of the experimental degrees-of-freedom as,

$$(\mathbf{K}^{*}_{EE} - \mathbf{K}^{*T}_{IE}\, \mathbf{K}^{*-1}_{II}\, \mathbf{K}^{*}_{IE})\, \mathbf{d}^{E}_{i+1} = (\mathbf{F}^{*}_{E_{i+1}} - \mathbf{K}^{*T}_{IE}\, \mathbf{K}^{*-1}_{II}\, \mathbf{F}^{*}_{I_{i+1}}) \tag{3.32}$$

If elastic elements are used in the formation of the substructured subassemblages , the submatrices $\mathbf{K}^{*}_{EI}$, $\mathbf{K}^{*}_{IE}$ and $\mathbf{K}^{*}_{II}$ are constant. Therefore, the matrix $(\mathbf{K}^{*}_{EE} - \mathbf{K}^{*T}_{IE}\, \mathbf{K}^{*-1}_{II}\, \mathbf{K}^{*}_{IE})$ can be assembled initially and will remain constant throughout the test. Similarly, the matrix product $\mathbf{K}^{*T}_{IE}\, \mathbf{K}^{*-1}_{II}$ need be formed only once in the beginning of the algorithm. The number of unknown displacements in Eq. (3.32) is significantly reduced when compared to Eqs. (3.30). Therefore, if the operations involved in the solution of Eq. (3.30) limit the real time interval

of each step , time can be saved if the size of the matrix equation is reduced. The displacements of the substructured subassemblages can be finally obtained by means of the following equation :

$$\mathbf{d}^{I}_{i+1} = \mathbf{K}^{*-1}_{II} \quad (\mathbf{F}^{*}_{I_{i+1}} - \mathbf{K}^{*}_{IE} \, \mathbf{d}^{E}_{i+1}) \tag{3.33}$$

However , if the substructured subassemblages are idealized by inelastic models, their stiffness characteristics must be evaluated each time the models enter new states. Therefore, the computational advantages of the condensation of the substructured degrees-of-freedom do not extend to nonlinear substructuring methods. Nevertheless, it may be possible to condense part of the substructured degrees-of-freedom if the analytical subassemblages are only locally nonlinear [25].

3.4 Experimental Error Propagation in Substructuring Algorithms

The cumulative effects of experimental errors on the pseudodynamic response of a structure have been investigated in previous studies and error compensation procedures have been developed to improve the accuracy of multiple degree-of-freedom testing of complete structures [9,24]. Since the displacement history of a structure advances in an incremental manner, the errors introduced at each time step are accumulated through the integration process. In pseudodynamic testing , experimental errors can be introduced in operations involving displacement-control , displacement-measurement and force-measurement. The errors can be systematic or random , depending on the performance of the experimental instruments. Systematic errors are usually associated with a resonance-like phenomena which may result in significant error propagation effects [9,24].

Experimental errors have been shown to cause the spurious growth of the higher frequency modes of multiple-degree-of-freedom systems. In pseudodynamic tests of complete structures , errors are associated with all the degrees-of-freedom present in the equations of

motion. However , when analytical substructuring is used to model selected subassemblages of the complete system , the degrees-of-freedom associated with the modeled components of the system are not controlled experimentally. Hence, no experimental errors are introduced into the system from the analytically specified subassemblages. This causes a reduction in the experimental error effects since the roundoff errors associated with the computations are much smaller than most experimental errors, but adds errors associated with the analytical model. As an illustrative example , a pseudodynamic test is numerically simulated, as shown in Fig. 3.5. In each step , displacement is computed and sent directly to the data acquisition system through a D/A converter. The restoring force is computed based on a simulated stiffness. The dynamic properties of the structure are also given in Fig. 3.5. No viscous damping is specified for the structure.

To simulate systematic errors , the computed displacement value at each degree-of-freedom is truncated in every time step. The free vibration response of the system is first investigated , by subjecting it to the pulse load shown in Fig. 3.6. The explicit Newmark method was used. The numerical results for the complete system are shown in Figs. 3.7,3.8 and 3.9. The "exact" response at each degree-of-freedom is also plotted . In addition, the systematic error signals are plotted for each degree-of-freedom in Fig. 3.10. A two second window of the error signals is enlarged to demonstrate the systematic pattern of the errors. It is apparent from the displacement history plots that the third mode dominated the response of the lower stories of the structure due to the rapid growth of the cumulative errors (Fig. 3.7).

The same structural system was also used for the simulation of a pseudodynamic test including substructuring concepts. In this case , systematic displacement errors were introduced into the bottom story. The top two degrees-of-freedom were analytically modeled with no simulated experimental errors. The response of the complete system was analyzed using both the explicit Newmark and the implicit-explicit method. The response histories obtained are shown in Figs. 3.7-3.9 . The error signals for the bottom degree-of-freedom are also plotted in Fig. 3.11. The spurious growth of the highest mode was significantly reduced.

Furthermore , we can observe that the implicit-explicit method has similar error-propagation characteristics with the Newmark method. From these numerical simulations , we can conclude that substructuring methods can reduce experimental error effects by eliminating some of the systematic error sources. However, any decrease in experimental errors will be offset by additional errors introduced by the analytical model of the substructured degrees of freedom.

CHAPTER 4

PSEUDODYNAMIC TESTING OF A TWO LATERAL DOF SYSTEM

4.1 Introduction

Previous studies at Berkeley have concentrated on evaluating the reliability of the pseudodynamic method by means of tests of single degree-of-freedom systems [9,24] . In these studies it has been demonstrated that the pseudodynamic method constitutes a reliable testing tool for the seismic performance of structures. In this chapter we will examine the implementation of the pseudodynamic method to a multiple-degree-of-freedom system. A simple steel specimen with two lateral degrees-of-freedom was selected. As such, it was idealized as having two concentrated masses at equal distances along its length (Fig. 4.1). The tests were planned based on the following objectives :

(i) to assess the performance of the pseudodynamic facilities at Berkeley in testing multiple-degree-of-freedom systems , and

(ii) to verify the application of substructuring techniques by use of a substructured model of the complete two degree-of-freedom system.

This chapter presents the test results of the complete specimen. Correlation of experimental results with analytical simulations for the complete system are discussed and conclusions are given regarding the efficiency of the pseudodynamic method to evaluate the seismic behavior of multiple degree-of-freedom structures. The test results involving the substructured model are described in Chapter 5.

4.2 Test Description

4.2.1 Features of the Test Specimen

The selected specimen consisted of a 96 in. (2.44 m) long , W 6×20 cantilever column of A36 steel as shown in Fig. 4.1 . The cantilever column was idealized as having two concentrated weights of w_2 = 2.087 kips (9.27kN), and w_1 = 3.207 kips (14.25kN) located at midheight and at the top of the column , respectively. With this design it was expected that no yielding would occur in the upper part of the column, if the applied ground motion was the El Centro 1940 (NS) earthquake excitation scaled to 0.5g peak acceleration. However, significant inelastic deformations would develop at the base of the cantilever. The specimen was free to rotate at the nodes at which the masses were concentrated. Thus, the specimen had four nodal degrees-of-freedom. However, no rotational masses were specified for the specimen; thus the rotations need not enter into the dynamic equations of motion. The rotations are effectively "condensed" to the two lateral translational degrees-of-freedom. Coupon tests were performed to determine the actual yield stress of steel. Two coupons were fabricated from the web and from the flange of the section. The test results are shown in Fig. 4.2 . The obtained yield stresses were 42.0 ksi (289.6 M Pa) for the flange and 44.8 ksi (308.9 M Pa) for the web.

4.2.2 Pseudodynamic Formulation

The inertial terms in the equations of motion are represented only by the lateral motion of the the concentrated masses at midheight and at the top of the cantilever. The weight of the column was relatively insignificant and thus not considered in the inertial terms. In addition, the cantilever was tested horizontally, so that P−Δ effects were disregarded. While these could be numerically simulated in the equations of motion [24], it was not believed necessary to do so for these tests. With these considerations , the equations of motion for the two degree-of-freedom column for time $(i+1)\Delta t$ are as follows :

$$\begin{bmatrix} m_1 & 0 \\ 0 & m_2 \end{bmatrix} \begin{bmatrix} a^1_{i+1} \\ a^2_{i+1} \end{bmatrix} + \begin{bmatrix} c_{11} & c_{12} \\ c_{21} & c_{22} \end{bmatrix} \begin{bmatrix} v^1_{i+1} \\ v^2_{i+1} \end{bmatrix} + \begin{bmatrix} r^1_{i+1} \\ r^2_{i+1} \end{bmatrix} = \begin{bmatrix} f^1_{i+1} \\ f^2_{i+1} \end{bmatrix} \qquad (4.1)$$

where

m_1, m_2 are the concentrated masses assigned to each degree-of-freedom

$c_{11}, c_{12}, c_{21}, c_{22}$ are the numerically specified viscous damping coefficients

r^1_{i+1}, r^2_{i+1} are the restoring forces measured at the two levels

$\mathbf{a}_{i+1}, \mathbf{v}_{i+1}, \mathbf{d}_{i+1}$ are the acceleration, velocity and displacement vectors, respectively, of the degrees-of-freedom considered

$\mathbf{f}_{i+1}$ is the excitation force vector , equal to $-\mathbf{m}\{1\}a^g_{i+1}$, with a^g_{i+1} being the discretized ground acceleration.

No viscous damping was numerically specified for the system. All the coefficients in the damping matrix were therefore assigned zero values. Damping due to frictional forces in the experimental process was approximately equal to 1% of critical in the first mode.

4.2.3 Test Setup and Instrumentation

A detailed test layout of the two degree-of-freedom experiment is shown in Fig. 4.3 . The column was tested in its weak axis. The lower end of the column was welded to a thick plate which was bolted to another plate attached to a concrete reaction block. A plate at the top of the column was bolted to a clevis attached to the end of the hydraulic actuator piston. At midheight, the clevis of the lower hydraulic actuator was attached to the web of the specimen.

The displacement at the top of the column was monitored by a position transducer (wire potentiometer). The displacement at midheight was measured by Linear Voltage Displacement Transducer (LVDT) installed within the actuator. Two additional LVDT's were positioned at midheight to measure the rotations that the column underwent at that point. This was achieved by computing the difference in in measured displacements at the ends of an 8 inch (20.3 cm) rod attached to the column only at its midheight. Later in this chapter,

the rotational values obtained are correlated with analytical predictions. The restoring forces were measured by load transducers (load cells) which were mounted on the hydraulic actuators. In addition, strain gauges were installed at the base and at midheight of the column to measure steel strains at these locations. At each location two strain gauges were installed on the top and bottom flanges at an equal distance from the web center line to allow curvature calculation. Therefore, it was possible to monitor the local inelastic behavior of the column. The experimental setup and instrumentations are shown by the photographs in Fig. 4.5.

As the schematic diagram in Fig. 4.4 indicates, a mini-computer was used to compute the column displacements and to acquire and store the test data obtained from the test. The displacement increments at each step were imposed on the specimen by the hydraulic actuators. The displacement and force measurements are transferred to the computer by the high-speed data acquisition system.

4.2.4 Test Sequence

The specimen was subjected to a series of ground motions as indicated in Table 4.1. Initially, a pulse load with acceleration magnitude 200 in/sec^2 ($5.08 \frac{m}{sec^2}$) was applied to assess the performance of the experimental system and measure the dynamic and damping properties of the specimen during the subsequent free vibration response. Subsequently, the El Centro 1940 NS earthquake excitation was applied at three different acceleration levels. The first excitation subjected the specimen to low amplitude elastic response. The second excitation induced response at its yield "strength" level and, during the third excitation, the column experienced significant inelastic deformations.

Table 4.1 - Test Sequence

Test	Ground Motion	Peak Acceleration (g)
Free Vibration	Pulse	0.52
Linear Elastic	El Centro 1940 NS	0.05
Strength Level	El Centro 1940 NS	0.08
Ductility Level	El Centro 1940 NS	0.5

4.3 Experimental Results

(i) *Free Vibration*

The free vibration response of the system obtained by pseudodynamic testing with a short initial acceleration pulse is shown in Figures 4.6(a) and 4.7(a). The displacement histories of the two degrees-of-freedom are plotted versus time. The second mode of vibration is apparent in the displacement history of the first (bottom) degree-of-freedom (Fig. 4.6(a)). The natural periods obtained from the experimental results were $T_1 = 0.423$ sec and $T_2 = 0.082$ sec. These values are slightly different from the analytically computed periods ($T_1 = 0.432$ sec , $T_2 = 0.077$ sec). The difference is mainly attributed to a slight base support flexibility. The gradual decrease of displacement amplitudes indicates that frictional forces in the clevises and at the support dissipated some energy during the response. The equivalent viscous damping as measured from the displacement amplitude decay of the second (top) degree-of-freedom was approximately 1% of critical damping of the first mode.

(ii) *Linear Elastic Response*

During the linear elastic test, the structure was subjected to the El Centro 1940 NS ground excitation scaled to 0.05g peak acceleration. Figures 4.8(a) and 4.9(a) illustrate the displacement history of the bottom and the top degrees-of-freedom, respectively. The maximum displacement for the bottom degree-of-freedom was 0.103 in. (2.6 mm) and for the top 0.304 in. (7.7 mm) . The system response was dominated by the first mode of vibration.

(iii) *Strength Level Response*

The specimen was subsequently subjected to the El Centro ground motion scaled to 0.08g peak acceleration. During this excitation, the maximum displacements for the lateral degrees-of-freedom were 0.181 in. (4.6 mm) and 0.515 in. (13.1 mm) as shown in Figs. 4.10(a) and 4.11(a) . No yielding was observed during this excitation.

(iv) *"Ductility" Level Response*

The El Centro seismogram was scaled to 0.5g peak acceleration for the "ductility" level earthquake. During this event, the specimen experienced significant inelastic deformations. It can be observed from the displacement time histories of the two degrees-of-freedom that the first period of vibration of the system was extended indicating a reduction in effective lateral stiffness (Figs. 4.12(a) , 4.13(a)). The observed period was 0.452 sec , which constituted a 7% increase over the period in the elastic range. In addition to period elongation, the specimen experienced residual displacements. Figure 4.14 shows the hysteretic relation of the base overturning moment and the curvature of the column at the support. The W 6×20 column yielded at a moment M_y = 268 k in (30.3 kN m). The maximum displacements were 1.017 in. (25.8 mm) for the first degree-of-freedom and 3.067 in. (77.9 mm) for the second.

4.4 Analytical Correlations

The experimental results were compared to analytical simulations of the response of the system to examine the reliability of multiple-degree-of-freedom pseudodynamic testing. In general, very good correlations were obtained for the pseudodynamic test results.

The analytical model which was used in the elastic simulations is shown in Fig. 4.15 . The simulations were performed with the DRAIN-2D2 computer program [22]. The specimen was idealized by two beam-column elements as shown in Fig. 4.15 . The base support was considered fixed. The specified mass and stiffness proportional viscous damping coefficient resulted in 1% of the critical damping of the first mode. Figures 4.5(b) and 4.6(b) illustrate the free vibration response of the system. Excellent correlation was obtained between analysis and experiment. Furthermore, simulations using the El Centro ground motion were performed. The analytical results are illustrated in Figures 4.7(b),4.8(b),4.9(b) and 4.10(b). Very good correlations were obtained for the earthquake response as well.

The inelastic analysis of the system was performed by use of the model shown in Fig. 4.16. Current beam-column elements which are used for the inelastic modeling of frame components assume that inelastic deformations concentrate in ideal "point" hinges at the ends of a member. In reality, inelastic deformations spread along a finite length. Therefore, the flexural post-yield behavior of the two degree-of-freedom system would not be realistically simulated by the use of only two elements connected at midheight. In order to simulate the spread of yielding behavior, the lower element was subdivided into small segments along the plastic hinging region of the base of the column. In this region the internal moment was expected to exceed the yield moment of the section due to strain hardening. The specified size of the segments was small, since yielding could spread only as a function of the length of the segments. Each small segment was modeled by a beam-column element. The yield surface of the element was assumed to be a bilinear moment-rotation ($M - \theta$) relationship with the strain hardening stiffness being 8% of the elastic stiffness (Fig. 4.15). This moment-rotation relationship is simpler than the actual hysteretic behavior exhibited by the specimen

(Fig. 4.14).

The results of the inelastic analysis using the El Centro 1940 NS ground motion scaled to 0.5g peak acceleration are shown in Figs. 4.11(b) and 4.12(b). The displacement histories of the two lateral degrees-of-freedom at midheight and at the top of the column are in excellent agreement with the pseudodynamic results.

4.5 Concluding Remarks

The results of the two degree-of-freedom experiment indicate that the pseudodynamic method can be reliably applied to multiple-degree-of-freedom structures. The control system proved to be very efficient in the tests of the two degree-of-freedom specimen. Based on the obtained time histories, it is apparent that no significant errors were introduced in the response of the system.

CHAPTER 5

PSEUDODYNAMIC TESTING OF A TWO LATERAL DOF SYSTEM INCLUDING SUBSTRUCTURING

5.1 Introduction

A number of tests have been conducted to assess the reliability and practicability of substructuring concepts as applied to pseudodynamic testing. In this chapter, the specimen tested in Chapter 4 is again considered. The complete specimen had two lateral degrees-of-freedom. However, the response was such that the inelastic deformations concentrated near the base. In this chapter, the possibility of using substructuring to analytically model the elastic upper portion of the system while testing the lower portion is investigated.

5.2 Test Description

5.2.1 Substructuring Formulation

The test sequence of the two lateral degree-of-freedom system presented in the previous chapter has been repeated with a substructured model of the test structure. To formulate a substructured model, the bottom half of the specimen was retained and the top half of the specimen was modeled analytically. Since the top part of the specimen remained elastic during the entire sequence of the experiments, it was possible to model the top half of the column as a linear elastic beam-column element. Therefore, the stiffness of the top part of the structure was held constant throughout these tests. Figure 5.1 illustrates the substructured model.

It must be noted that the experimental specimen cannot be considered as a simple cantilever column because, in general, the internal moment and rotation at midheight of the

complete two degree-of-freedom specimen are not zero. Therefore, to achieve the proper boundary conditions the experimental specimen in Fig. 5.1 should be subjected to an imposed rotation (and moment) at the top. This consideration necessitates the introduction of a rotational degree-of-freedom at the midheight of the column. Therefore, the test specimen has one translational and one rotational degree-of-freedom to be experimentally controlled. The control mechanism used is fully described in Section 5.2.2 .

Generally, in dynamic structural analysis rotational inertial masses are not usually prescribed to rotational degrees-of-freedom at the ends of members. Thus, the complete specimen in Chapter 4 was idealized as having only two dynamic degrees-of-freedom. When zero mass is associated with any structural degree-of-freedom, the corresponding natural frequency is infinitely large. Implicit integration methods can be successfully used with systems with such massless degrees-of-freedom. However, explicit methods cannot be used, since a sufficiently small time step cannot be found to prevent the solution from becoming unstable. Thus, the implicit-explicit algorithm was used for all the cases considered for this specimen. The analytical part of the system, which consisted of the top elastic column element, was considered as an implicit element. The experimental specimen was considered as an explicit element, and thus, a rotational mass was needed at the midheight node of the system connecting the two parts to satisfy the stability criteria required by Eq. 3.27.

When damping is disregarded, the equations of motion for the combined system corresponding to the degrees-of-freedom shown in Fig. 5.1 become :

$$\begin{bmatrix} m_1 & 0 & 0 & 0 \\ 0 & m_2 & 0 & 0 \\ 0 & 0 & m_3 & 0 \\ 0 & 0 & 0 & 0 \end{bmatrix} \begin{bmatrix} \alpha_1 \\ \alpha_2 \\ \alpha_3 \\ \alpha_4 \end{bmatrix} + \frac{2EI}{L^3} \begin{bmatrix} 6 & -6 & -3L & -3L \\ -6 & 6 & 3L & 3L \\ -3L & 3L & 2L^2 & L^2 \\ -3L & 3L & L^2 & 2L^2 \end{bmatrix} \begin{bmatrix} d_1 \\ d_2 \\ \Theta_3 \\ \Theta_4 \end{bmatrix} + \begin{bmatrix} R_1^* \\ 0 \\ M_3^* \\ 0 \end{bmatrix} = - \begin{bmatrix} m_1 \\ m_2 \\ 0 \\ 0 \end{bmatrix} \alpha_{i+1}^g \qquad (5.1)$$

where :

m_1 , m_2 are the translational masses specified for the complete two lateral degree-of-freedom system (as in Section 4.2);

m_3 is the rotational mass of the midheight rotational degree-of-freedom (equal to 5.0 kip sec^2 / in);

E,I,L are the modulus of elasticity, the moment of inertia, and the length, respectively, of the analytical portion of the model;

R_1^* is the restoring force measured for the lateral degree-of-freedom 1 ;

M_3^* is the restoring moment measured for the rotational degree-of-freedom 3.

With these considerations, the test procedure for each integration step followed the pattern indicated in Fig. 3.6. That is, the explicit displacements $\bar{d}_1$ and $\bar{\Theta}_3$ were computed and applied to the experimental specimen; the restoring forces R_1^* and M_3^* were measured from the load transducers; and the "generalized" equations of motion were solved to determine d_1 , d_2 , Θ_3 and Θ_4.

5.2.2 Test Setup and Instrumentation

The test layout of the substructured model is shown in Fig. 5.2. A W 6×20 section, identical to that of the complete two lateral degree-of-freedom column, was used as the test specimen. The base support of the column was also the same. The first lateral degree-of-freedom was attached to a hydraulic actuator with the same connection detail as in the test of the complete system. A second hydraulic actuator was attached at a location on the test specimen slightly above the first one in order to impose a rotation at midheight of the system. The clevis at the end of the piston was bolted to a plate which was welded at the end of the extension of the column (Fig. 5.2).

A special detail was fabricated to monitor the displacement and the rotation of the specimen at the first level (Fig. 5.3). A short cantilevered rod was welded at the center line of the top flange at this level. Two displacement transducers (LVDT's) were installed to

measure the displacements of the base and the free end of the rod. The relative displacement of the two transducers divided by the length of the rod gave a measure of the rotation at the first level. The rotation measurement was used in controlling the rotation at the top of the test specimen The transducer controlling the lateral displacement of the first level was directly attached to the base of the rod in order to obtain good accuracy in measuring the specimen's rotation. If the same transducer had been attached at some other point of the column section (e.g. the web) differential displacements between the attachment point and the base of the rod would have likely introduced errors in the rotation measurement that would adversely affect results. It should also be noted that it was not necessary for the top LVDT to be aligned with the center line of the top actuator.

The distance between the hydraulic actuators was 17 inches (43.1 cm). To minimize displacement control and force feedback errors, the gain settings of the actuator controllers was significantly increased above that used for the complete specimen. In this way, the sensitivity of the actuators was conditioned to maintain about the same speed of displacement change in this test. Figure 5.4 contains photographs of the experimental setup.

5.2.3 Test Sequence

The specimen was subjected to the sequence of excitations shown in Table 4.1. At first, the specimen was subjected to a free vibration response generated by a pulse load of acceleration 200 in/sec^2 (5.08 $\frac{m}{sec^2}$). The El Centro 1940 NS accelerogram was then applied, with the accelerations scaled accordingly to obtain (i) linear elastic response, (ii) "strength" level response and (iii) inelastic "ductility" level response.

5.3 Experimental Results

(i) *Free Vibration Test*

Figures 5.5(a) and 5.6(a) illustrate the time histories of the lateral displacements of the two levels during the free vibration test. In addition, Figs. 5.7(a) and 5.8(a) show the time histories of the rotations at the first and second levels of the system. We can observe from these time histories that the second mode of vibration of the system again participated significantly in the overall response. Because of the addition of the rotational mass at the first level, the first natural period was slightly longer than the first period of the complete system. The first period T_1 was found to be 0.489 sec (vs. 0.423 sec). The second period T_2 was equal to 0.070 sec, which is shorter than the equivalent period (0.082 sec) of the complete system. Hence, the dynamic characteristics of the system experienced a small change which is attributed to the extra rotational mass. Frictional forces in the system introduced damping in the response. The equivalent viscous damping coefficient measured from the displacement time histories was about 1% of the critical damping of the first mode.

(ii) *Linear Elastic Response*

The elastic response of the system due to the El Centro 1940 excitation with 0.05g peak acceleration is shown in Figs. 5.9(a) and 5.10(a). The system vibrated primarily in its first mode. The maximum lateral displacements obtained were 0.115 in. for the first level and 0.353 in. for the second level. Comparing these results with these in Chapter 4, we can observe that the additional rotational mass had a negligible effect on the lateral displacement envelope of the system.

(iii) *"Ductility" Level Response*

For the "ductility" level event, the El Centro accelerogram was scaled to 0.5g peak acceleration as in the case of the complete system. The specimen experienced inelastic deformations near the base support. The maximum displacements obtained were 1.261 in. (32.0 mm) (Fig. 5.11(a)) for the first level and 3.110 in. (79.0 mm) for the top level (Fig. 5.12(a)). When these displacements are compared to the values obtained from the complete system, we

can see that for the first level there is a 23% difference , while for the second (top) level there is only a 1% difference. Based on the displacement time history, the fundamental period of the system after the test specimen yielded was found to be 0.500 seconds. The observed differences in the displacement envelopes and the period of vibration are due to the added rotational mass. However, in the case of the displacements, the midheight rotational mass had a negligible effect for the upper level of the system.

Based on the first level displacement history (Fig. 5.11), we can observe an increasing contribution of the second mode of vibration near the end of the time history. This was not observed at the first level. Similar behavior has been observed in previous research at Berkeley [9] and has been attributed to the effects of experimental errors. This phenomenon occurred in this test because of difficulties in precisely controlling rotations. This was partially due to the small backlash in the clevises. In addition, the actuators were connected to the specimen a small distance apart resulting in strong cross coupling of these actuators. Consequently, the actuator forces were very sensitive to deformation errors. These force errors tend to propagate in the computed response as discussed in Ref. [9]. To alleviate this problem, a greater separation between the actuators and better clevises could have been used. Of course, numerical methods could also be used to suppress the propagation of errors in the higher modes. Since this test was intended to assess the numerical substructuring procedures, it was not believed necessary to eliminate these experimental error effects.

5.4 Analytical Correlations

It is believed that the discrepancies between results of the complete structure test and the substructured test are attributable to the altered dynamic characteristics resulting from the added rotational mass moment of inertia considered at the first level. To confirm this, a series of analyses were performed. The analytical model used in the correlation studies of the complete system was also adopted for the analyses of the pseudodynamic tests with substructuring. The DRAIN-2D 2 program was again used to simulate the elastic and inelastic

performance of the system. A rotational mass moment of inertia was added to the midheight rotational degree-of-freedom to conform with the substructured pseudodynamic model. The specified viscous damping coefficient was 1% of critical of the first mode.

The displacement time histories for the free vibration response of the system to the pulse excitation described in Section 5.2.3 are illustrated in Figs. 5.5(b),5.6(b),5.7(b) and 5.8(b). Excellent agreement was obtained between analytical and experimental results indicating that discrepancies were associated with the rotational mass.

The analytical simulations of the elastic response based on the El Centro record are shown in Figs. 5.9(b) and 5.10(b). Again, there is very good agreement between analytical and experimental results.

In the simulation of the inelastic response of the system, the analytical model included the spread of yielding by using closely spaced nodes near the column base. The model was still a simple bilinear hysteretic relationship. The displacement time histories of the lateral degrees-of-freedom are illustrated in Figs. 5.11(b) and 5.12(b). In general, good correlation was obtained between the pseudodynamic tests and the analytical simulations. For the first story response, there are few discrepancies in the amplitude of the displacements near the end of the time history. These are attributed to the experimental error propagation effects. The second mode vibration amplified the displacement response toward the end of the record. No experimental error effects directly influenced the second level displacement ; and there is very good agreement between the pseudodynamic results and analysis at this location. In addition, the analytical model experienced a displacement drift which was not observed in the pseudodynamic response. This is attributable to the simplified hysteretic model used. The offset is less significant in the displacement response of the second level.

5.5 Added Mass Effects

The distribution of the inertial masses determines which of the two substructuring algorithms described in Chapter 3 is most appropriate. When the implicit-explicit algorithm is

used and rotational masses are needed for the experimental degrees-of-freedom, the natural frequencies of the structure are slightly changed as indicated above. The magnitude selected for the additional masses is determined by the stability conditions of the algorithm (Eq. 3.27). Consequently, the change in the natural frequencies is directly related to the integration time step which is used. If the integration step is shortened, the additional masses can be significantly reduced. Therefore, it is possible to minimize the added mass effects by using small time steps. However, this will increase the total number of steps required to complete a certain length of excitation. Thus, the duration of the test will be increased. If a fast pseudo-dynamic system (which can complete all the tasks involved for each integration step in a very small real time interval) is available, shorter integration steps can be considered without increasing the total duration of the experiment to unacceptable levels. Thus, these added mass effects can be considered a trade off between accuracy and convenience.

The added mass effects are also minimized when large analytical substructures are considered. If the complete system has a large mass distributed over a number of degrees-of-freedom, the added masses required at the boundary degrees-of-freedom should not influence the dynamic characteristics significantly. Consequently, the dominant natural frequencies of the overall system should not be altered considerably. The consequence of these effects can be analytically investigated for a particular structure.

5.6 Conclusions

Based on the results of the experiments of the two-degree-of-freedom system with substructuring, the following conclusions can be obtained :

(1) Substructuring techniques can be successfully applied to pseudodynamic testing to reduce the size of an experimental specimen when the remaining part of the structure can be modeled analytically with confidence. Realistic boundary conditions must be considered for the structural subassemblages.

(2) The analytical algorithms which are involved in substructuring gave reliable results in comparison with analytical simulations. The implicit-explicit algorithm used necessitated rotational masses at the boundary between the explicit and implicit portions. These masses affected the dynamic characteristics of the structure. The effect was easily calculable and could be controlled by reducing the mass to an acceptable level.

(3) Based on the results obtained it appears that rotations can be controlled experimentally with relatively good accuracy. The device which monitored the specimen's rotations is practical and reliable. During each test it was possible to record both the command signal and the measured rotation. The two quantities were identical, thus, verifying the reliability of the rotational control. However, good equipment and instrumentation is required.

(4) Due to the short distance between the two electro-hydraulic actuators, high gains were selected in the actuator controllers to insure reliable displacement control. If the actuators were separated by a larger distance, the controller gains could have been reduced. It is recommended that, in similar tests, the interaction of the actuators should be reduced in order to minimize force-feedback errors resulting from displacement control errors. This can be achieved by selecting a bigger lever arm at the location at which the rotation is controlled.

CHAPTER 6

SUBSTRUCTURING METHODS FOR INTERNAL EQUIPMENT IN STRUCTURES

6.1 Introduction

Severe seismic events may cause damage to mechanical equipment and other nonstructural components which are mounted on structures. Contained equipment in earthquake-loaded structures may experience accelerations much greater than those in the primary structure [29]. For design purposes, it is important to evaluate the effects of the equipment-structure interaction on the behavior of the equipment. Shaking table tests of equipment-structure systems may be very expensive to perform, since the cost of the primary structure must be included in the experiment. In addition, it may not be possible to use significantly reduced scaled models in such tests if one is interested in assessing the adequacy of attachment or other details. While pseudodynamic tests would permit tests of components at full-scale [6,7], one still encounters the cost of constructing the entire equipment-structure system. However, if substructuring techniques are used in conjunction with pseudodynamic testing, the dynamic and mechanical response of the equipment can be evaluated without the need for constructing the structural system. According to the substructuring concept, an analytical model of the primary structure may be formed which interacts with the pseudodynamically tested equipment specimen. Therefore, the experimental behavior of the equipment under a prescribed earthquake excitation can be examined without the need to construct a physical specimen of the containing structure.

Clearly, the type of specimens tested in this fashion must be carefully considered. For example, the component to be tested should possess a limited number of degrees-of-freedom, have mass concentrated at a few locations and be insensitive to viscous damping and rate loading effects. In addition, the equipment should be rigidly connected to the structure since sliding friction may be rate sensitive. However, many types of mechanical equipment and nonstrutural components might be tested. In particular, performance tests for methods of attaching equipment can be performed in this manner as can tests of components that are sensitive to relative displacements and accelerations.

Related work has been done at the University of Tokyo [30] for a special problem involving evaluation of retrofitting methods for attaching single-degree-of-freedom equipment in nuclear reactors. This approach is extended in this chapter to more complex systems and the theoretical considerations are generalized. In addition, the results of a pseudodynamic test of an equipment-structure system are presented and correlated with analytical predictions. Conclusions are also given about the effectiveness of the method.

6.2 Implementation Method

In this section we will examine the numerical implementation of substructuring concepts to pseudodynamic tests of equipment-structure systems or other similar types of grouped subassemblages. These systems possess distinct features which differentiate them from systems of the type described in Chapter 5 :

(i) The support of the experimental specimen does not represent ground conditions. The tested equipment is attached to a floor of the primary structure (Fig. 6.1). Therefore, the equipment support motion, i.e. the floor response, is not a prescribed acceleration history. In fact, the response of the floor is an unknown quantity which is computed at every step of the integration process. In addition, when multiple pieces of equipment are attached to different floors of the structure (Fig. 6.2) (or when a piece of equipment is attached to several locations in the structure), their bases have different acceleration time histories.

(ii) During a real earthquake-induced structure excitation, the floors may displace and rotate in any direction. It is difficult to simulate the complex motion of the equipment support in the laboratory. Therefore, the experimental specimen is supported with a fixed base and the relative displacements are imposed on the equipment with respect to the support movement (Fig. 6.1).

With these considerations in mind, we can proceed with the mathematical formulation of equipment-structure substructuring methods. To simplify the following development, we consider a one-story structure with a single piece of equipment mounted on it as shown in Fig. 6.3. The equipment-structure interaction is assumed to occur in a three-dimensional space. Thus, there are six degrees-of-freedom assigned to each nodal point. The displacement vectors of the two nodes are given by the vectors $\mathbf{d}^1$ and $\mathbf{d}^2$ for the structure and the equipment, respectively, where

$$\mathbf{d}^1 = \begin{bmatrix} d_1^1 \\ d_2^1 \\ d_3^1 \\ d_4^1 \\ d_5^1 \\ d_6^1 \end{bmatrix} \quad \text{and} \quad \mathbf{d}^2 = \begin{bmatrix} d_1^2 \\ d_2^2 \\ d_3^2 \\ d_4^2 \\ d_5^2 \\ d_6^2 \end{bmatrix}$$

During a pseudodynamic test, the structure is represented by an analytical model and the base support of the equipment is assumed fixed. To obtain realistic deformations for the test specimen, relative displacements ($\bar{\mathbf{d}}^2$) with respect to the structure's displacements ($\mathbf{d}^1$) at the attachment point must be imposed on the equipment node. The relative displacement vector $\bar{\mathbf{d}}^2$ is given by the formula,

$$\bar{\mathbf{d}}^2 = \mathbf{d}^2 - \mathbf{T}\ \mathbf{d}^1 \tag{6.1}$$

where $\mathbf{T}$ is a transformation matrix.

To evaluate the transformation matrix $\mathbf{T}$, consider the sets of displacements $\mathbf{u}^1$ and $\mathbf{u}^2$ of points P_1 and P_2, respectively (shown in Fig. 6.4) located at the ends of a rigid chord.

Assuming small displacements, the displacements $\mathbf{u}^2$ of point P_2 due to a given set of displacements $\mathbf{u}^1$ at P_1 are found to be :

$$u_x^2 = u_x^1 + (z_2 - z_1)\, u_{yy}^1 - (y_2 - y_1)\, u_{zz}^1 \tag{6.2}$$

$$u_y^2 = u_y^2 - (z_2 - z_1)\, u_{zz}^1 + (x_2 - x_1)\, u_{zz}^1 \tag{6.3}$$

$$u_z^2 = u_z^1 + (y_2 - y_1)\, u_{zz}^1 - (x_2 - x_1)\, u_{yy}^1 \tag{6.4}$$

$$u_{xx}^2 = u_{xx}^1 \tag{6.5}$$

$$u_{yy}^2 = u_{yy}^1 \tag{6.6}$$

$$u_{zz}^2 = u_{zz}^1 \tag{6.7}$$

or in matrix form,

$$\mathbf{u}^2 = \mathbf{T}\ \mathbf{u}^1 \tag{6.8}$$

where

$$\mathbf{T} = \begin{bmatrix} 1 & 0 & 0 & 0 & (z_2-z_1) & -(y_2-y_1) \\ 0 & 1 & 0 & -(z_2-z_1) & 0 & (x_2-x_1) \\ 0 & 0 & 1 & (y_2-y_1) & -(x_2-x_1) & 0 \\ 0 & 0 & 0 & 1 & 0 & 0 \\ 0 & 0 & 0 & 0 & 1 & 0 \\ 0 & 0 & 0 & 0 & 0 & 1 \end{bmatrix} \tag{6.9}$$

Substituting the transformation matrix $\mathbf{T}$ back into Eq. (6.1), we obtain the values of the displacements which are imposed on the test specimen.

During a pseudodynamic test the base support of the equipment is fixed. However, the support node is treated as a free node in the equations of motion. Therefore, in the equations of motion, all the degrees-of-freedom which are assigned to the support node are active and, in general, they have nonzero displacement values. These displacements are the support displacements induced by the earthquake excitation and Eq. 6.1 is used to determine the displacements to be imposed on the equipment.

In addition to the transformation of displacements, appropriate adjustments must be made to the restoring force values obtained from the specimen before they are fed back into the equations of motion. The effect of the specimen on the support degrees-of-freedom can be evaluated by translating the restoring forces applied to the specimen to the support node. The force translation matrix is found from static equilibrium relations. Considering Fig. 6.4 again, if the set of forces $\mathbf{F}^2$ acts on point P_2, it is found that these actions are transferred to point P_1 according to the following small displacement transformation :

$$\mathbf{F}^1 = \mathbf{T} \quad \mathbf{F}^2 \tag{6.10}$$

where $\mathbf{T}$ is the previously defined displacement transformation matrix. Therefore, the restoring force vector of the attachment degrees-of-freedom is a combination of two factors : (i) the transformed restoring forces applied to the equipment and (ii) the analytically computed restoring forces contributed by the analytical model.

As a consequence of these differences, new operations must be added to the numerical pseudodynamic algorithm which controls an experiment. Figures 6.5 and 6.6 show the modified flow diagrams for the Newmark explicit and the implicit-explicit algorithms, respectively.

The Newmark explicit algorithm (Fig. 6.5) involves the following tasks :

(i) The displacements ($\mathbf{d}_{i+1}$) of all the degrees-of-freedom at the current time step are evaluated based on parameters of the previous step.

(ii) The relative displacements ($\overline{\mathbf{d}}^E_{i+1}$) of the equipment with respect to the support degrees-of-freedom are calculated from the absolute equipment displacements ($\mathbf{d}^E_{i+1}$) and the translated displacements of the support ($\mathbf{T}\mathbf{d}^F_{i+1}$).

(iii) These relative displacements are imposed on the equipment specimen and the restoring forces ($\mathbf{R}^{*E}_{i+1}$) are measured by load transducers.

(iv) The restoring forces of the support degrees-of-freedom ($\mathbf{R}^{*F}_{i+1}$) are computed by combining the analytically determined internal forces due to the deformation ($\mathbf{d}^F_{i+1}$) of the analytical substructure with the transformed equipment restoring forces ($\mathbf{T}^T\mathbf{F}^{*E}_{i+1}$).

(v) The restoring forces of the remaining degrees-of-freedom of the analytically modeled structure are computed.

(vi) The accelerations and the velocities of all the degrees-of-freedom are computed using the basic Newmark procedure.

The implicit-explicit algorithm performs the following operations :

(i) Explicit displacements $\mathbf{d}_{i+1}^{E}$ and $\mathbf{d}_{i+1}^{F}$ are calculated for the equipment and the support degrees-of-freedom.

(ii) The relative displacements $(\overline{\mathbf{d}}_{i+1}^{E})$ of the equipment with respect to the support degrees-of-freedom are calculated based on the absolute equipment displacements $(\mathbf{d}_{i+1}^{E})$ and the translated displacements of the support $(\mathbf{T}\mathbf{d}_{i+1}^{F})$.

(iii) The relative displacements $\overline{\mathbf{d}}_{i+1}^{E}$ are imposed on the equipment specimen and the restoring forces $(\mathbf{R}_{i+1}^{*E})$ are measured by load transducers.

(iv) The restoring forces $\mathbf{R}_{i+1}^{*E}$ are translated to the support degrees-of-freedom.

(v) The generalized force vector is computed as before based on excitation, inertial and damping parameters in addition to the experimentally measured restoring forces.

(vi) The analytical stiffness matrix for all the substructured elements is computed.

(vii) The solution of the simultaneous equations $\mathbf{K}^{*}\ \mathbf{d}_{i+1} = \mathbf{F}_{i+1}^{*}$ gives the displacement vector of all the degrees-of-freedom.

(viii) Finally, the acceleration and velocity vectors are computed for all the degrees-of-freedom.

Comments :

For simplicity, the algorithms presented above were formulated for equipment with a single node. The same basic algorithms may be used to test multiple-node equipment specimens. Figure 6.7 illustrates an example of a multiple-node equipment specimen, which can be tested pseudodynamically using substructuring for the supporting structure. During the test, the mathematical operations involved in the computation of relative displacements and the translation of forces must be performed for the two nodal points pictured in Fig. 6.7.

Similarly, equipment-structure substructuring methods can also be used for testing the upper stories of a structure pseudodynamically when the lower stories are modeled analytically. Figure 6.8 demonstrates the application of this concept to a three-story shear building. The upper story is tested pseudodynamically as a specimen with a single lateral degree-of-freedom, while the bottom two stories are modeled analytically. These methods can also be extended to cases where the equipment is attached to the structure at more than one location.

When the supporting structure becomes large enough to require excessive storage capacity or computational effort, non-active degrees-of-freedom can be condensed out. This is especially useful where structures remain elastic or inelastic deformations are concentrated in a few locations.

6.3 Verification Tests

6.3.1 Test Description

Verification tests were performed to examine the reliability of equipment-structure substructuring methods. The equipment-structure assemblage selected is illustrated in Fig. 6.9. It consisted of a cantilever equipment specimen mounted on top of an x-braced bent. The structure is derived from one tested in Reference 2. For simplicity in this example, it is assumed that the structure should remain elastic during the excitation. The equipment and its attachments could, however, yield. The braces of the frame were modeled by analytical elastic truss elements. The columns and beams were analytically modeled by elastic beam

elements. The member sizes are given in Table 6.1.

Table 6.1 - Member Sizes

Member No.	Description
Columns 3,4,5,6	Tube 8 in. (outer diameter) × 0.158 in. (thickness)
Beams 1,2	W 10×22 wide flange section
Beam 7	Tube 2.5 in. × 0.049 in.
Braces 1,2	Tube 2.5 in. × 0.049 in.
Braces 3,4	Tube 3.0 in. × 0.083 in.

It was assumed that the braced bent carried a concentrated weight of 40 kips at the top. No gravity and P–Δ effects were considered. The experimental specimen was represented by a W 6×20 section, which was 48 inches (121.9 cm) long. The base of the W 6×20 section was welded to a steel plate which, in turn, was bolted to a reaction block. It was assumed that the test specimen carried a concentrated weight of 1.0 kip at its top end. Therefore, the experimental specimen was considered a single-degree-of-freedom cantilever column. The column was tested horizontally so that gravity effects were not taken into account. Figure 6.10 illustrates the layout of the experiment. The displacement of the top end of the column was monitored by an external LVDT. The restoring force of the specimen was measured by a load cell which was mounted on the piston of the actuator. Two tests were performed with this system. The results of these tests are presented in the subsequent sections.

6.3.2 Substructuring Formulation

The following idealizations were made in the analytical model of the braced bent :

(i) The ground supports of the columns were assumed to be fixed.

(ii) The diagonal braces were connected to the columns with a pin connection.

(iii) The connections of the columns with the beams were moment resisting.

(iv) The beams were assumed to be axially rigid. Therefore, the ends of these members had identical horizontal displacements at each integration step.

(v) The vertical degrees-of-freedom of all the nodes were constrained.

Based on these simplifying assumptions, the braced bent model had seven degrees-of-freedom (Fig. 6.9(b)). The rotational degrees-of-freedom 4,5,7 and 8 and the translational degree-of-freedom 6 were not assigned any mass. Therefore, the implicit-explicit numerical algorithm was selected to control the pseudodynamic test. The members of the braced bent were treated as the implicit elements and the experimental specimen was considered as the explicit element. As shown in Fig. 6.9(b), the boundary node of the experimental specimen and the analytical substructure, i.e. node 2, was allowed to translate and rotate in the plane of the frame. Since the rotational degree-of-freedom lies in the interface of the two subassemblages, a rotational mass was assigned to node 2 in order to satisfy the stability conditions of the implicit-explicit algorithm. The specified rotational mass was 5.0 k sec^2 in to achieve a reasonable integration time step. All the members in the frame were assumed to remain elastic throughout the tests. Therefore, the stiffness matrix of the analytical substructure was not modified during the integration process.

6.3.3 Experimental Results

(i) *Free Vibration*

The equipment-structure system was subjected initially to a free vibration response. A ground pulse of acceleration magnitude 200 in/sec^2 was applied to the braced bent. The

displacement time histories of the top level and the equipment relative to the ground are shown in Figs. 6.11(a) and 6.12(a), respectively. The maximum displacements obtained were 0.147 in. (3.7 mm) for the top level and 0.182 in. (4.6 mm) for the equipment. There is no observable decay in the amplitudes since the only damping introduced in the system was that caused by the frictional forces in the experimental apparatus. This damping effect was negligible in the response of the bent and it did not affect the response of the equipment significantly. The relative displacement history of the equipment with respect to the top level is plotted in Fig. 6.13(a). These displacements were the ones actually imposed on the specimen. The contribution from the second mode of vibration of the system is apparent only in the relative deformation of the equipment. However, no growth of the second mode response was observed, since the experimental errors were minimal.

(ii) *Earthquake Excitation*

The system was subsequently tested using the El Centro 1940 NS accelerogram, which was scaled to 0.4g peak ground acceleration.

To simplify the subsequent analytical correlations, the excitation was selected such that the equipment remained elastic. This is not a necessary restriction for the technique. The displacement time histories of the equipment and the top level relative to the ground are shown in Figs. 6.14(a) and 6.15(a). The maximum displacement obtained for the equipment was 1.168 in. (29.7 mm). The maximum displacement of the deck level was 0.956 in. (24.3 mm). In addition, the relative displacement time history of the equipment with respect to the deck level is shown in Fig. 6.16(a). The maximum relative displacement of the top of the specimen with respect to its base was found to be 0.248 in. (6.3 mm). Larger amplitudes in the negative displacement direction can be observed in the later portions of the displacement time history. This is attributed to the imperfect base flexibility conditions ; the flexibility of the base was larger in that direction. Ideal "fixed" base conditions are usually difficult to obtain in an experiment.

6.3.4 Analytical Correlations

Very good agreement was obtained between the results of the experiments and analytical simulations of the response of the system under the same ground excitations. The experimental specimen was idealized as an elastic column element. The braced bent model was identical to the one used as the substructured subassemblage of the experiment. The free vibration response of the analytical model is shown in Figs. 6.11(b), 6.12(b) and 6.13(b). The analytical simulation of the response due to the El Centro excitation is shown in Figs. 6.14(b),6.15(b) and 6.16(b). Table 6.2 lists the maximum displacements obtained from all the tests and the analytical simulations.

Table 6.2 Maximum Displacements

		Equipment		Top (in)
		Relative to Base (in)	Relative to Ground (in)	
Free Vibration	Test	0.041	0.182	0.147
	Anal.	0.042	0.182	0.147
El Centro	Test	0.248	1.168	0.956
	Anal.	0.204	1.133	0.955

The small difference observed in the relative displacements of the equipment with respect to its base is due to the flexibility of the support in the experimental setup. In the analytical simulations idealized "fixed" support conditions were used.

6.4 Conclusions

The results of the pseudodynamic tests of the equipment-structure system described in this chapter demonstrate the practicability and efficiency of substructuring methods in assessing the seismic performance of equipment and other nonstructural components. Furthermore, the same methods can be used to test structural subassemblages which are not directly attached to the ground.

The good correlation of the analytical simulations and the experimental results has shown that such experiments can be controlled accurately and reliably in spite of the fact that relatively small displacements may be imposed on the test specimen.

It is clear from the test that it is difficult to perfectly fix equipment to the structure. Thus, analytical idealizations assuming rigid connections may result in erroneous results. By testing the entire equipment-support assembly pseudodynamically, a more realistic representation of the equipment-structure interaction can be obtained.

CHAPTER 7

NONLINEAR SUBSTRUCTURING

7.1 Introduction

The applications of substructuring concepts to pseudodynamic testing are further examined in this chapter considering substructured subassemblages which exhibit nonlinear behavior. In the previous chapters, the substructured subassemblages were modeled with elastic elements : (i) in Chapter 5, the top part of the two-degree-of-freedom structure was modeled with an elastic beam-column element, and (ii) in Chapter 6, the braced frame was represented by an assembly of elastic beam-column and truss elements. In this chapter, nonlinear hysteretic elements are used to model the inelastic behavior of the substructured subassemblages in a steel frame. The behavior of the frame to a specified ground motion is examined by testing part of the frame pseudodynamically and modeling the hysteretic behavior of the remaining components with inelastic elements. The results of this experiment are compared with analytical simulations to evaluate the reliability and practicability of applying nonlinear substructuring to the pseudodynamic test method. Recommendations are offered concerning the needs for enhancing and extending the inelastic analytical elements which may be integrated with the current substructuring options. In addition, this experiment is carried out using the standard explicit integration procedure, rather than the implicit-explicit method used in the previous tests.

7.2 Test Description

7.2.1 Frame Description

A simple three-story steel frame was used as basis of the test system. The steel frame is shown in Fig. 7.1. To simplify this example, it consisted of a one bay shear building. Each of the three stories was 96 inches (243.8 cm) high. For dynamic analysis purposes with horizontal ground excitation, the prototype structure was idealized as having three lateral degrees-of-freedom as shown in Fig. 7.1. The masses are concentrated at the story levels. The beams were assumed to be rigid. The columns were W 6×20 wide flange sections and they were aligned with their weak axis perpendicular to the plane of the frame. Table 7.1 lists the mass and elastic stiffness characteristics of each story.

Table 7.1 - Frame Characteristics

Story No.	Weight (kips)	Elastic Stiffness (k/in)
1	2.0	10.46
2	2.0	10.46
3	4.0	10.46

During the test, the top two stories were modeled analytically and the bottom story was tested pseudodynamically. With an inflection point at the midheight of the first story, the experimental specimen was reduced to a single degree-of-freedom cantilever column. Figure 7.1 illustrates the test specimen and the substructured subassemblage.

7.2.2 Pseudodynamic Formulation

Three lateral degrees-of-freedom were considered for the combined system. Each degree-of-freedom was assigned a concentrated mass. No viscous damping was specified for the system and P–Δ effects were disregarded. Based on these considerations, the equations of motion for the combined system are :

$$\begin{bmatrix} m_1 & 0 & 0 \\ 0 & m_2 & 0 \\ 0 & 0 & m_3 \end{bmatrix} \begin{bmatrix} a^1_{i+1} \\ a^2_{i+1} \\ a^3_{i+1} \end{bmatrix} + \begin{bmatrix} R^A_1 \\ R^A_2 \\ R^A_3 \end{bmatrix} + 2 \begin{bmatrix} R^E_1 \\ 0 \\ 0 \end{bmatrix} = - \begin{bmatrix} m_1 \\ m_2 \\ m_3 \end{bmatrix} a^g_{i+1} \qquad (7.1)$$

where

m_1 , m_2 and m_3 are the masses of the floors given in Table 7.1,

$R^E_{1_{i+1}}$ is the restoring force of the first story column measured directly from the experimental specimen when subjected to a displacement of 0.5 d^1_{i+1},

$R^A_{1_{i+1}}$, $R^A_{2_{i+1}}$ and $R^A_{3_{i+1}}$ are analytical restoring forces computed based on the calculated interstory drifts and the hysteretic model assumed for the story.

Since there are no massless degrees-of-freedom, the Newmark explicit algorithm could be used as the integration method. Figure 7.2 illustrates the tasks which are performed during each time step of the integration process. First, the displacement value of each degree of freedom is computed based on the displacement, velocity and acceleration values of the previous time step. Restoring force values are then computed from the experimental specimen and from the inelastic analytical models of the substructured stories. From the story displacements we can compute the drifts of each substructured story. Based on the drift values, the restoring forces of the substructured stories are calculated from the inelastic analytical model (See Section 7.2.4). These forces are fed back to the equations of motion. The computed displacement of the experimental specimen is imposed on the cantilever column and the restoring force of the column is measured by the load transducer. This restoring force is then also inserted in the equations of motion and the acceleration vector of the current time step is finally computed. The entire process is repeated for each integration time step.

7.2.3 Experimental Setup

The pseudodynamic test setup of the first story column is shown in Fig. 7.2. The specimen, a W 6×20 wide flange section, was tested in its weak axis direction. One hydraulic actuator was used to impose specified displacements at the top of the column. A load transducer was attached to the piston of the actuator to measure the restoring force of the test specimen. The specimen was connected to the actuator with a clevis. No moment was imposed at the top of the specimen since this point simulated the inflection point of the first story column. The displacements were controlled using an external displacement transducer (LVDT).

7.2.4 Inelastic Analytical Model

The inelastic behavior of the top two (substructured) stories was modeled by means of the Menegotto-Pinto nonlinear model. The hysteretic pattern of the Menegottto-Pinto model is shown in Fig. 7.3. The governing equations for this behavior are

$$\bar{R} = b\,\bar{d} + \frac{(1-b)\,\bar{d}}{(1+\bar{d}^{r})^{1/r}} \tag{7.2}$$

where

$$\bar{R} = \frac{R}{r_y} \tag{7.3}$$

$$\bar{d} = \frac{d}{d_y} \tag{7.4}$$

$$k = \frac{r_y}{d_y} \tag{7.5}$$

Equation (7.2) is used when tensile or compressive loading occurs. The loading curve is defined by the initial elastic stiffness k, the strain hardening stiffness bk and the curvature parameter r. Unloading occurs on a straight line with slope equal to the initial elastic stiffness k. After a permanent plastic deformation is incurred, the displacement control parameters are shifted by this amount. The Menegotto-Pinto model was selected for the

substructuring idealization because it was simple and could still reasonably simulate the inelastic hysteretic behavior of the steel columns used. Of course, the accuracy of the results are limited by the accuracy of the inelastic model used.

7.3 Experimental Results

The test system was subjected to a single earthquake excitation. The inelastic behavior of the frame was examined considering 10 seconds of the 1940 El Centro (NS) ground motion scaled to 1.0g peak acceleration. The parameters which were selected for the substructured stories are listed in Table 7.2. The same table also lists the parameters which were selected in modeling the experimental specimen for the analytical correlations which are described in Section 7.4.

Table 7.2 - Modeling Parameters

Story	Experiment				Analytical Simulation			
No.	k (k/in)	d_y (in)	β	r	k (k/in)	d_y (in)	β	r
1	-	-	-	-	9.96	1.120	0.15	1.5
2	10.46	1.067	0.08	2.0	10.46	1.067	0.08	2.0
3	10.46	1.067	0.08	2.0	10.46	1.067	0.08	2.0

The displacement time histories of the three degrees-of-freedom are shown in Figs. 7.4,7.5 and 7.6. The maximum displacements obtained during the experiment are listed in Table 7.3. The corresponding values from analytical simulations are shown in the same table, too. Additionally, the story shear vs. interstory drift relationships for all three stories are illustrated in Figs. 7.7(a),7.8(a) and 7.9(a). The experimental specimen experienced significant inelastic deformations as demonstrated in the hysteretic behavior of the first story. The

second story acquired a permanent plastic deformation which is shown in the shift of the corresponding hysteretic loop. The experimental results are next compared to analytical simulations to verify the reliability of nonlinear substructuring techniques.

7.4 Analytical Correlations

Excellent analytical correlations were obtained for the pseudodynamic test results. As shown in Table 7.2, the top two stories were modeled with the same parameters which were used in the pseudodynamic tests. The selected parameters for the first story are also shown in Table 7.2. The displacement time histories of the three stories are plotted in Figs. 7.4,7.5 and 7.6. Good correlations were obtained for all three displacement time histories. Furthermore, the shear vs. drift hysteretic loops are plotted in Figs. 7.7(b),7.8(b) and 7.9(b). The hysteretic loops matched very well with the pseudodynamic test results.

7.5 Conclusions and Recommendations

The results of the pseudodynamic tests with nonlinear substructuring indicate that substructuring techniques may be applied with confidence to structures with substructured subassemblages which involve changes in stiffness during an experiment. Based on the results of the experiments described in the previous section, additional conclusions can be obtained :

(1) When nonlinear subassemblages are modeled analytically, it is not necessarily efficient to condense the analytical degrees-of-freedom to the experimental boundaries. The state determination for each inelastic analytical element must be performed at every integration step and appropriate changes, if any, must then be made to the analytical stiffness matrix. If such changes in stiffness occur frequently, the condensation process may increase the computation time by more than it saves.

(2) Viscous damping did not play an important role in the behavior of the three-story frame. The energy losses due to frictional forces in the experimental setup were negligible compared to the hysteretic energy dissipation of the specimen. This is readily seen from the correlation of the results between experiment and analysis.

(3) The standard explicit integration appears to work well. It has the added convenience that the algorithm does not need the stiffness of the analytical substructures. Thus, models such as these based on the Menegotto-Pinto formulation, can be used without the complexity of forming the stiffness matrix. If the stiffness formulation is more convenient, the restoring force can be represented by conventional incremental load procedures based on tangent stiffness.

The modeling capabilities of substructured subassemblages can be greatly enhanced by expanding the current substructuring element library. Since the accuracy of substructuring techniques is directly related to the realism of the mathematical models which are used in the representation of structural components, future developments should include these tasks as well.

CHAPTER 8

CONCLUSIONS

8.1 Summary

The fundamental theories regarding the application of substructuring concepts to pseudodynamic testing have been examined. The basic algorithms for substructuring have been developed and discussed. The Newmark Explicit and the Implicit-Explicit numerical integration methods have been considered and guidelines for their proper use were given. Studies were performed to assess the characteristics of experimental error propagation on the substructuring algorithms. Verification tests were performed to test the reliability of the developed substructuring techniques. In these tests, both elastic and inelastic structural subassemblages were considered. Experiments were also performed to demonstrate the application of substructuring techniques to pseudodynamic tests of mounted equipment on structures. The results of pseudodynamic experiments correlated well with analytical simulations.

8.2 Conclusions

The results of this investigation have shown that substructuring techniques can provide reliable means to combine analytically modeled subassemblages with pseudodynamically tested specimens. Substructuring concepts are practical and efficient to implement in pseudodynamic experiments and they provide significant economies in the experimental investigation of structural systems. Furthermore, the versatility of the substructuring ideas is demonstrated by their broad spectrum of applications in the pseudodynamic test method. In addition to conventional structural subassemblage tests, equipment and soil-structure interaction pseudodynamic investigations were shown to be feasible by means of substructuring.

The substructuring techniques considered were based on well-established numerical methods. The characteristics of the integration algorithms are well known, thus, their proper use can be achieved without numerical stability problems. Since analytical subassemblages are not associated with experimental errors, substructuring techniques were shown to reduce experimental error propagation effects as compared to pseudodynamic tests of complete structures. Therefore, the spurious growth of the higher frequency modes in multiple-degree-of-freedom systems can be limited substantially by use of substructuring.

In conclusion, the findings indicate that when realistic analytical models are used for the substructured subassemblages, substructuring techniques in pseudodynamic testing constitute a very powerful tool in the experimental investigation of the seismic performance of structural systems.

8.3 Recommendations

As mentioned in the previous section, reliable results can be obtained provided realistic analytical models are used for the substructured subassemblages. Therefore, more and better analytical elements need to be incorporated in the available pseudodynamic systems to provide greater versatility and reliability in modeling substructured components. Furthermore, optimization of the computational schemes involved in the substructuring algorithms will contribute significantly in increasing the speed of a pseudodynamic test. If this is achieved, smaller integration time steps may be selected without unduly prolonging the test. This is especially important in the implicit-explicit methods so that any artificially added mass at the boundaries can be made significantly small.

As mentioned in Chapter 2, in some cases, the interface of the test specimen and the modeled substructure may require a large number of degrees-of-freedom, which renders the experiment difficult and inefficient to control. However, it may be possible for certain systems to simplify the interface conditions without significantly affecting the overall behavior of the test system. Further research is needed to investigate whether certain boundary degrees-

of-freedom can be disregarded and allow for a bigger variety of structures to be tested efficiently by means of substructuring techniques. In addition, improvement of displacement and rotation control mechanisms may further reduce experimental errors.

REFERENCES

1. Takanashi, K., et al., "Nonlinear Earthquake Response Analysis of Structures by a Computer-Actuator On-Line System", *Bull. of Earthquake Resistant Structure Research Center*, Institute of Industrial Science, University of Tokyo, No. 8, 1975.

2. Ghanaat, Y. and Clough, R. W., "Shaking Table Tests of a Tubular Steel Frame Model", *UCB/EERC-82/02*, Earthquake Engineering Research Center, University of Californnia, Berkeley, 1982.

3. Takanashi, K., et al., "Inelastic Response of H-Shaped Columns to Two-Dimensional Earthquake Motions", *Bull. of Earthquake Resistant Structure Research Center*, Institute of Industrial Science, University of Tokyo, No. 13, 1980.

4. Okada, T., et al., "A Simulation of Earthquake Response of Reinforced Concrete Building Frames to Bi-Directional Ground Motion by IIS Computer-Actuator On-Line System", *Proceedings*, 7th World Conference on Earthquake Engineering, Istanbul, Turkey, 1980.

5. Watabe, M., et al., "Feasibility of Pseudodynamic Testing System", *Progress Report on U.S.-Japan Large-Scale Aseismic Experiments for Building Structures*, Building Research Institute, Ministry of Construction, 13th Joint Meeting, US-Japan Panel on Wind and Seismic Effects, Tsukuba, 1981.

6. Okamoto, S., et al., "A Progress Report on the Full-Scale Seismic Experiment of a Seven-Story Reinforced Concrete Building", Building Research Institute, Ministry of Construction, Tsukuba, 1982.

7. Yamanouchi, H., et al., "Test Results of Full-Scale Six-Story Steel Building", Building Research Institute, Ministry of Construction, 4th Joint Technical Coordinating Committee Meeting, U.S.-Japan Cooperative Research Program, Tsukuba, Japan, 1983.

8. McClamroch, N. H., Serakos, J., and Hanson, R. D., "Design and Analysis of the Pseudodynamic Test Method", *UMEE 81R3*, University of Michigan, Ann Arbor, 1981.

9. Shing, P.B., and Mahin, S. A., "Experimental Error Propagation in Pseudodynamic Testing", *UCB/EERC-83/12*, Earthquake Engineering Research Center, University of California, Berkeley, 1983.

10. Clough, R. W. and Penzien, J., *Dynamics of Structures*, McGraw-Hill, 1975.

11. Bathe, K. and Wilson, E. L., *Numerical Methods in Finite Element Analysis*, Prentice Hall, 1976.

12. Newmark, N. M., "A Method of Computation for Structural Dynamics", *Journal of the Engineering Mechanics Division*, ASCE, No. EM 3, Vol. 85, 1959.

13. Row, D.G., Powell, G.H., and Mondkar, D.P., "2D Beam-Column Element for the ANSR-II Program", *Report No. UCB/EERC-79/30*, Earthquake Engineering Research Center, University of California, Berkeley, December 1979.

14. Wilson, E.L., "CAL 78 User Information Manual", *Report No. UC-SESM 79-1*, University of California, Berkeley, November 1978.

15. Hanson, R.D., and McClamroch, N.H., "Pseudodynamic Test Method for Inelastic Building Response", *Proceedings*, Eighth World Conference in Earthquake Engineering, San Francisco, July 1984.

16. McClamroch, N.H., Serakos, J., and Hanson, R.D., "Design and Analysis of the Pseudodynamic Test Method", *Report UMEE 81R3*, University of Michigan, September 1981.

17. U.S.-Japan Planning Group, "Recommendations for a U.S.-Japan Cooperative Research Program Utilizing Large-Scale Testing Facilities", *Report No. UCB/EERC-79/26*, Earthquake Engineering Research Center, University of California, Berkeley, September 1979.

18. Shing, P.B., Mahin, S.A. and Dermitzakis, S.N., "Evaluation of On-Line Computer Control Methods for seismic Performance Testing", *Proceedings*, Eighth World Conference in Earthquake Engineering, San Francisco, July 1984.

19. Hughes, T.G.R., and Liu, W.K., "Implicit-Explicit Finite Elements In Transient Analysis: Implementation and Numerical Examples", *ASME, Journal of Applied Mechanics*, Vol. 45, pp. 369-372, June 1978.

20. Hughes, T.G.R., and Liu, W.K., "Implicit-Explicit Finite Elements In Transient Analysis: Stability Theory", *ASME, Journal of Applied Mechanics*, Vol. 45, pp. 365-368, June 1978.

21. Kannan, A.E., and Powell, G.H., "DRAIN-2D : A General Purpose Computer Program for Dynamic Analysis of Inelastic Plane Structures", *Report No. EERC/UCB-73-6 and 73-22*, Earthquake Engineering Research Center, University of California, Berkeley, April 1973.

22. Golafshani, A.A., "DRAIN-2D2 : A Program for Inelastic Seismic Response of Structures", *Ph.D. Dissertation*, University of California, Berkeley, April 1982.

23. Bolt, B.A., "Earthquakes : A Primer", Freeman ,1978.

24. Shing, P.B. and Mahin, S.A., "Pseudodynamic Test Method For Seismic Performance Evaluation : Theory and Implementation", *Report No. UCB/EERC-84/01*, Earthquake Engineering Research Center, University of California, Berkeley, January 1984.

25. Row, D.G. and Powell, G.H., "A Substructure Technique For Nonlinear Static and Dynamic Analysis", *Report No. UCB/EERC-78/15*, Earthquake Engineering Research Center, University of California, Berkeley, 1978.

26. Midorikawa et al., "Preliminary Analysis of the Full-Scale Six-Story Steel Building", Third JTCC, *U.S.-Japan Cooperative Research Program, Building Research Institute*, Ministry of Construction, Japan, July 1982.

27. Yamanoushi et al., "Design of the Full-Scale Six-Story Steel Building", Third JTCC, *U.S.-Japan Cooperative Research Program, Building Research Institute*, Ministry of Construction, Japan, July 1982.

28. Okamoto et al., "System Check of New BRI Computer On-Line Testing", Third JTCC, *U.S.-Japan Cooperative Research Program, Building Research Institute*, Ministry of Construction, Japan, July 1982.

29. Mahin, S.A. and Williams, M. , "Computer Controlled Seismic Performance Testing", *Proceedings*, Second ASCE-EMD Specialty Conference on Dynamic Response of Structures, Atlanta, Georgia, Jan. 1981.

30. Okada, T., et al., "Nonlinear Earthquake Response of Equipment Anchored on R/C Building Floor", *Bull. ERS Research Center*, No. 13, Institute of Industrial Science, Univ. of Tokyo, 1980.

31. Der Kiureghian, A., Sackman, J.L., Nour-Omid, B., "Dynamic Response of Light Equipment in Structures", *Report No. UCB/EERC-81/05*, Earthquake Engineering Research Center, University of California, Berkeley, 1981.

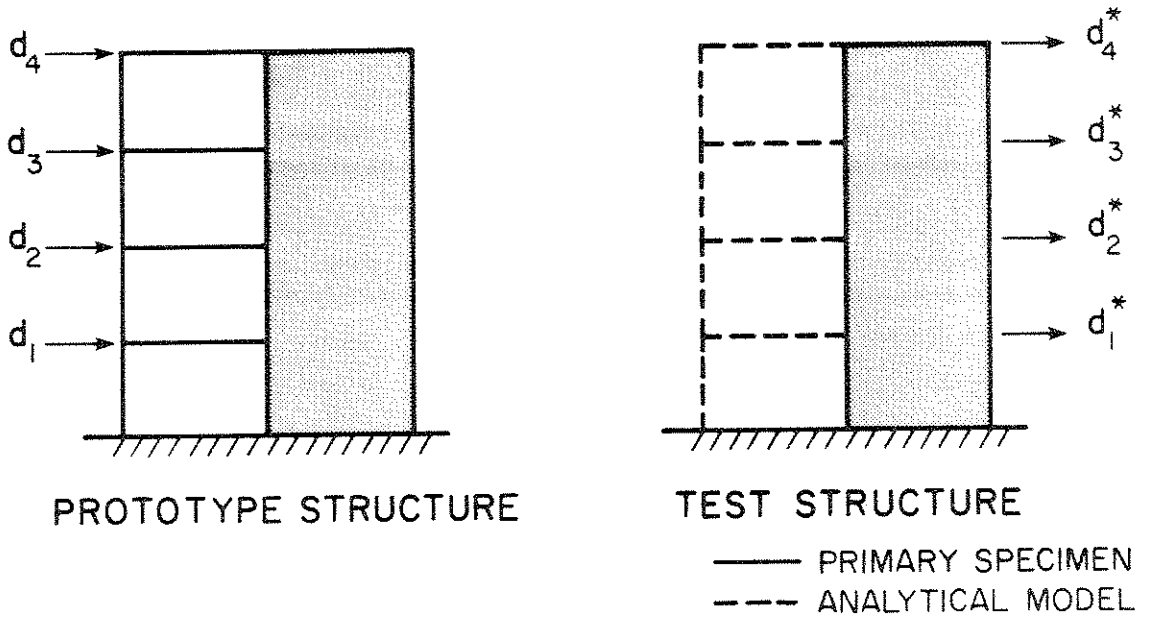

Fig. 2.1 Reduction of Full-Size Prototype Specimen Using Substructuring

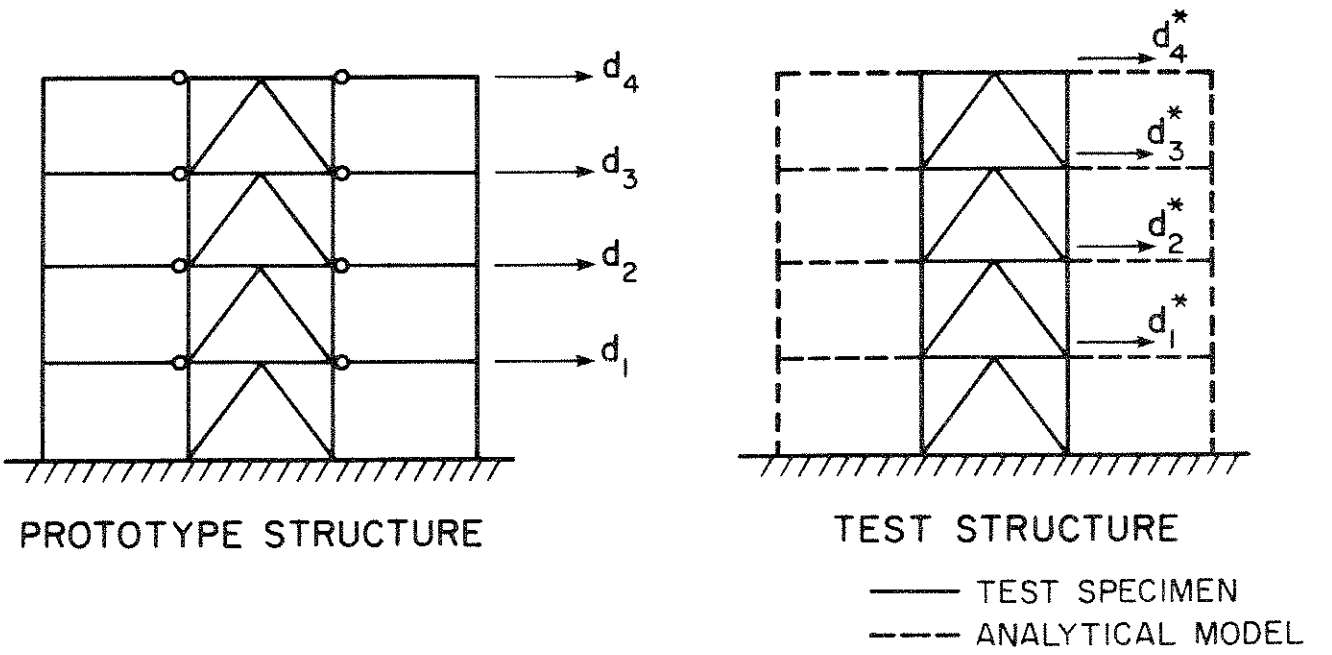

Fig. 2.2 Pseudodynamic Testing of Critical Lateral Load Resisting Components

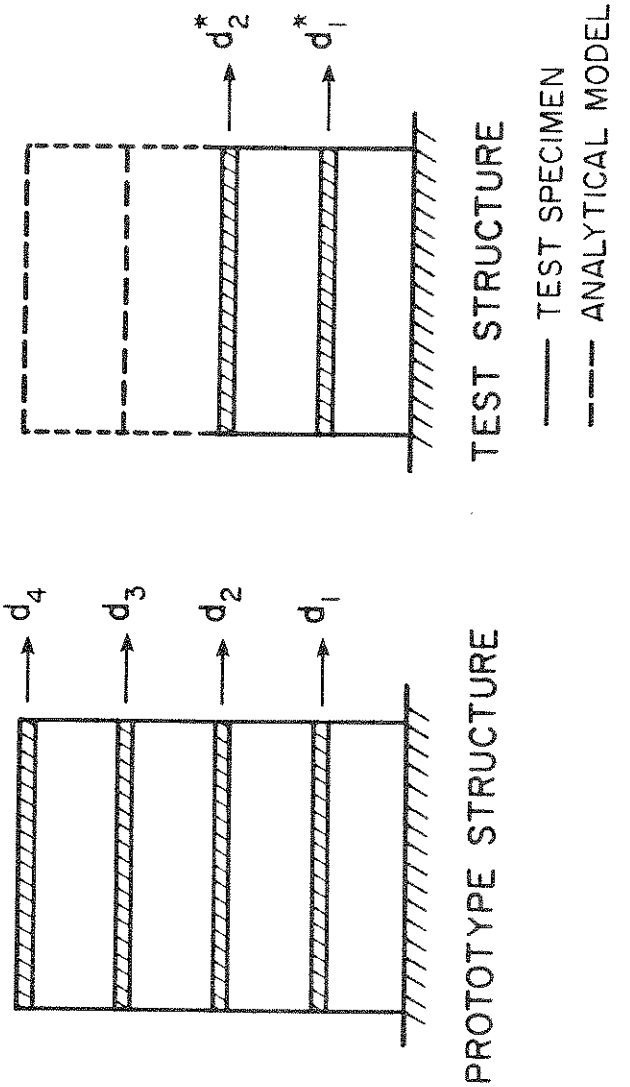

Fig. 2.3 Reduction of the Experimental Degrees-of-Freedom of a Prototype Structure

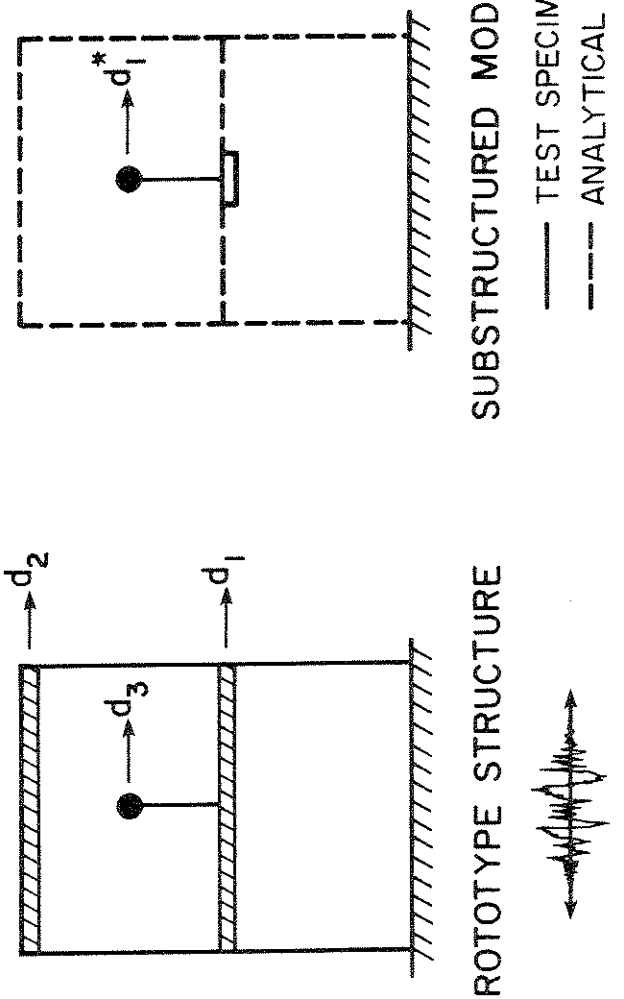

Fig. 2.4 Testing of Equipment Using Substructuring of Supporting Frame

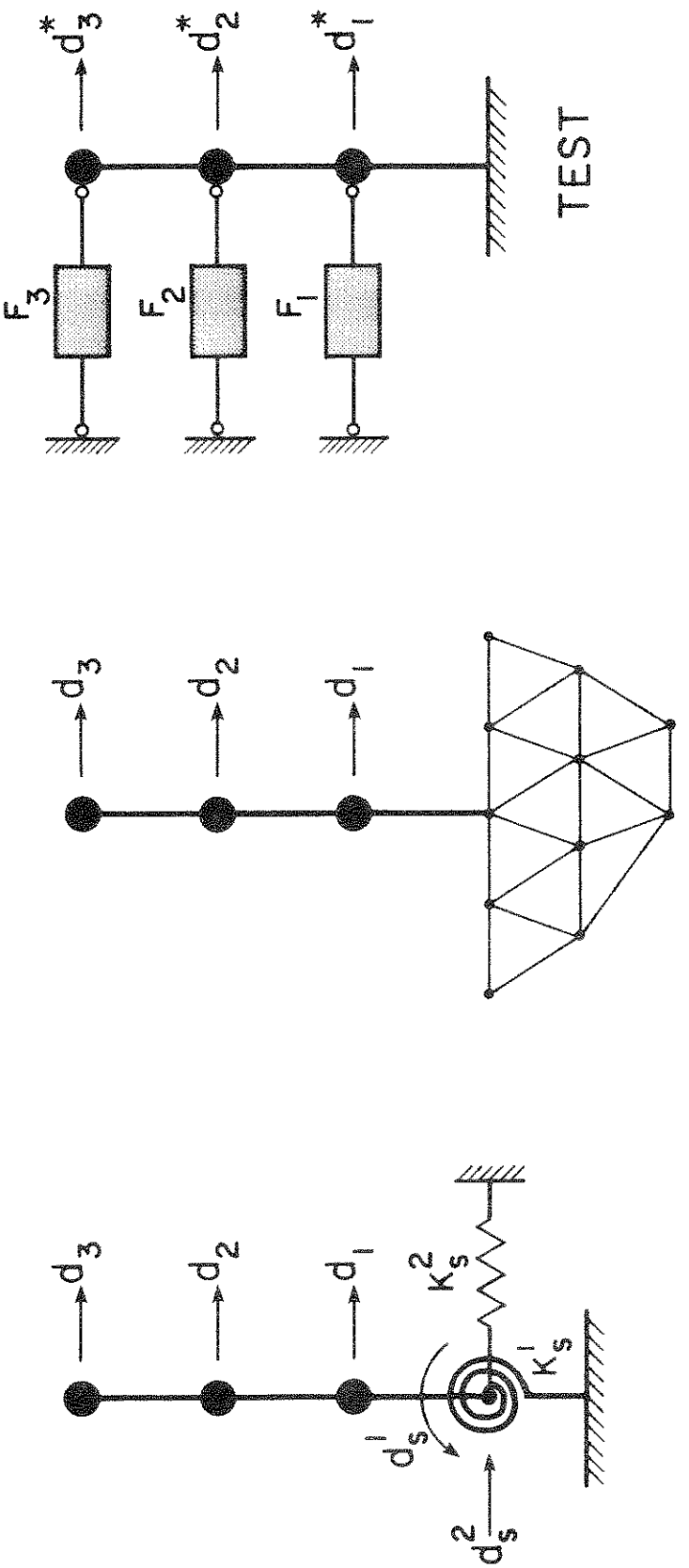

Fig. 2.5 Modeling of Soil-Structure Interaction Using Substructuring

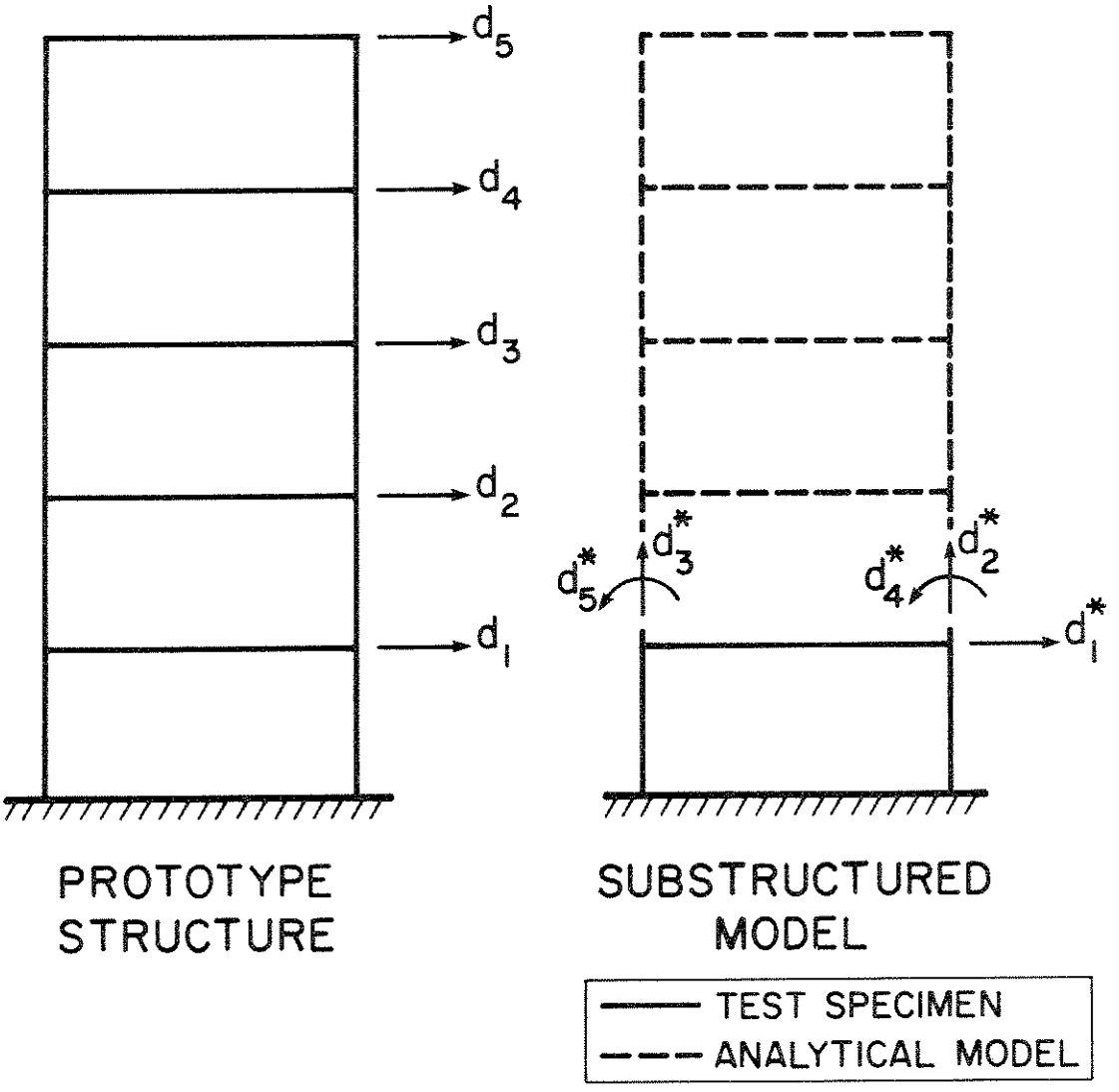

Fig. 2.6 Prototype and Substructured Model of a Five-Story Frame

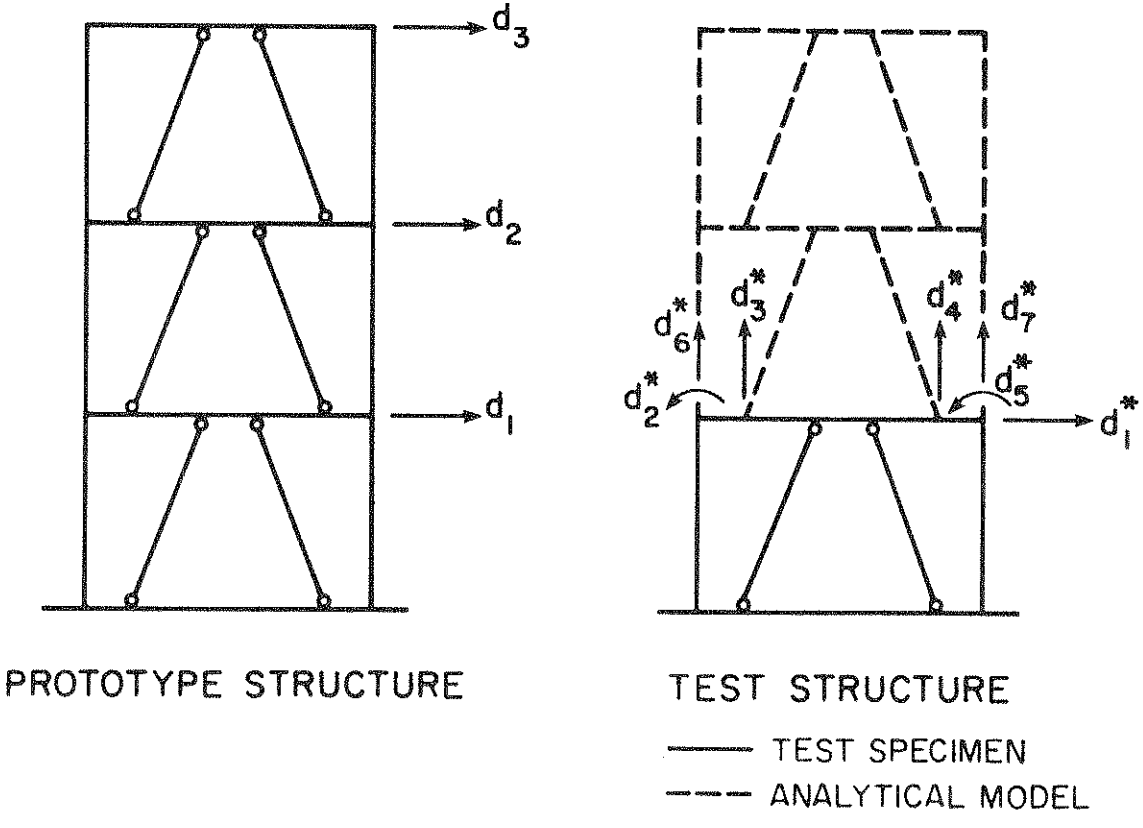

Fig. 2.7 Introduction of Additional Experimental Degrees-of-Freedom

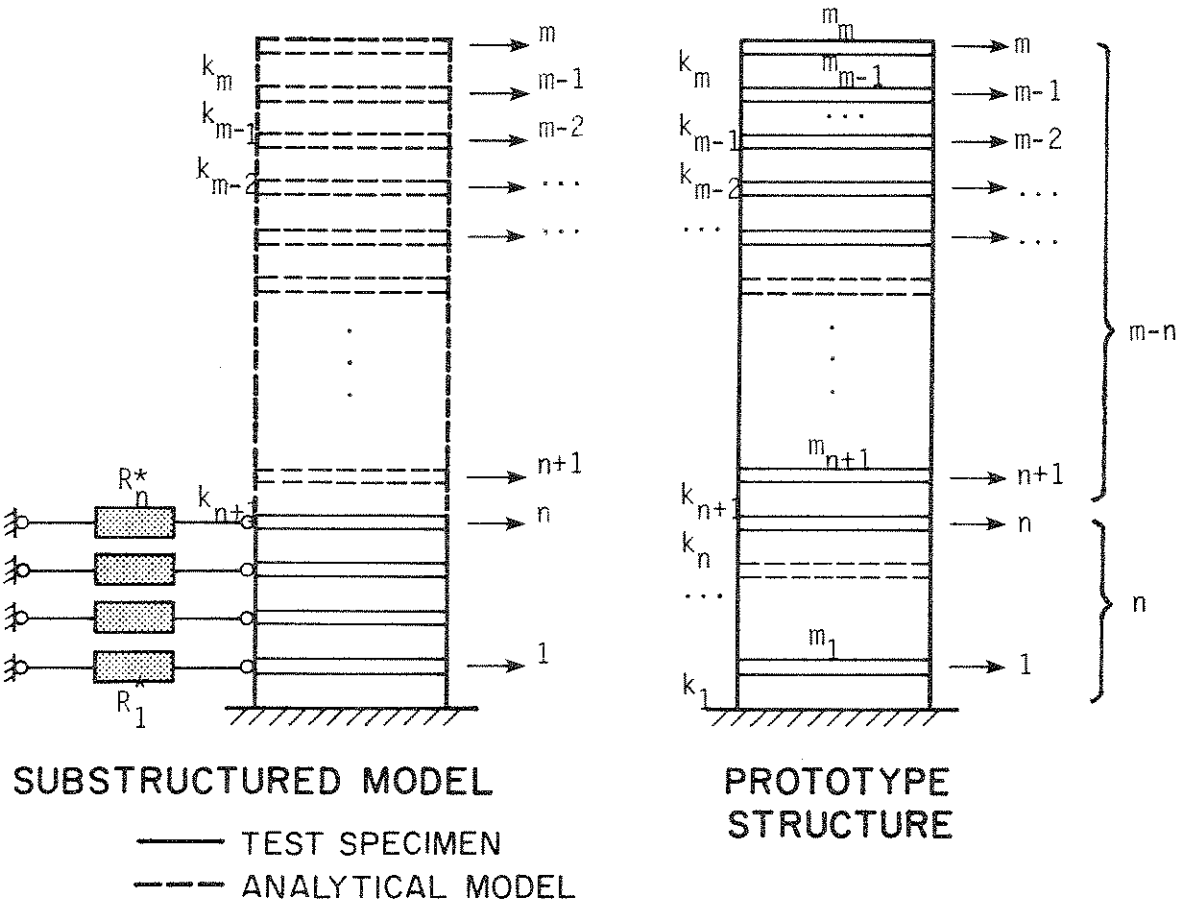

Fig. 3.1 Application of Substructuring Concepts in the Pseudodynamic Test of an M-Story Shear Building.

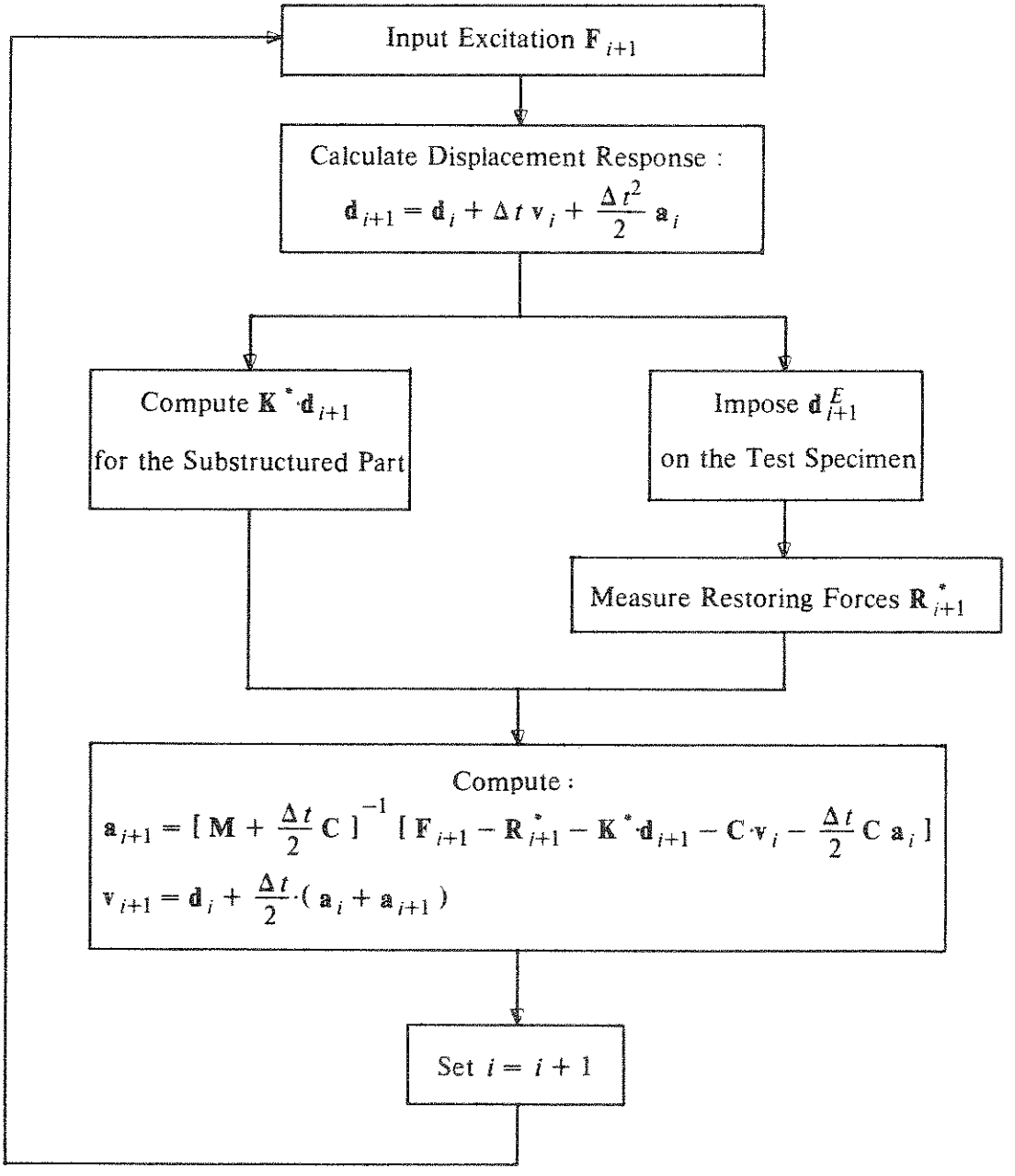

Fig. 3.2 Pseudodynamic Algorithm for Substructuring Applications Using the Newmark Explicit Integration Method

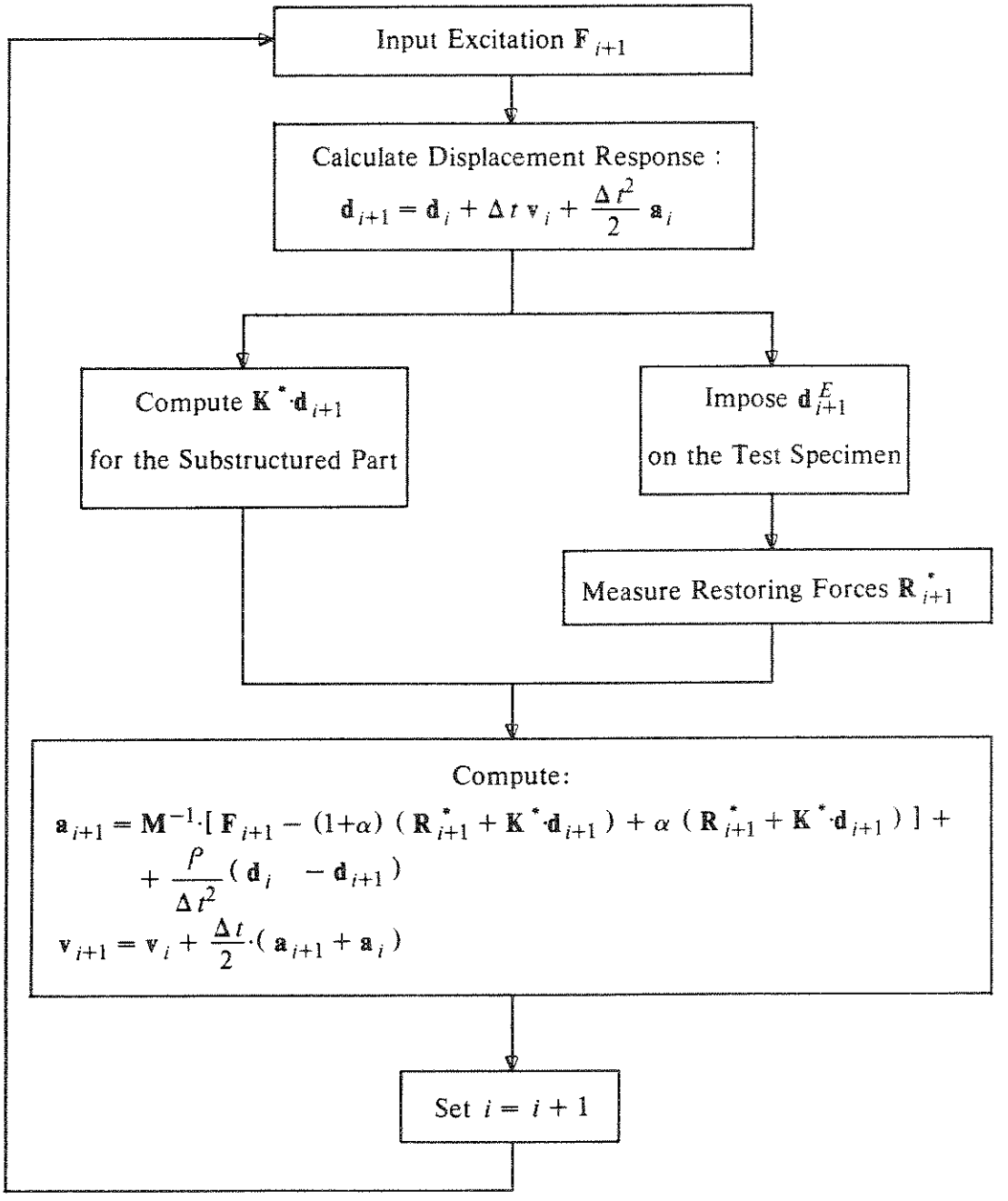

Fig. 3.3 Pseudodynamic Algorithm for Substructuring Applications Using the Modified Newmark Explicit Integration Method

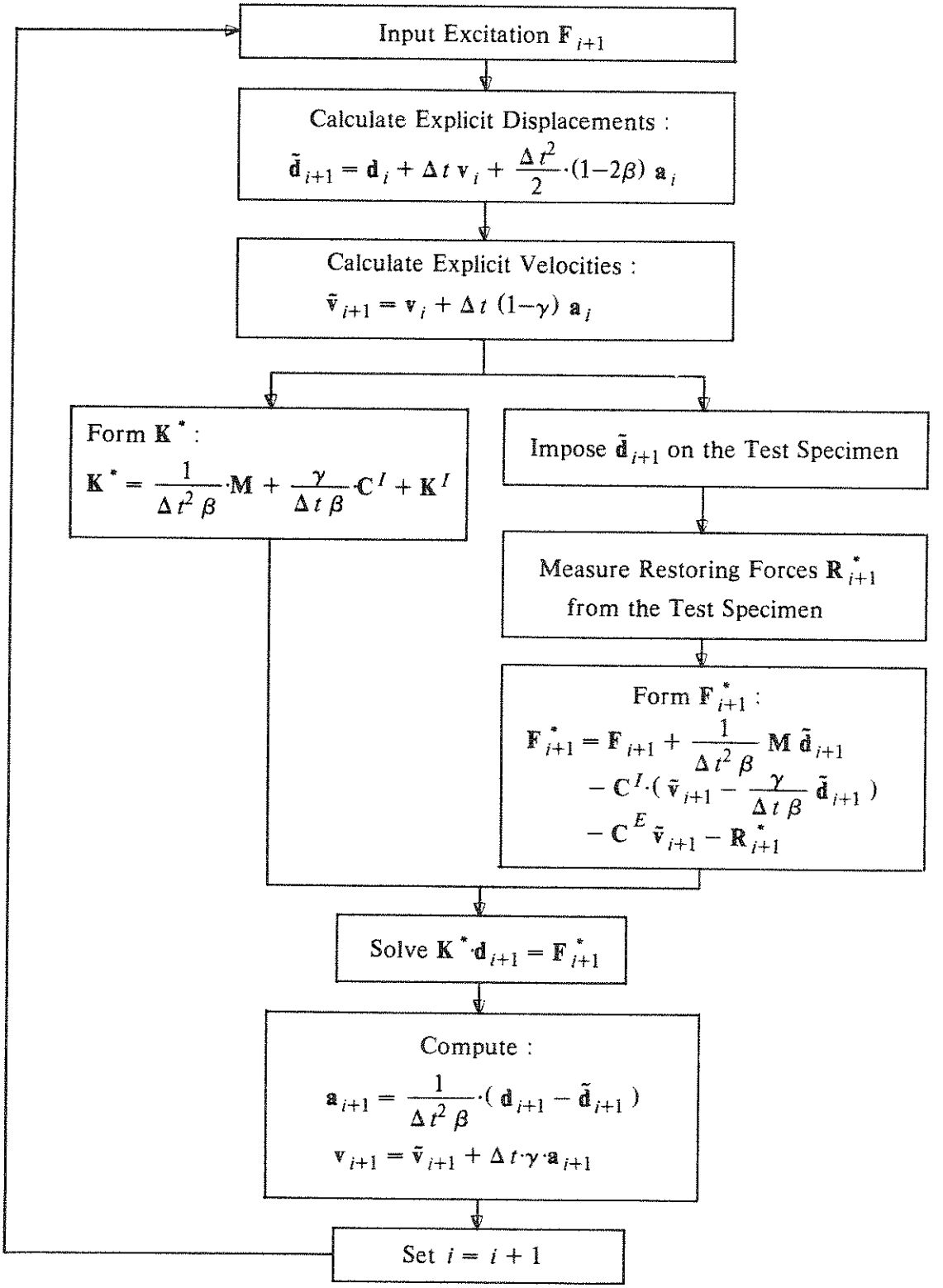

Fig. 3.4 Pseudodynamic Algorithm for Substructuring Applications Using the Implicit-Explicit Integration Method

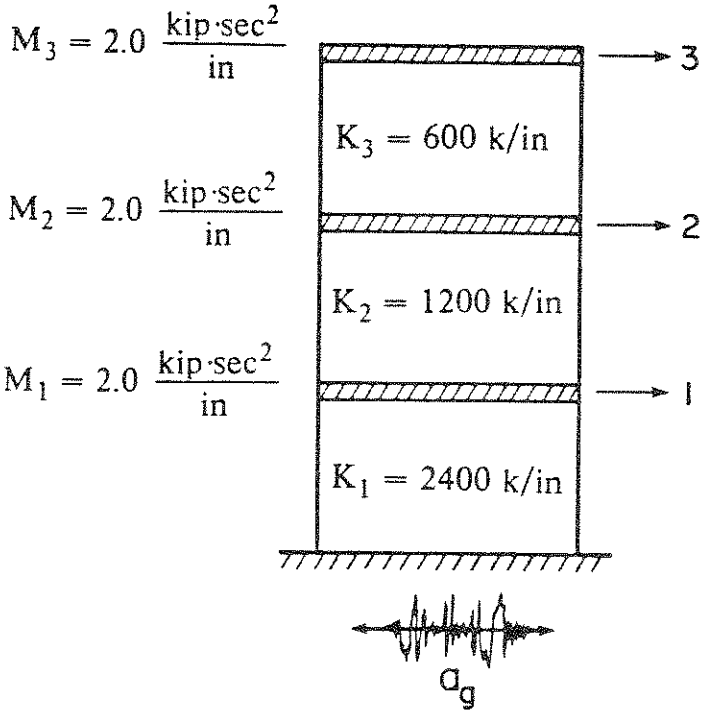

$$T = \begin{bmatrix} 0.54 \\ 0.23 \\ 0.14 \end{bmatrix} \text{ sec}$$

$$\omega = \begin{bmatrix} 11.62 \\ 27.5 \\ 45.9 \end{bmatrix} \frac{\text{rad}}{\text{sec}}$$

$$\Phi = \begin{bmatrix} 0.198 & -0.872 & 12.100 \\ 0.548 & -1.522 & -6.260 \\ 1.000 & 1.000 & 1.000 \end{bmatrix}$$

Fig. 3.5 Three-Story Frame Used in Error Analysis

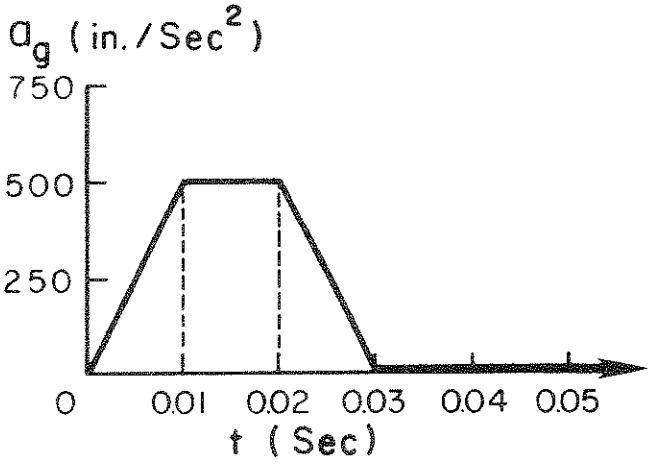

Fig. 3.6 Pulse Ground Acceleration

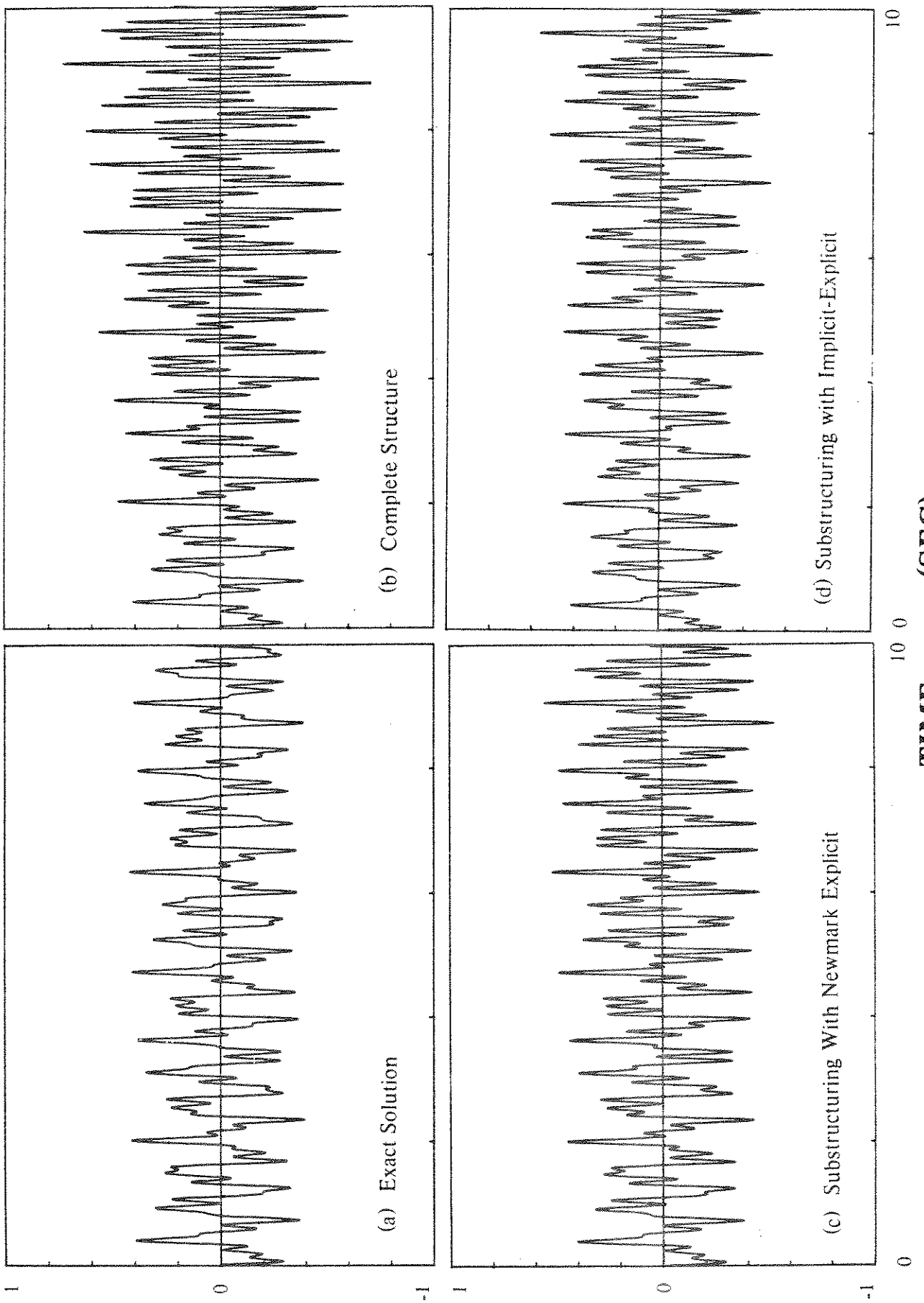

Fig. 3.7 Displacement History of First Story; Simulation of Experimental Error Effects in the Response of a Three Story Frame.

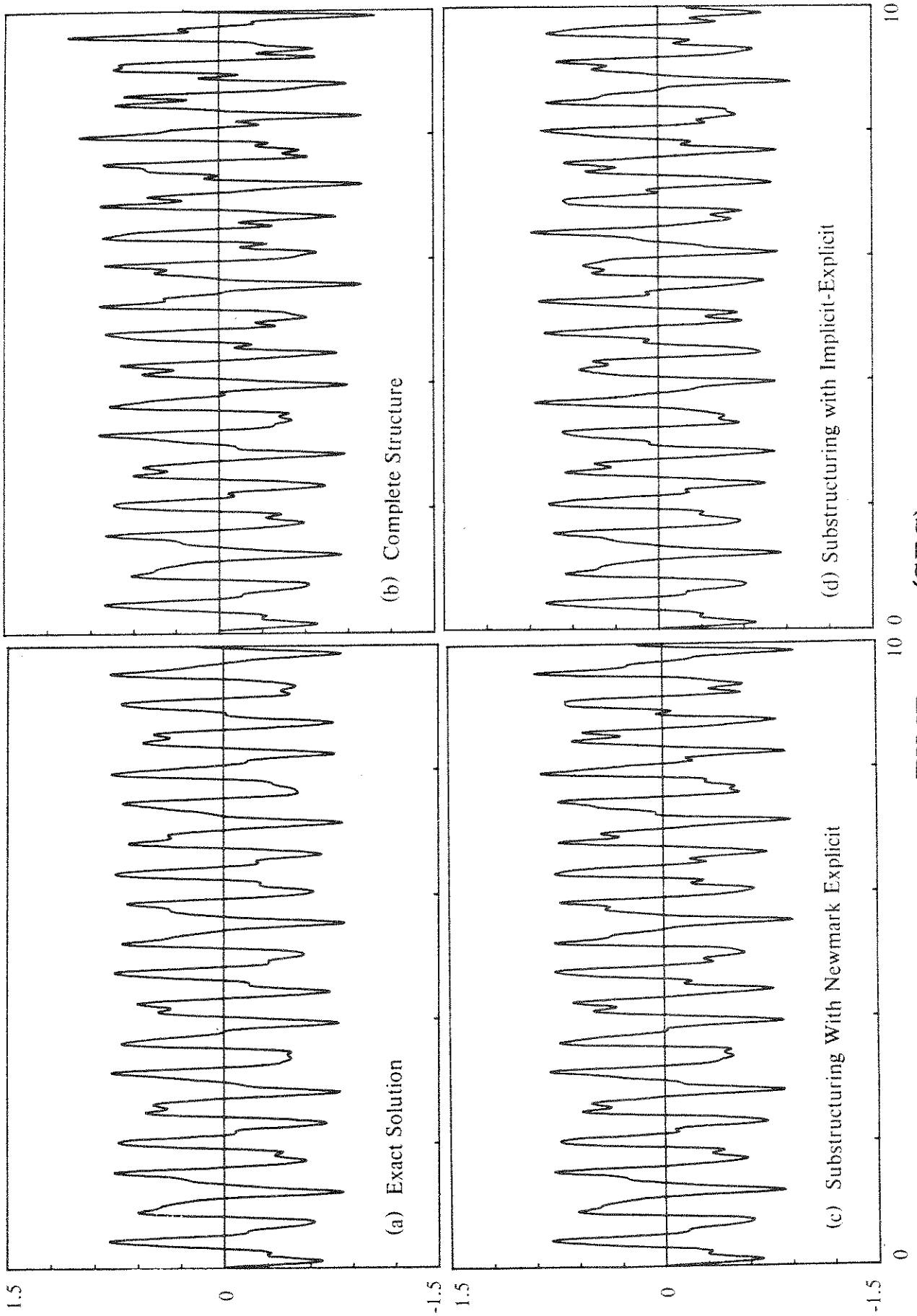

Fig. 3.8 Displacement History of Second Story; Simulation of Experimental Error Effects in the Response of a Three Story Frame.

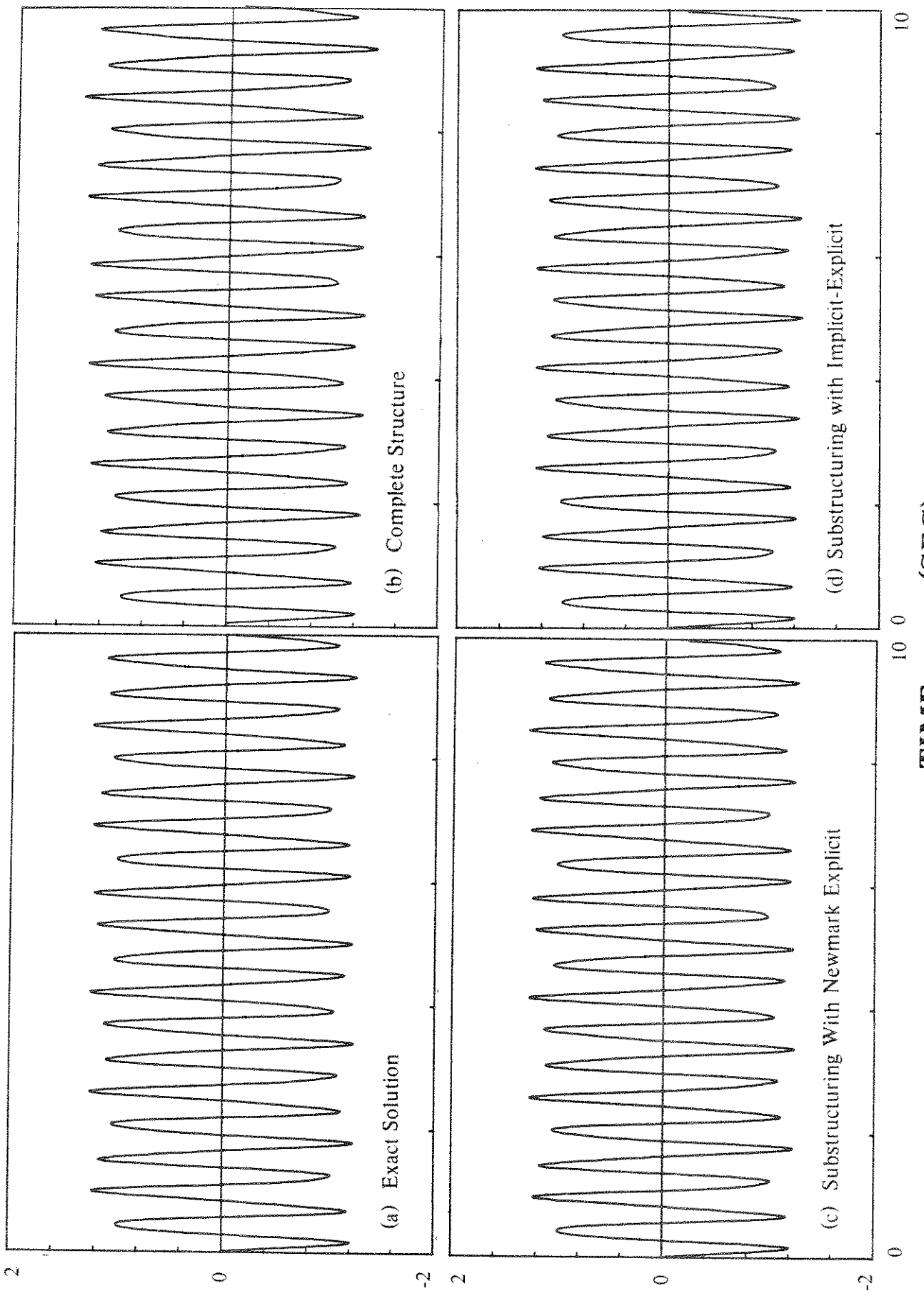

Fig. 3.9 Displacement History of Third Story; Simulation of Experimental Error Effects in the Response of a Three Story Frame.

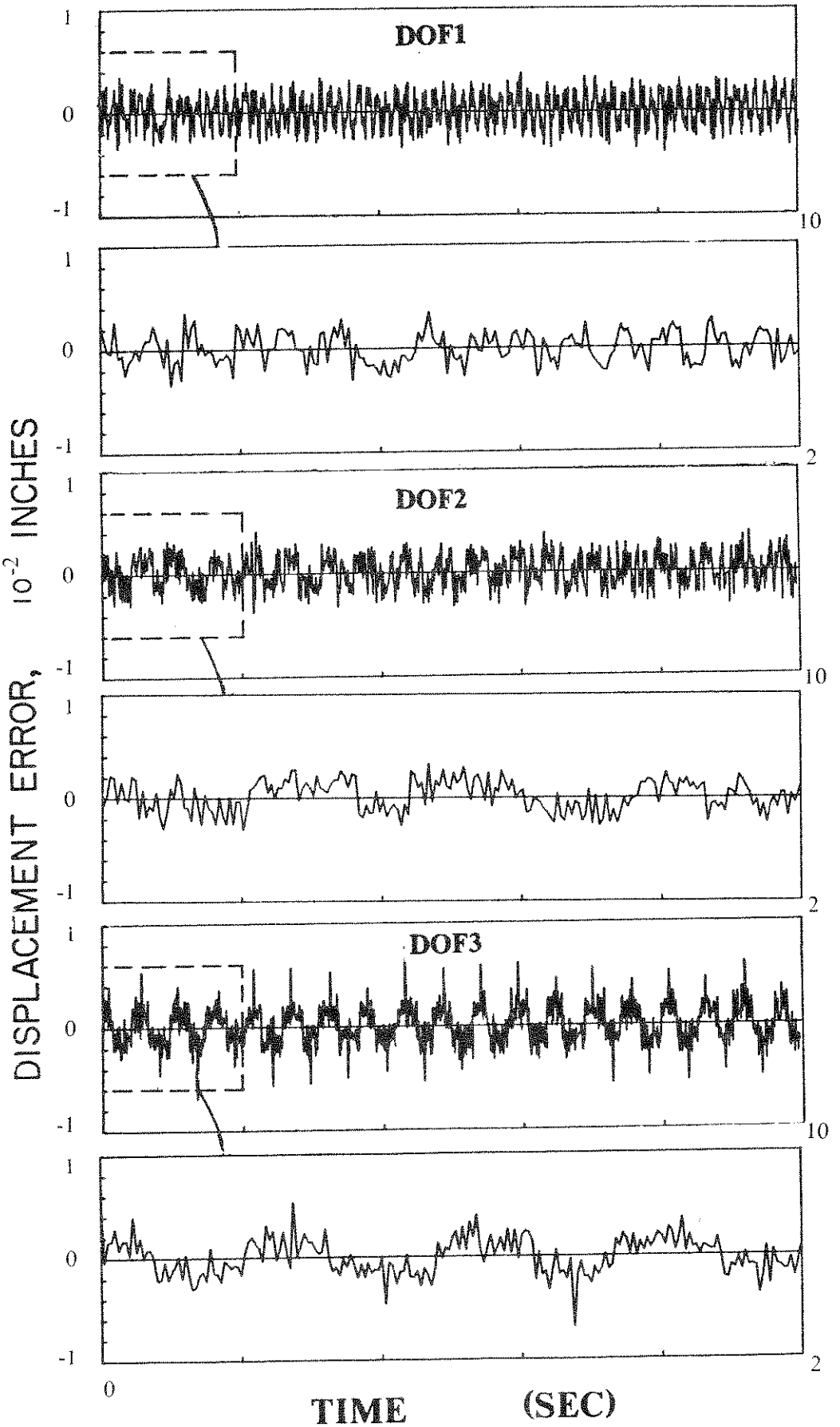

Fig. 3.10 Systematic Experimental Errors; Numerically Simulated Pseudodynamic Response of a Complete Three Story Frame

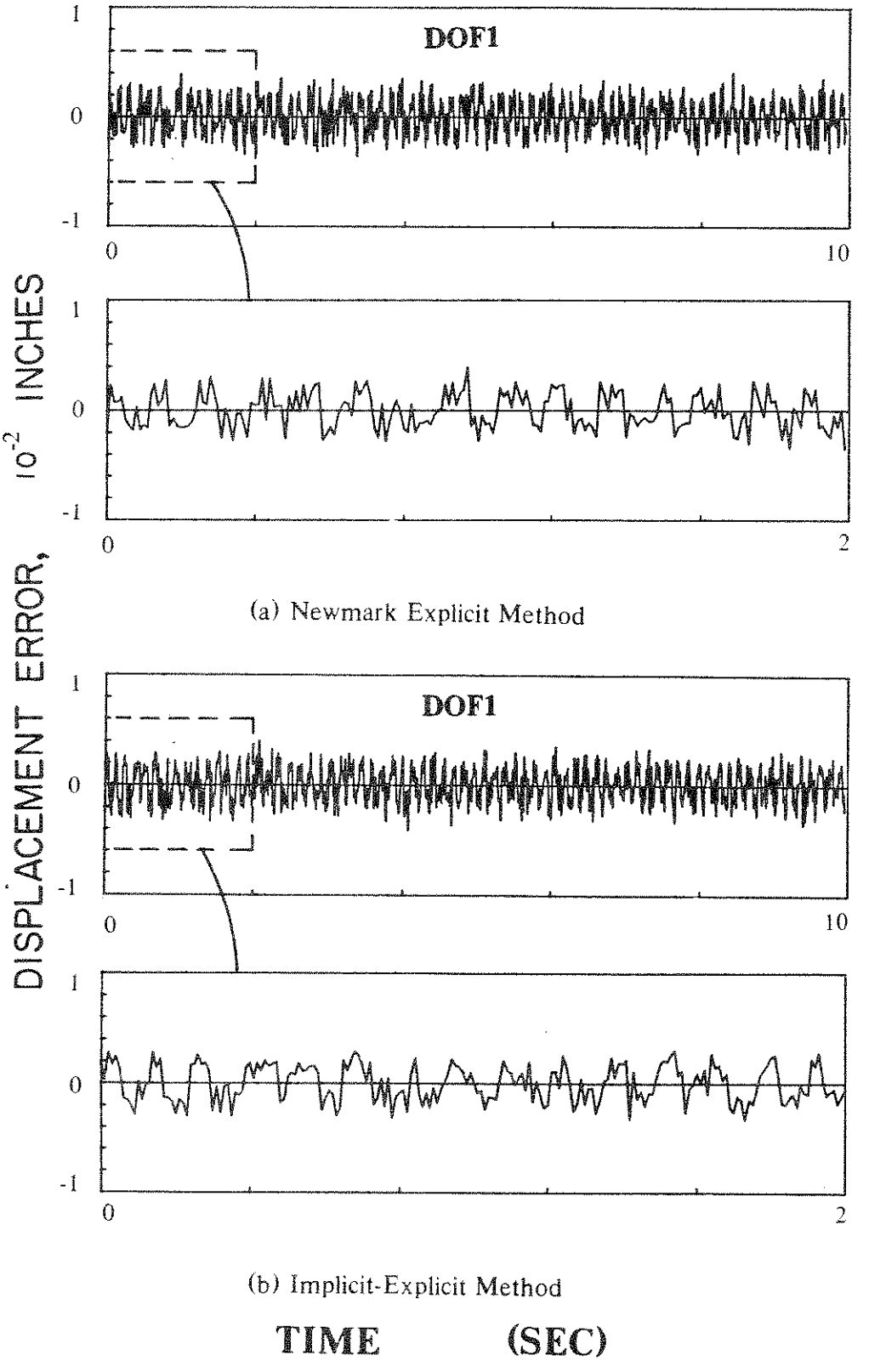

Fig. 3.11 Systematic Experimental Errors in the First Story Displacement
(Simulation of Pseudodynamic Response Using Substructuring)

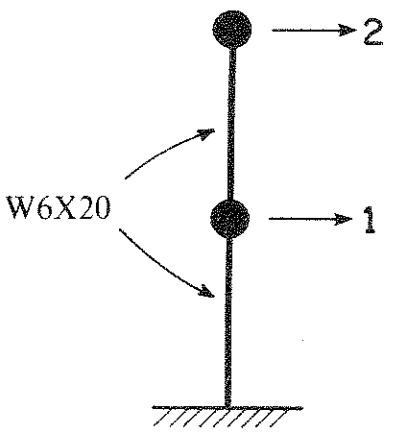

$$m_2 = 0.00543 \ \frac{\text{kip}\cdot\text{sec}^2}{\text{in}}$$

$$m_1 = 0.00828 \ \frac{\text{kip}\cdot\text{sec}^2}{\text{in}}$$

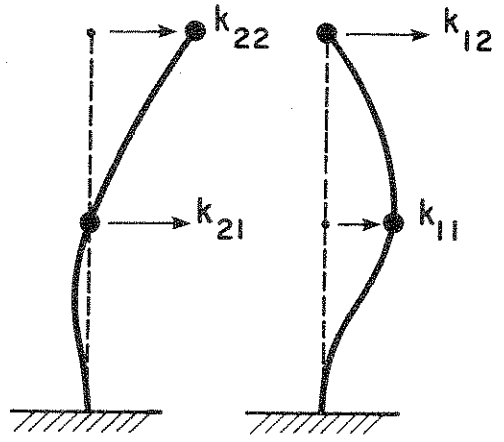

$$\mathbf{K} = \begin{bmatrix} 47.8 & -14.9 \\ -14.9 & 5.97 \end{bmatrix} \frac{\text{k}}{\text{in}}$$

$$\Phi = \begin{bmatrix} 1.00 & 1.00 \\ 2.95 & -0.51 \end{bmatrix} \qquad \omega = \begin{bmatrix} 14.54 \\ 81.59 \end{bmatrix} \frac{\text{rad}}{\text{sec}} \qquad \mathbf{T} = \begin{bmatrix} 0.432 \\ 0.077 \end{bmatrix} \text{sec}$$

Fig. 4.1 Two-Degree-of-Freedom Steel Specimen With Calculated Stiffness and Dynamic Characteristics

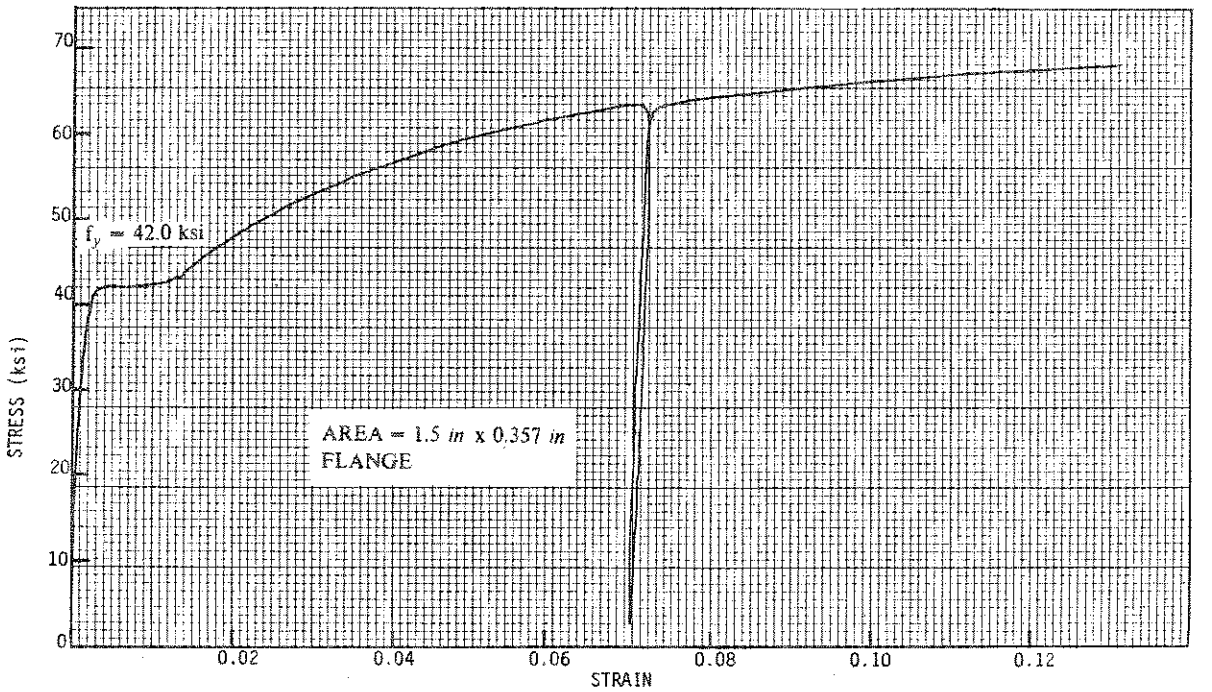

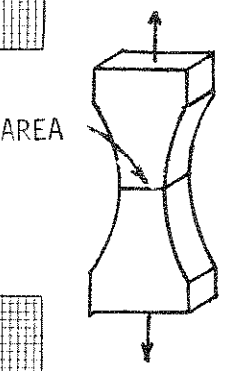

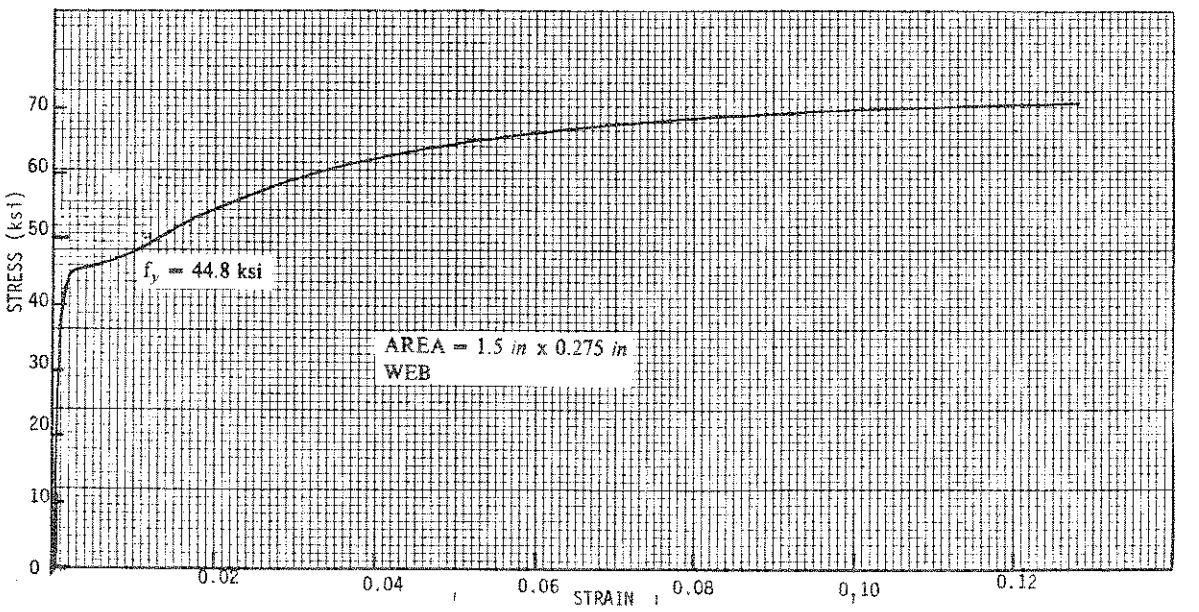

Fig. 4.2 Coupon Test Results

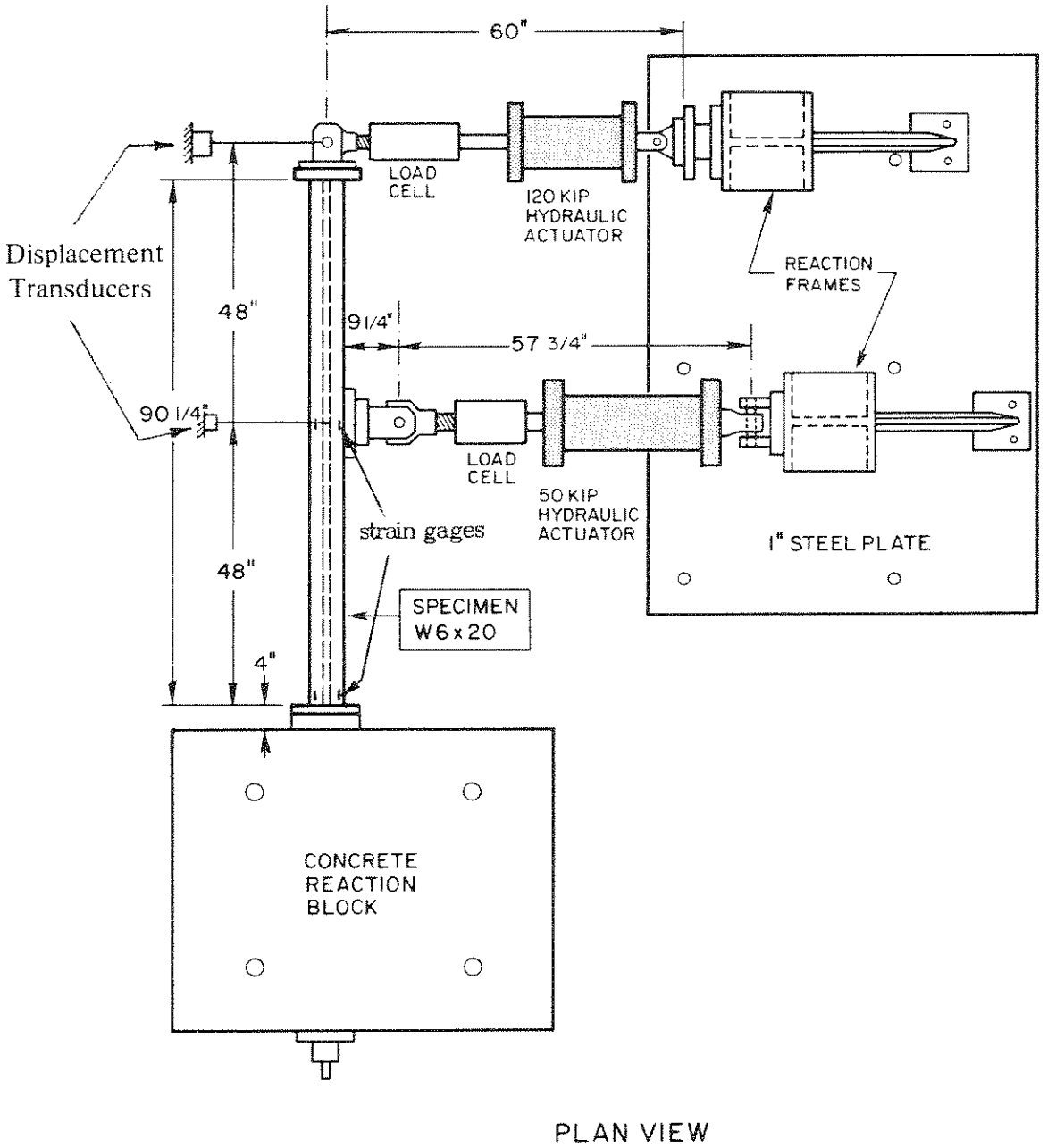

Fig. 4.3 Plan View of the Two-Degree-of-Freedom Test Layout

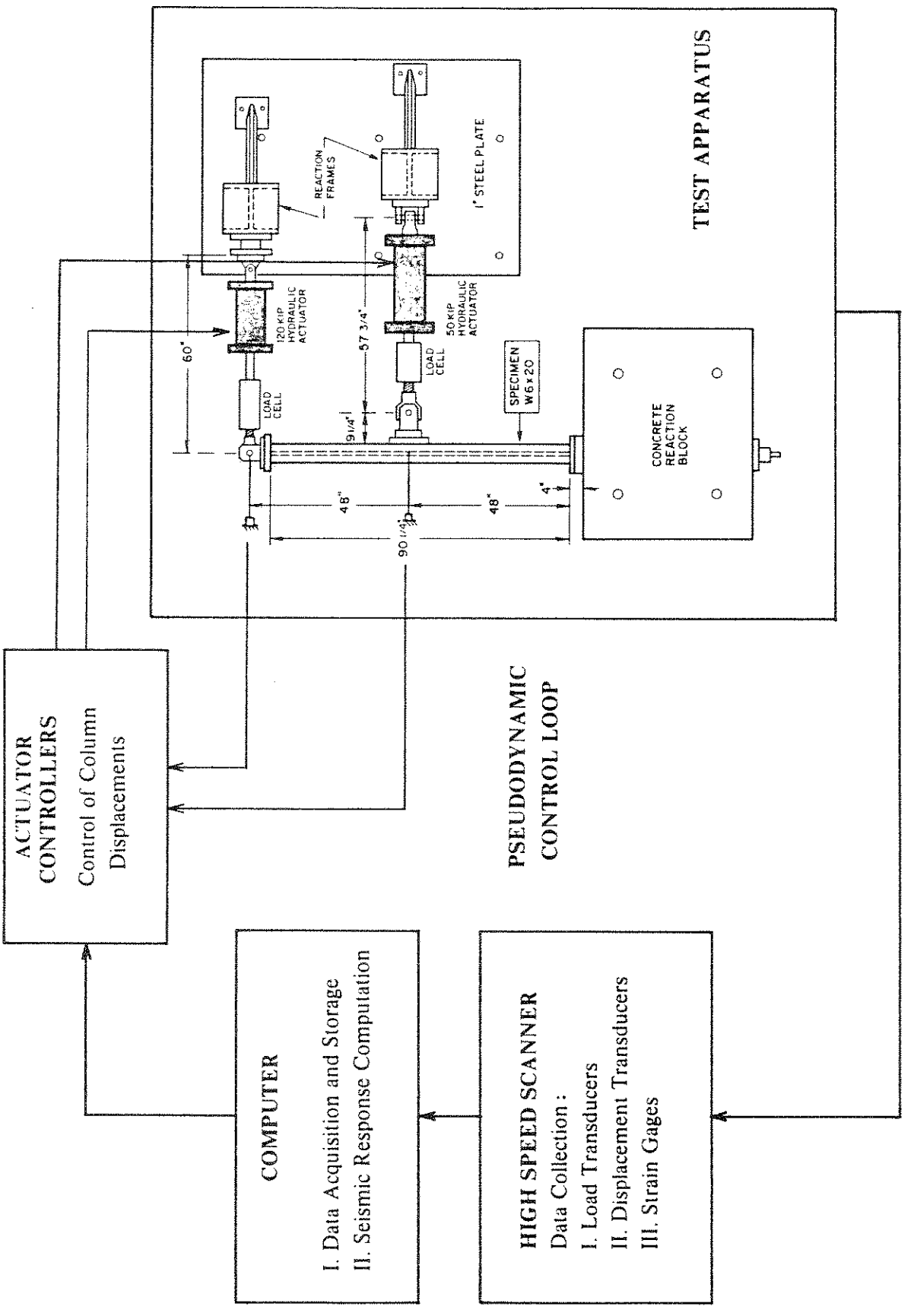

Fig. 4.4 Schematic of Pseudodynamic Control Loop

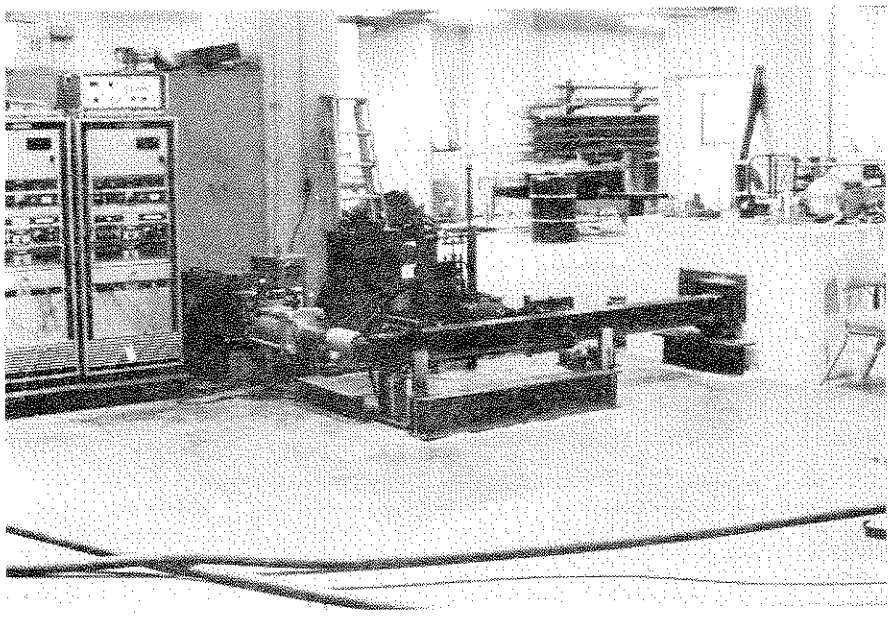

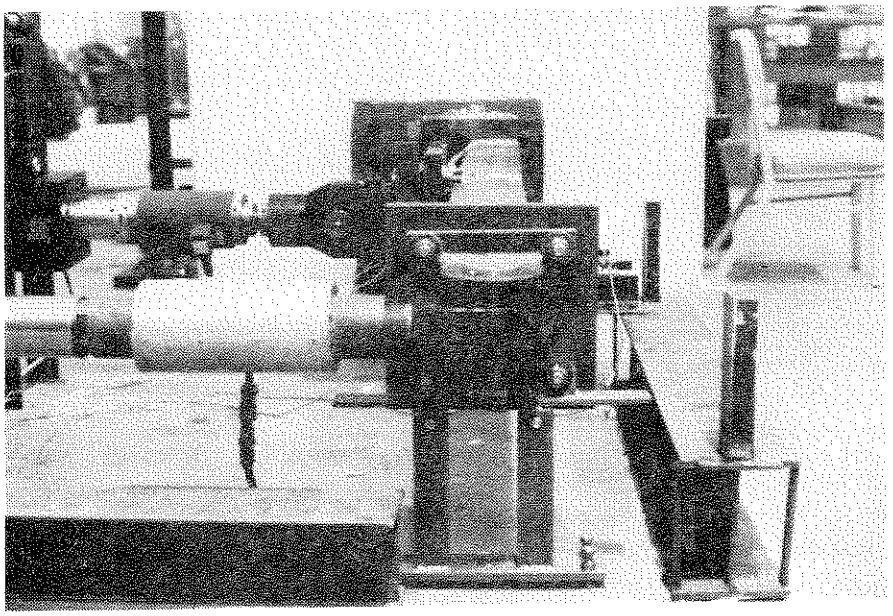

Fig. 4.5 Photographs of Pseudodynamic Test Setup and Instrumentation

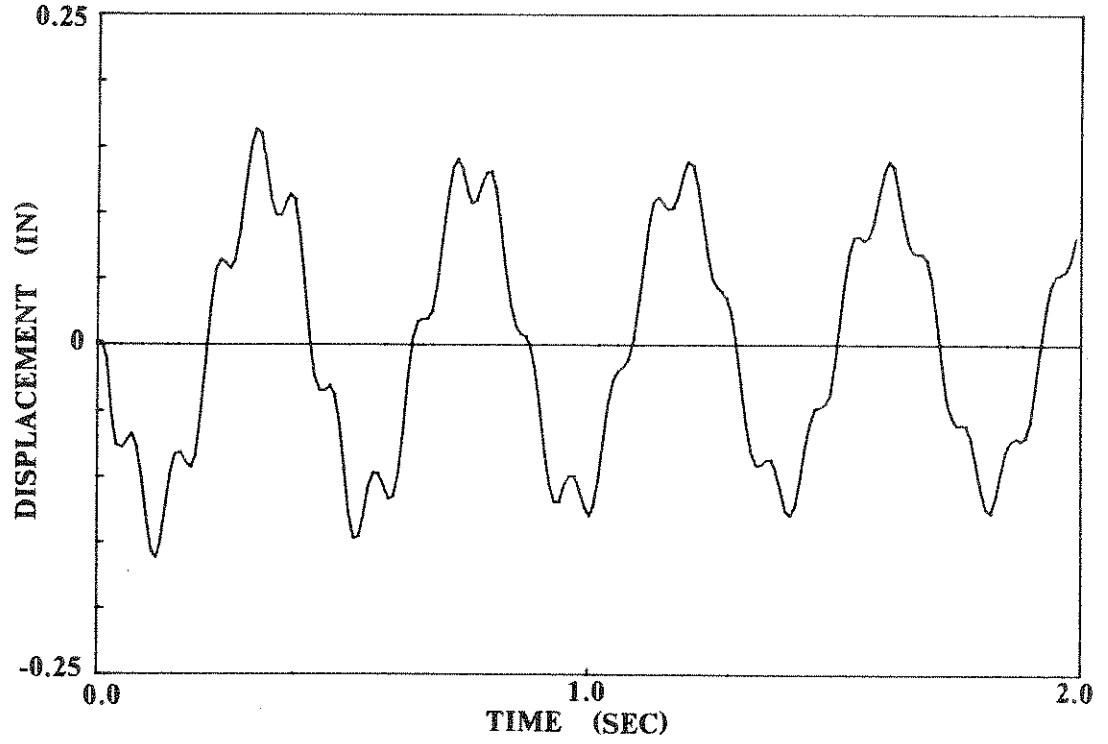

(a) Pseudodynamic Test

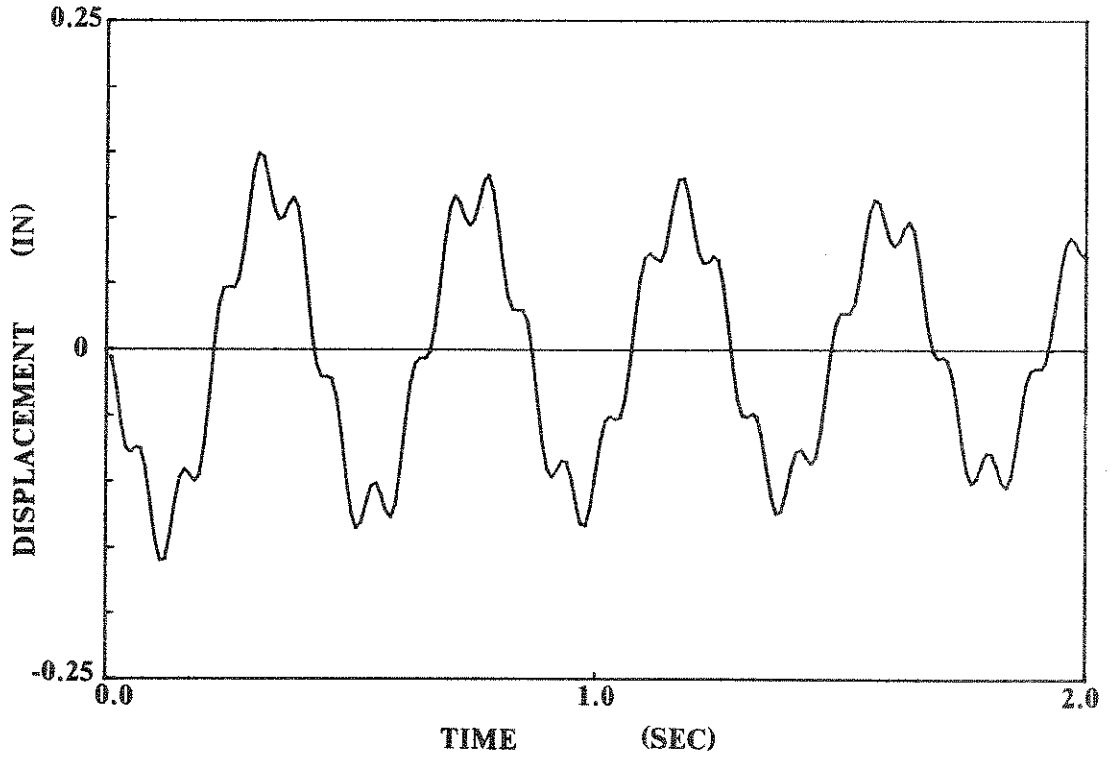

(b) Analytical Simulation

Fig. 4.6 Free Vibration Response of DOF1

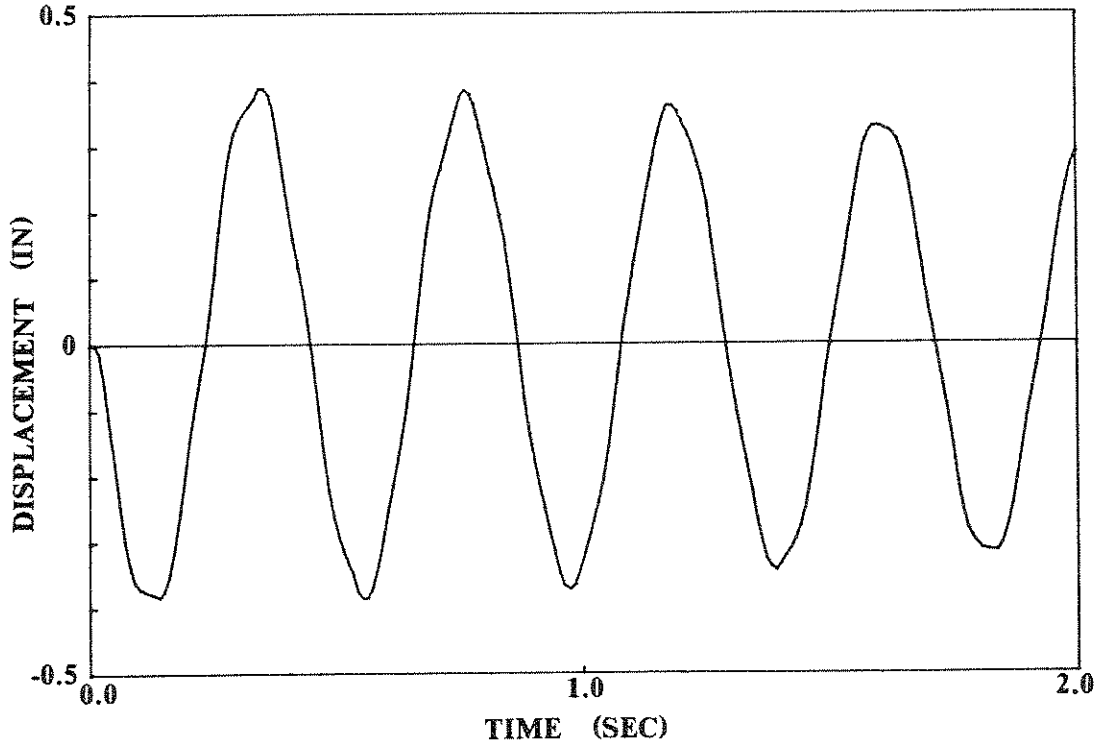

(a) Pseudodynamic Test

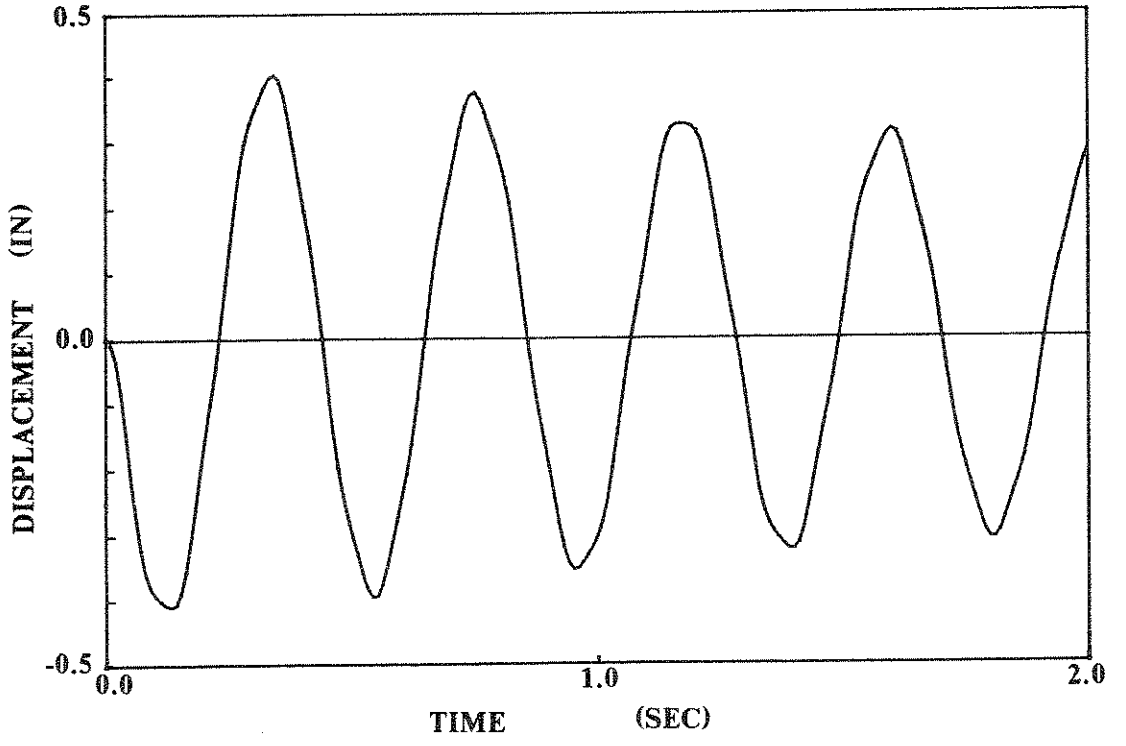

(b) Analytical Simulation

Fig. 4.7 Free Vibration Response of DOF2

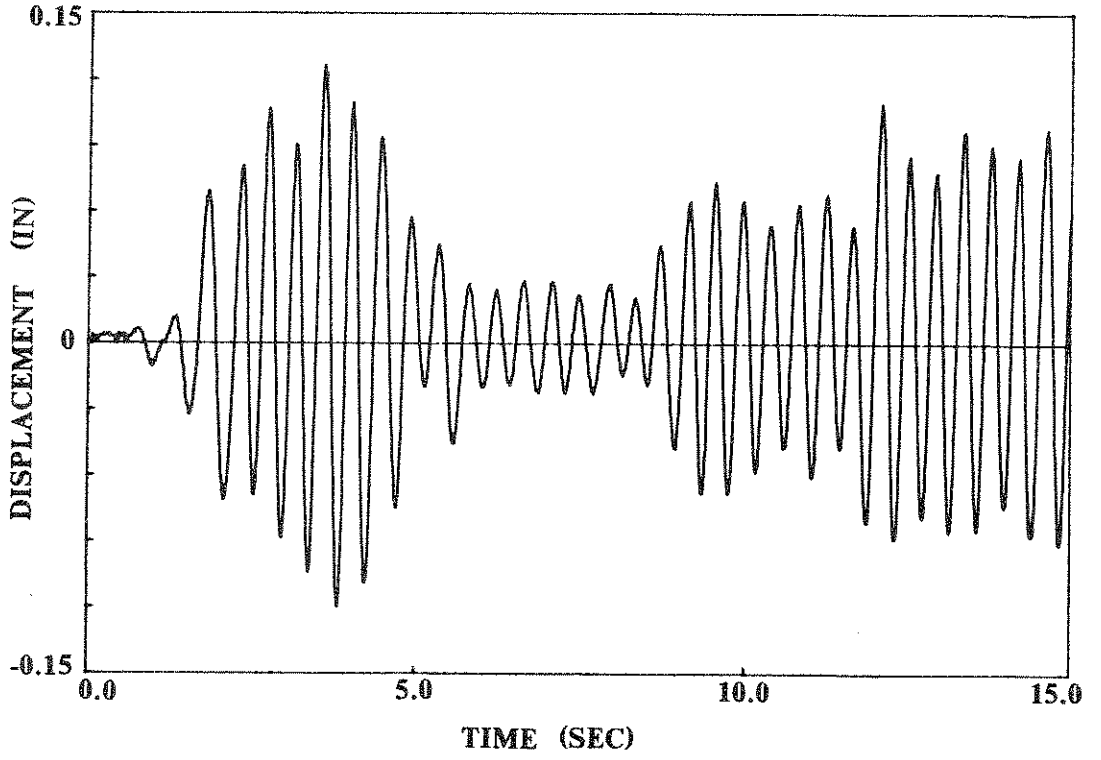

(a) Pseudodynamic Test

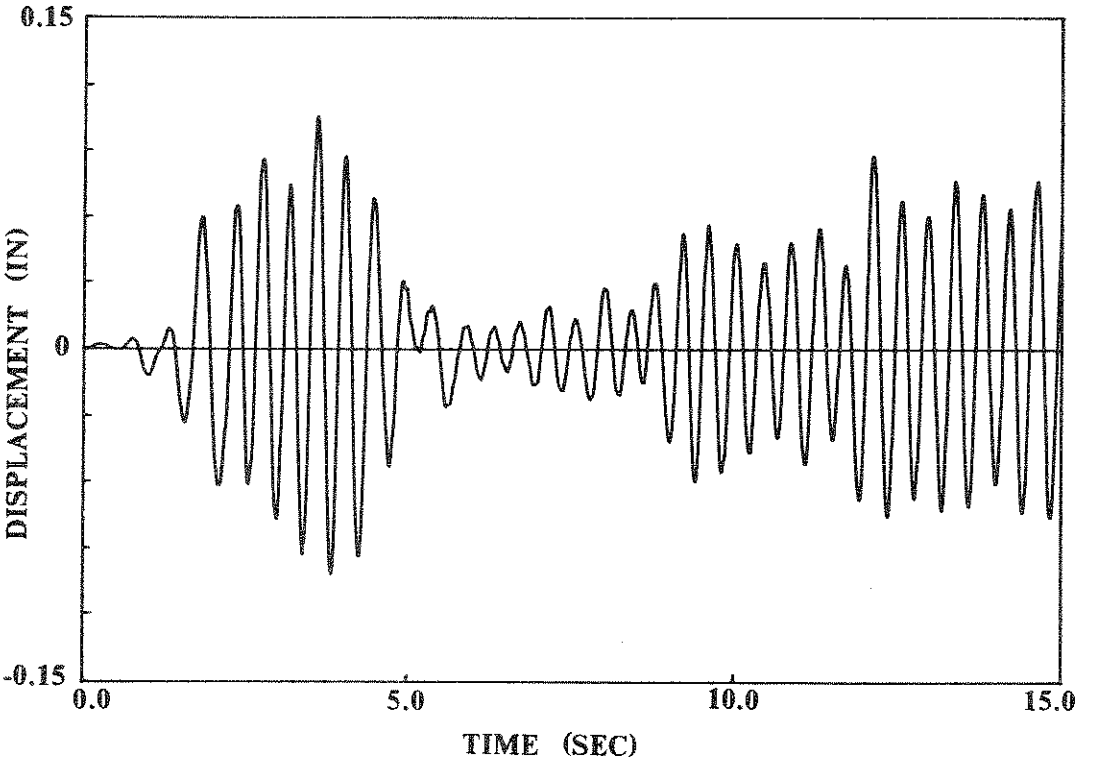

(b) Analytical Simulation

Fig. 4.8 Displacement Time History of DOF1
(El Centro 0.05g Ground Motion)

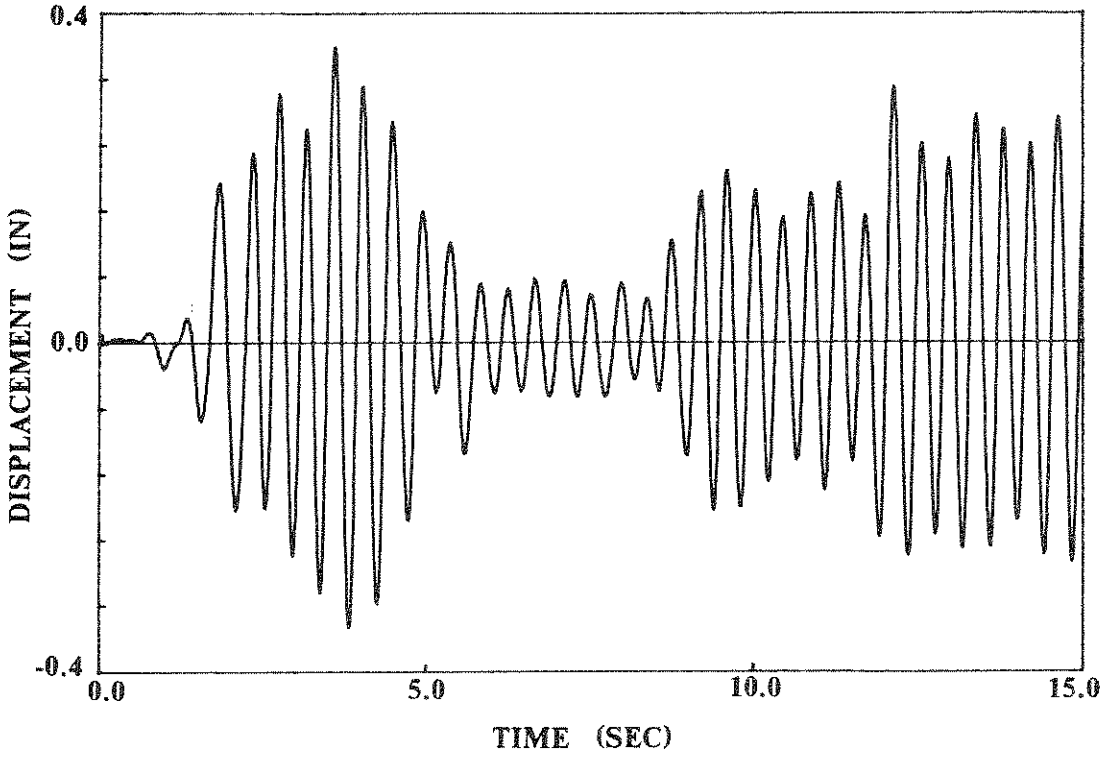

(a) Pseudodynamic Test

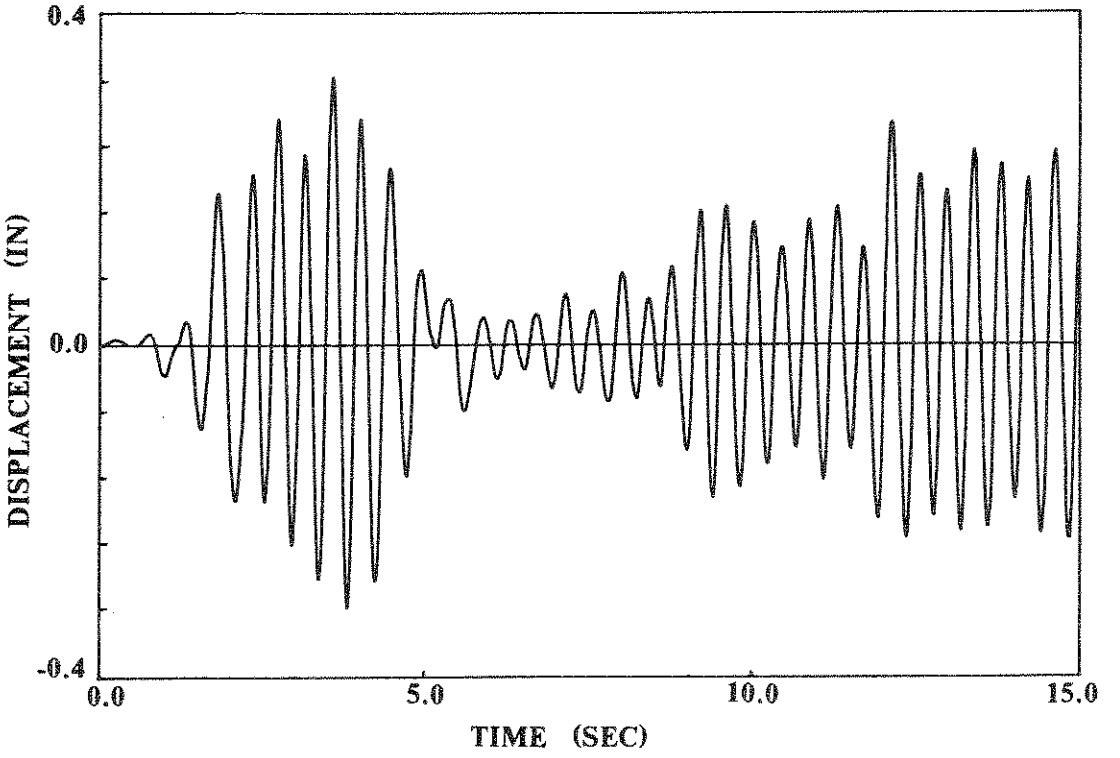

(b) Analytical Simulation

Fig. 4.9 Displacement Time History of DOF2
(El Centro 0.05g Ground Motion)

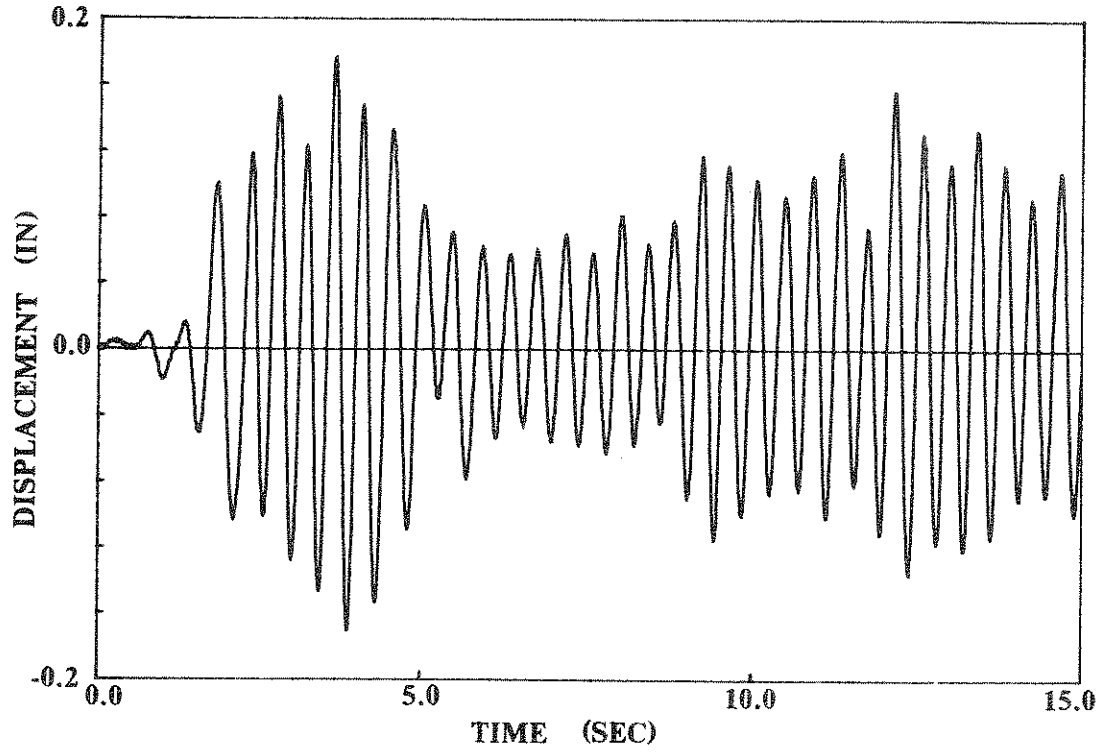

(a) Pseudodynamic Test

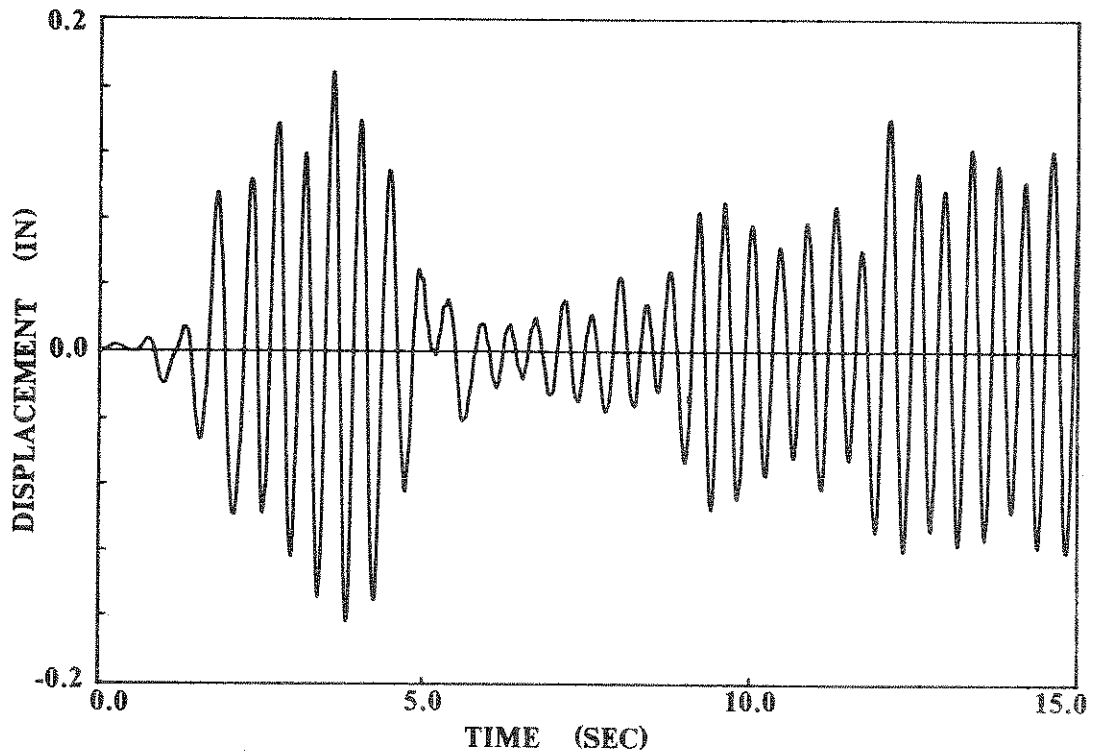

(b) Analytical Simulation

Fig. 4.10 Displacement Time History of DOF1
(El Centro 0.08g Ground Motion)

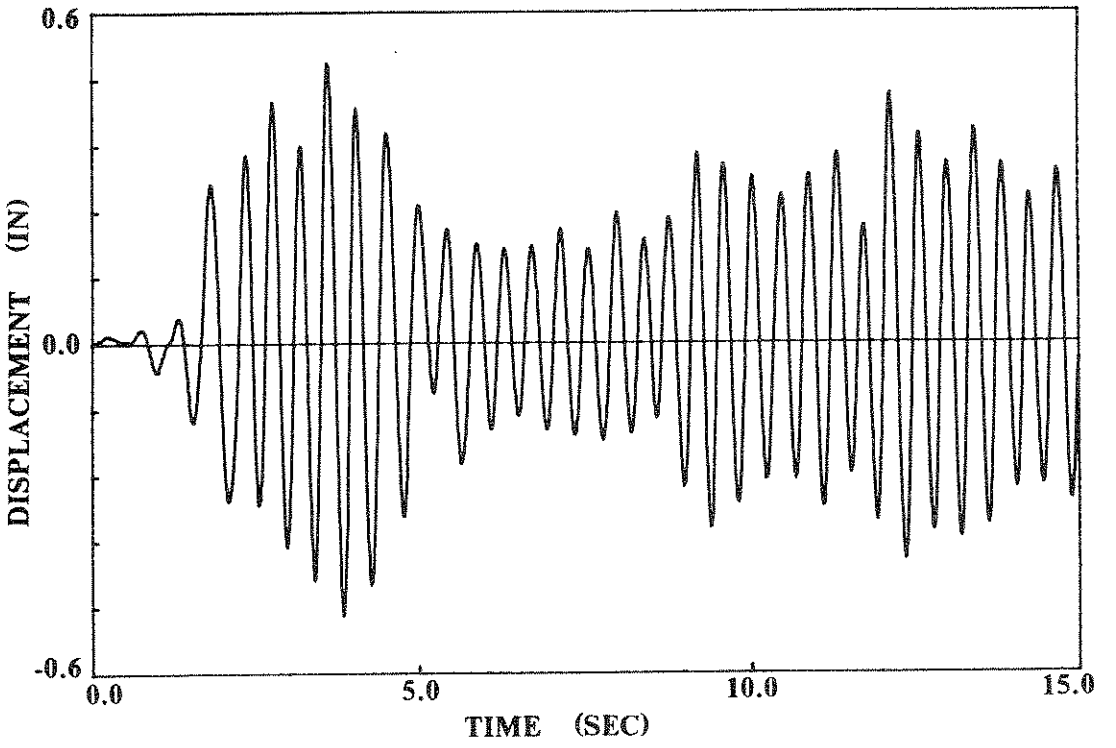

(a) Pseudodynamic Test

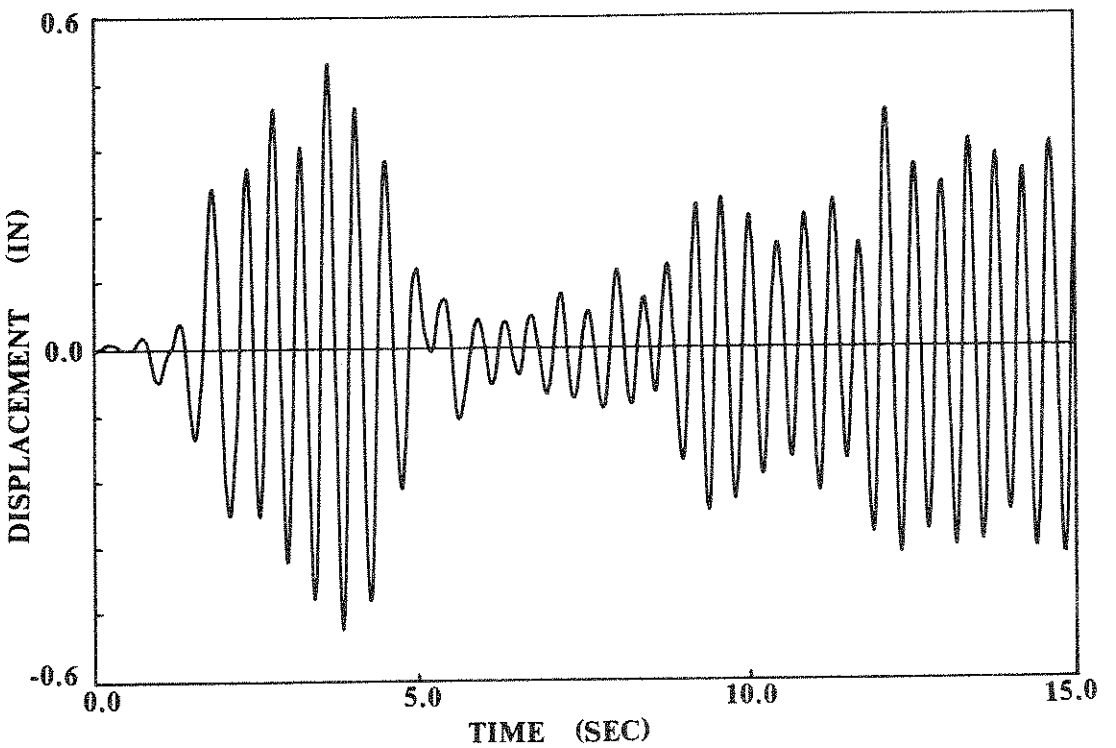

(b) Analytical Simulation

Fig. 4.11 Displacement Time History of DOF2
(El Centro 0.08g Ground Motion)

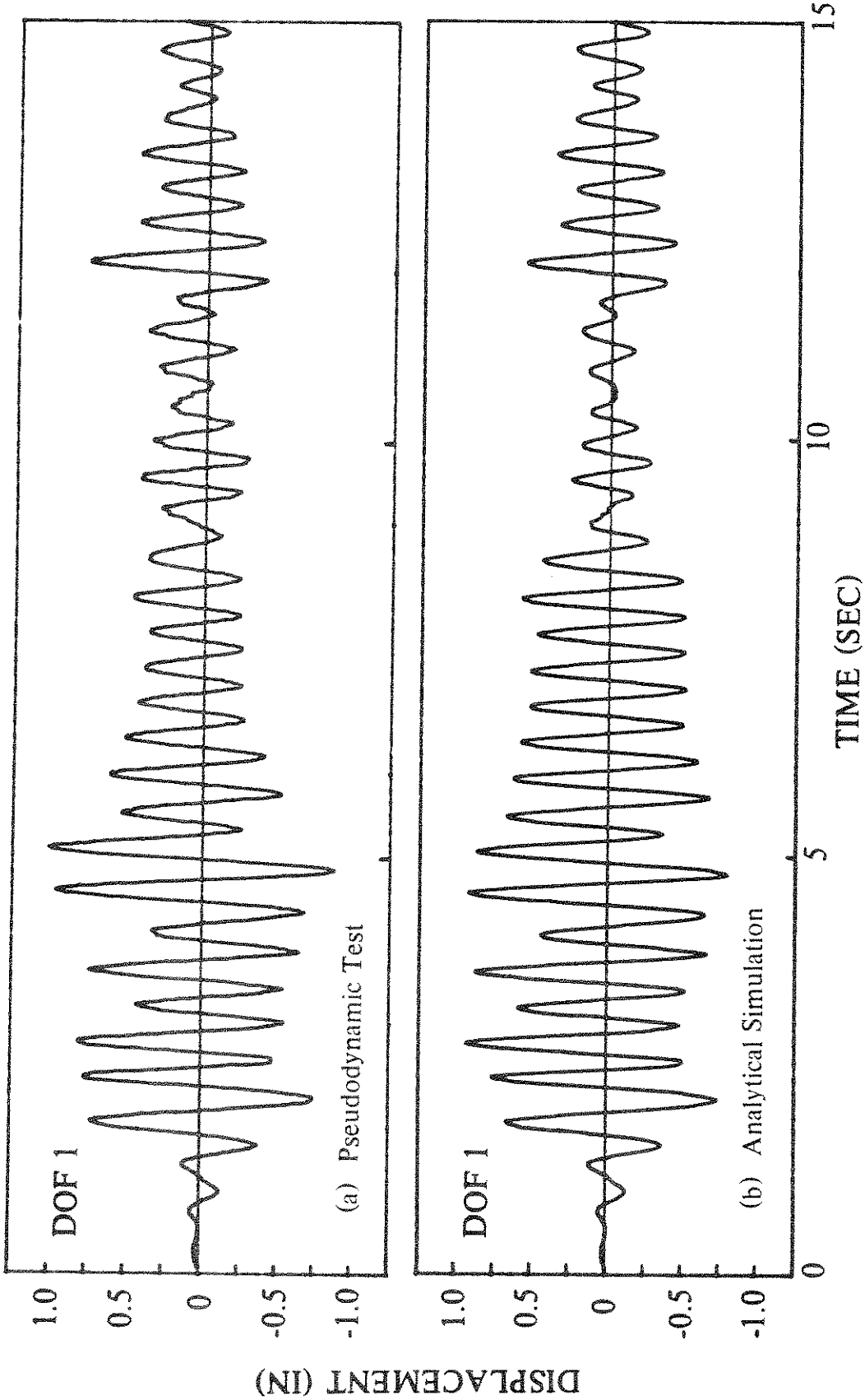

Fig. 4.12 Displacement Time History of DOF1 (El Centro 0.5g Ground Motion)

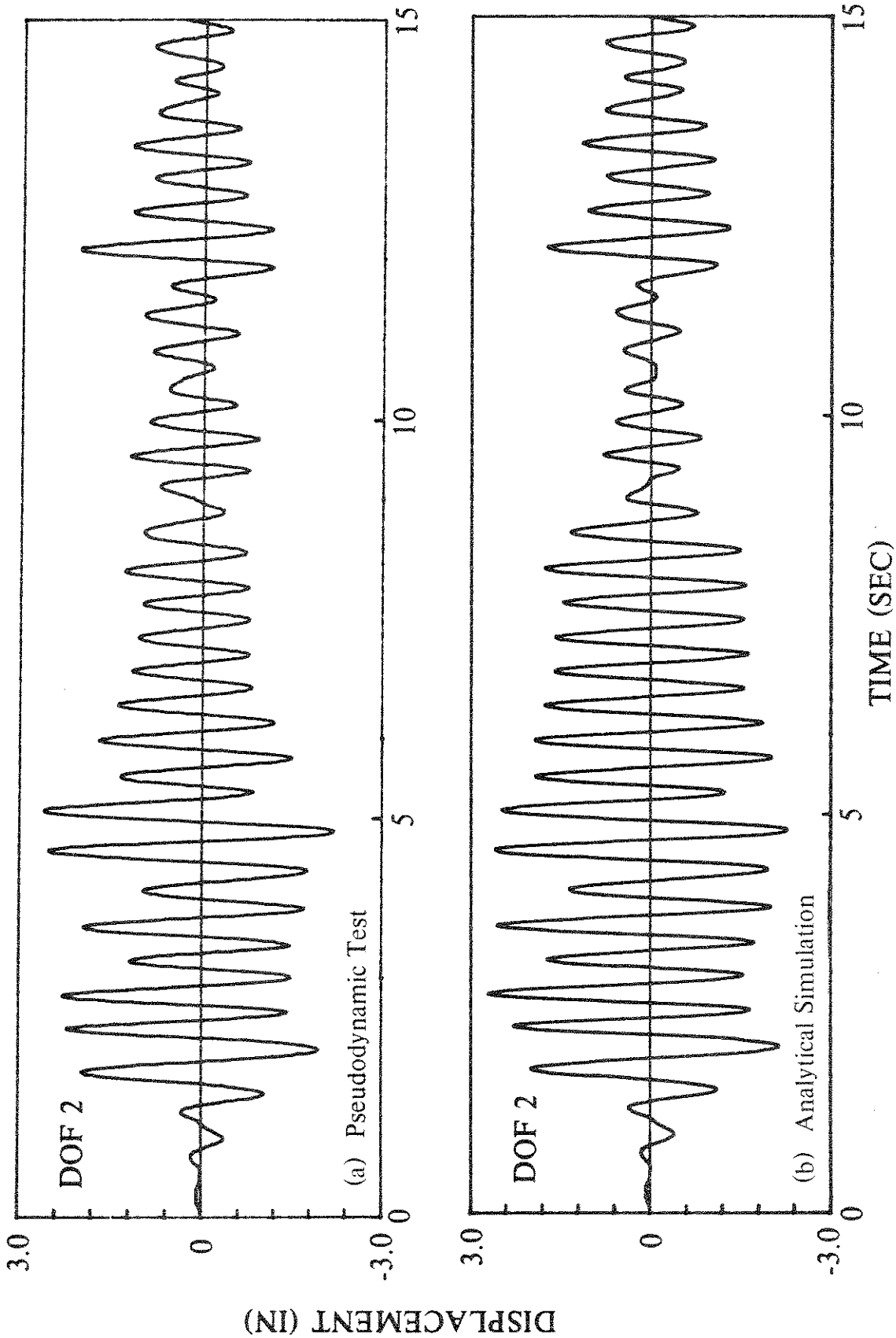

Fig. 4.13 Displacement Time History of DOF2 (El Centro 0.5g Ground Motion)

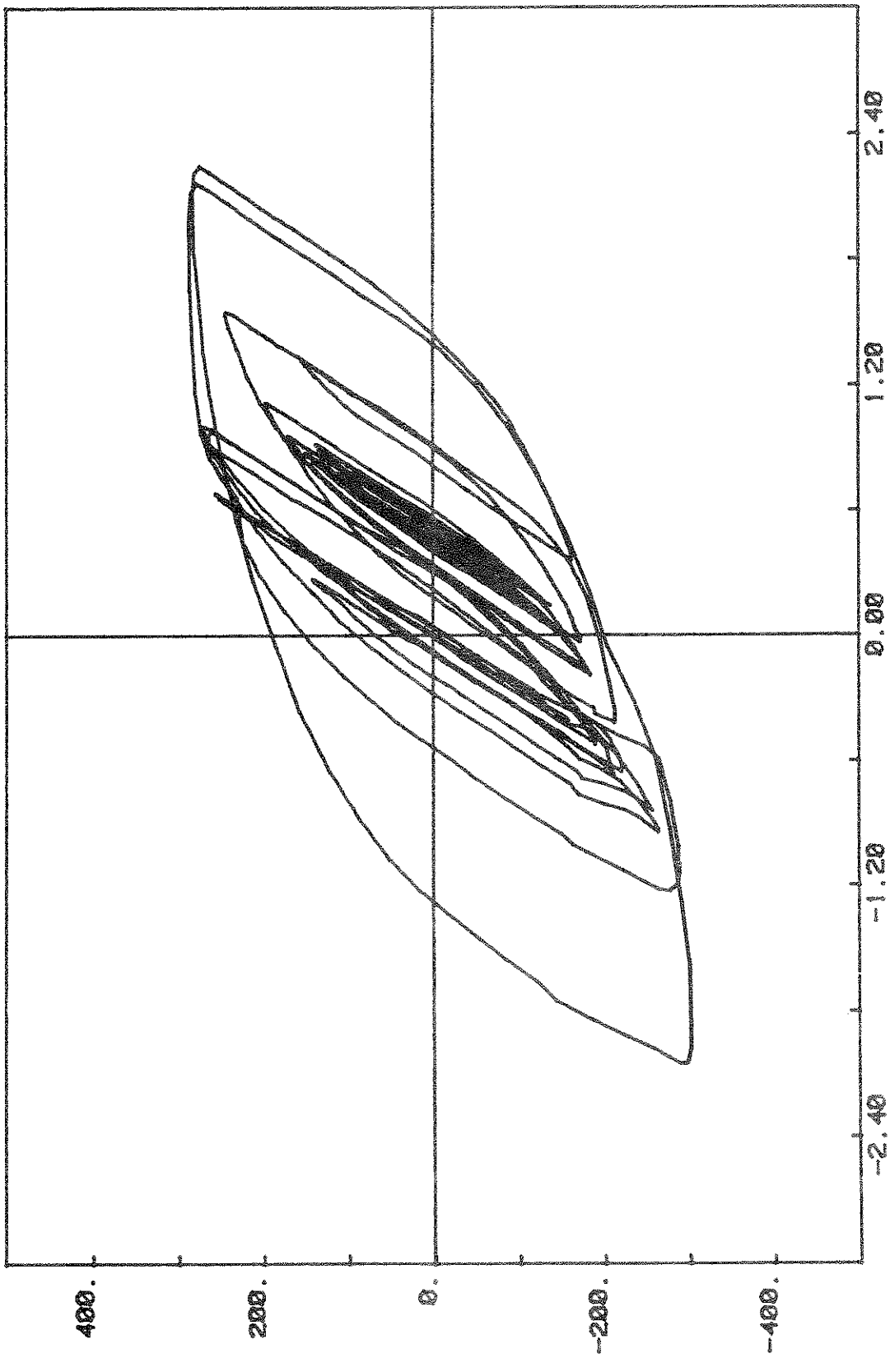

Fig. 4.14 Overturning Moment-Curvature Hysteretic Relation at the Support of the Column

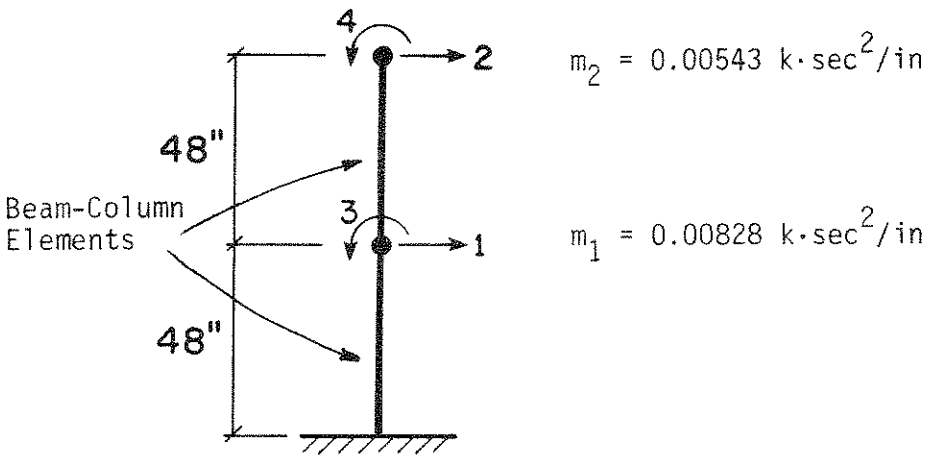

Fig. 4.15 Analytical Model for Elastic Response of the Two-Degree-of-Freedom System

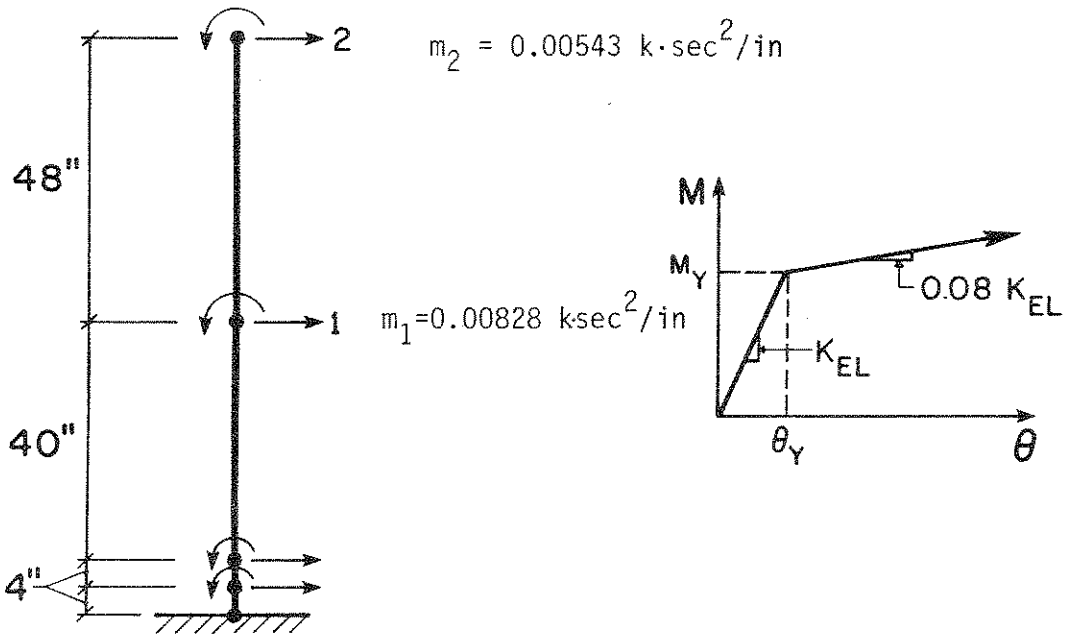

Fig. 4.16 Analytical Model for Inelastic Response of the Two-Degree-of-Freedom System

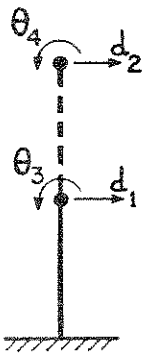

Fig. 5.1 Two Degree-of-Freedom Substructured Model

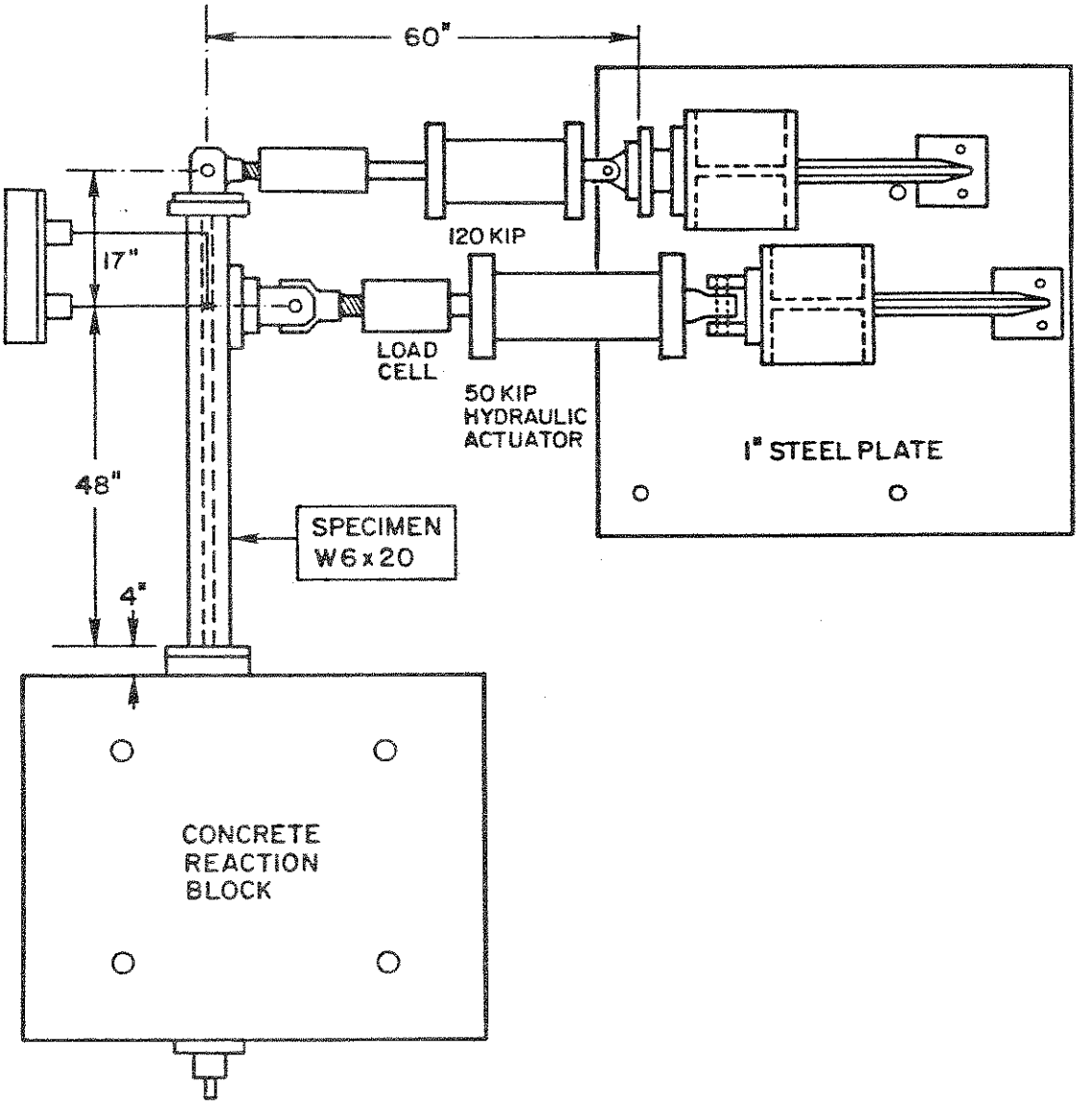

Fig. 5.2 Test Layout of Two-Degree-of-Freedom System with Substructuring (Compare with Fig. 4.3)

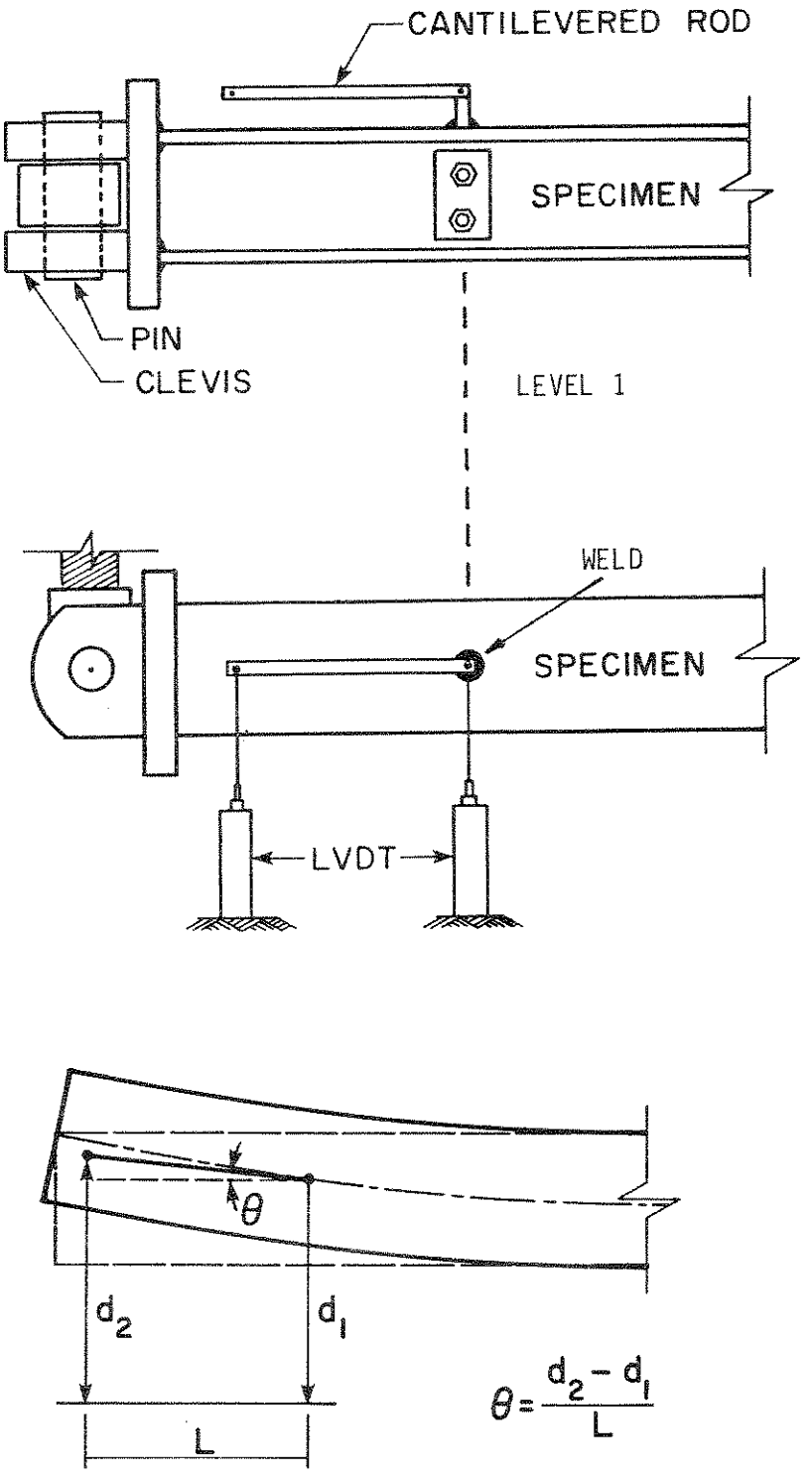

Fig. 5.3 Special Detail for Displacement and Rotation Measurement of First Level

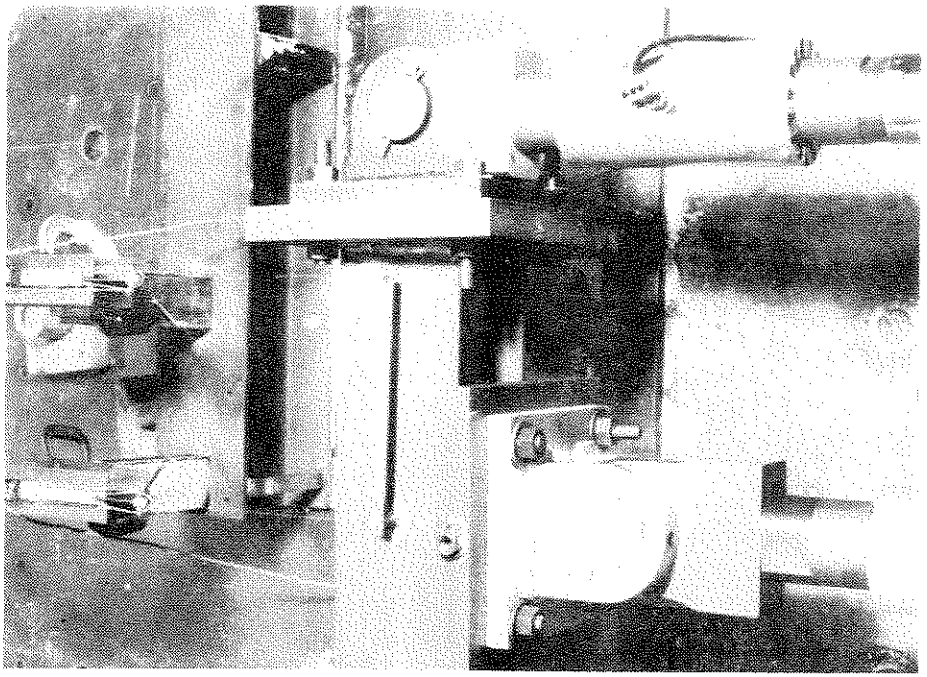

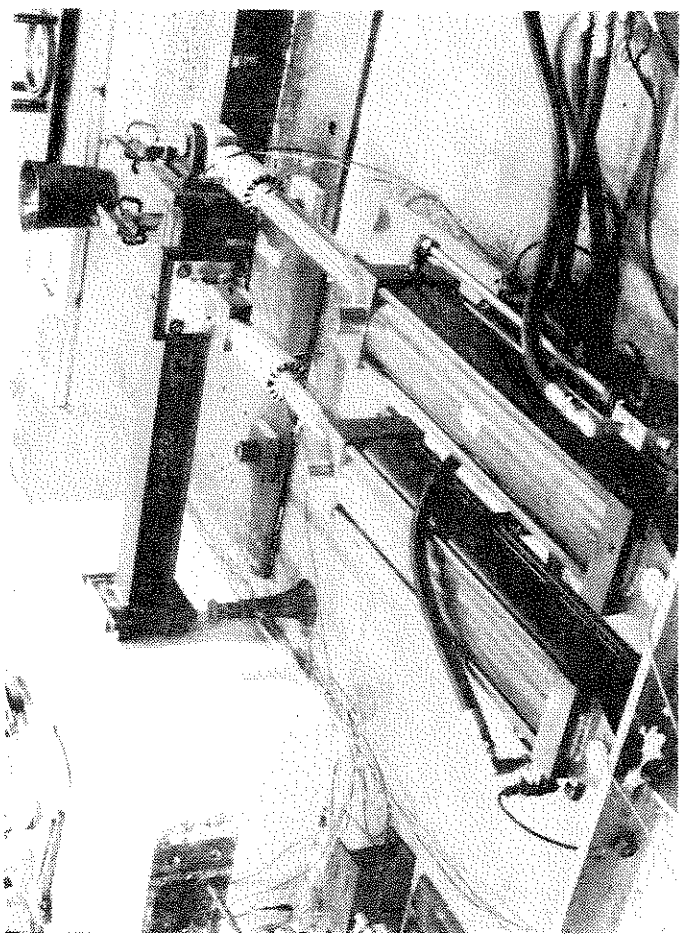

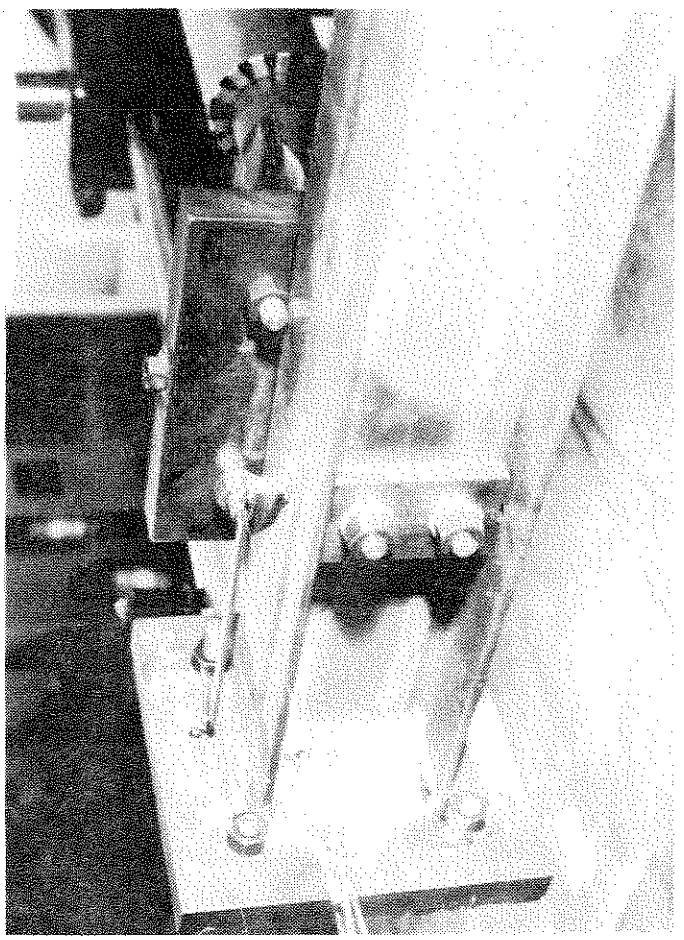

Fig. 5.4 Photographs of Pseudodynamic Test Setup and Instrumentation

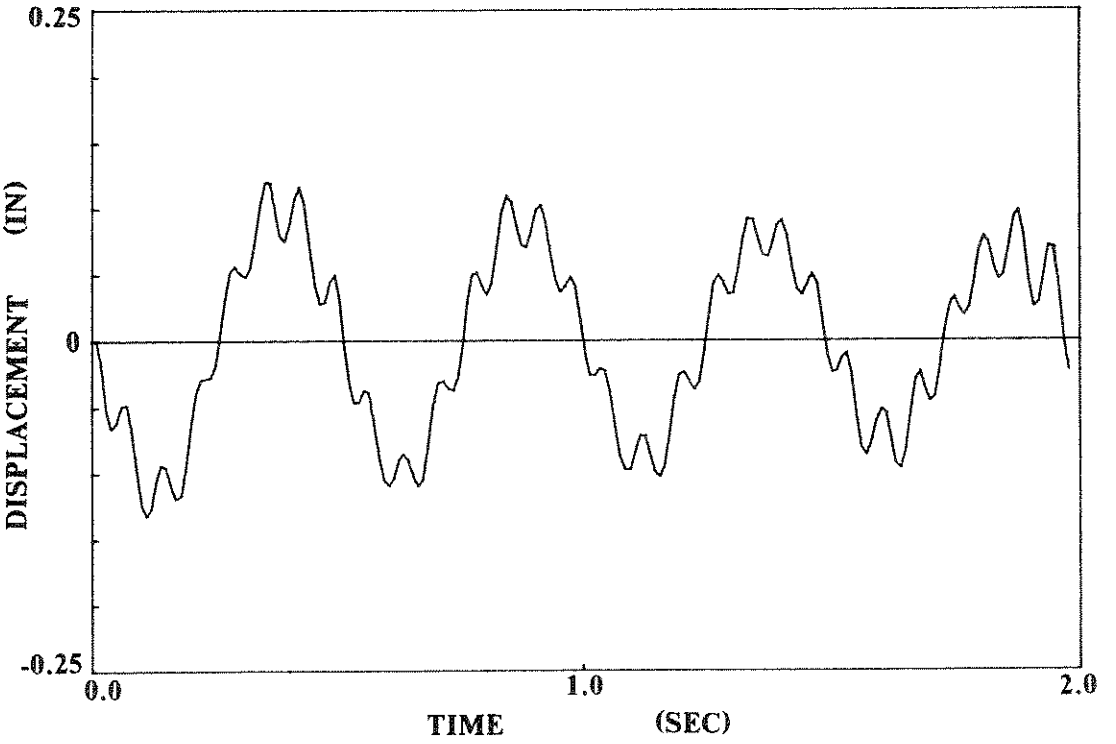

(a) Pseudodynamic Test

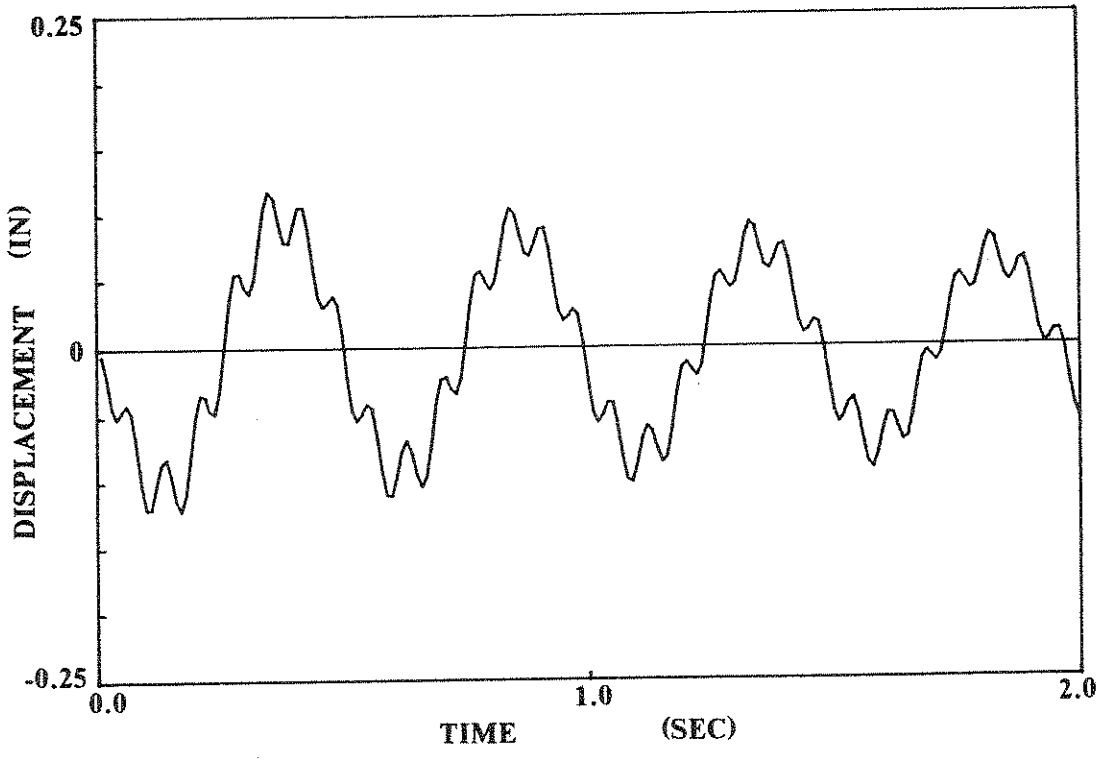

(b) Analytical Simulation

Fig. 5.5 Free Vibration Response of First Level

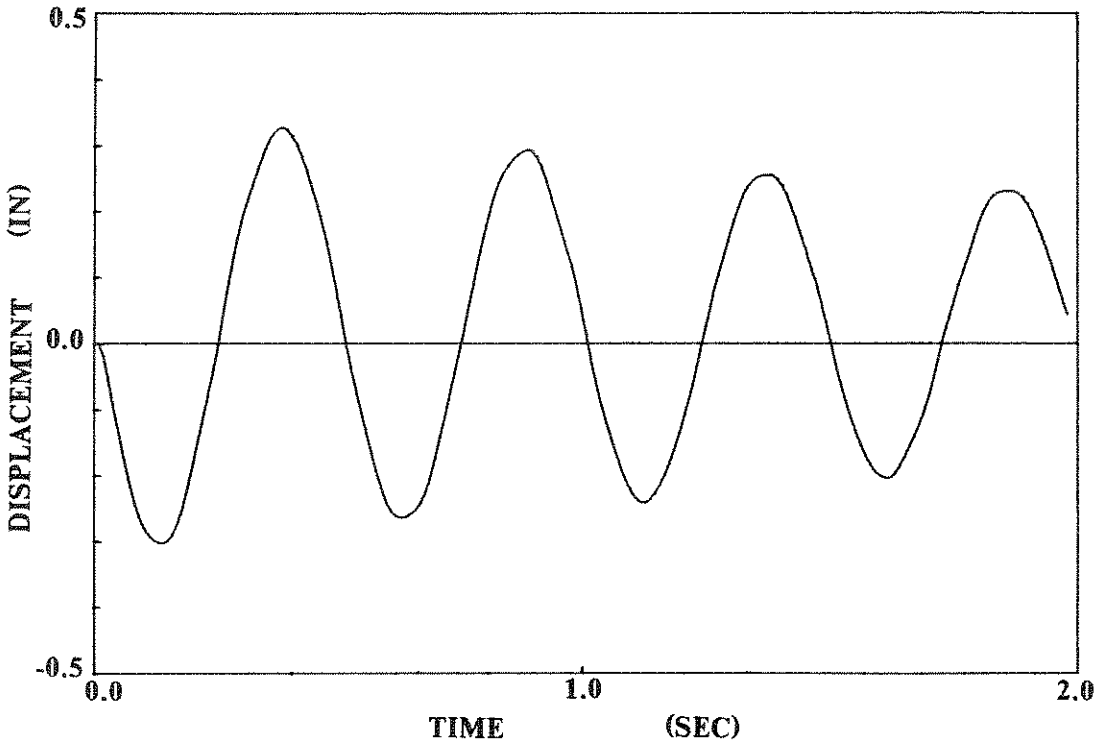

(a) Pseudodynamic Test

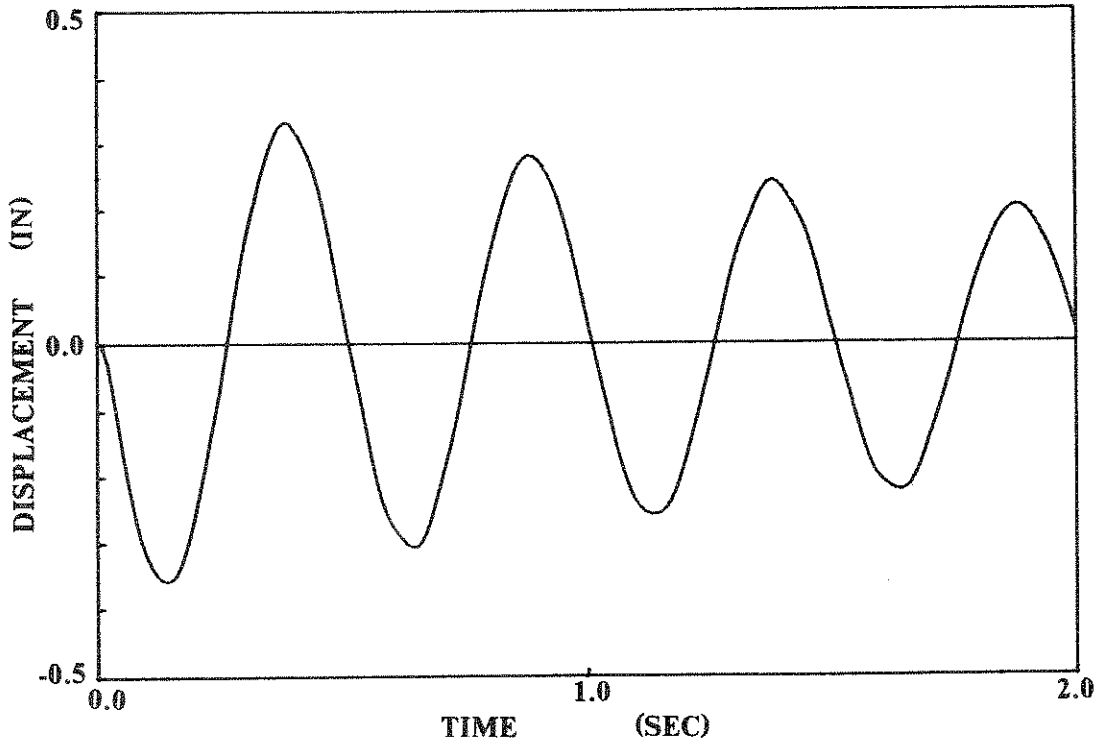

(b) Analytical Simulation

Fig. 5.6 Free Vibration Response of Second Level

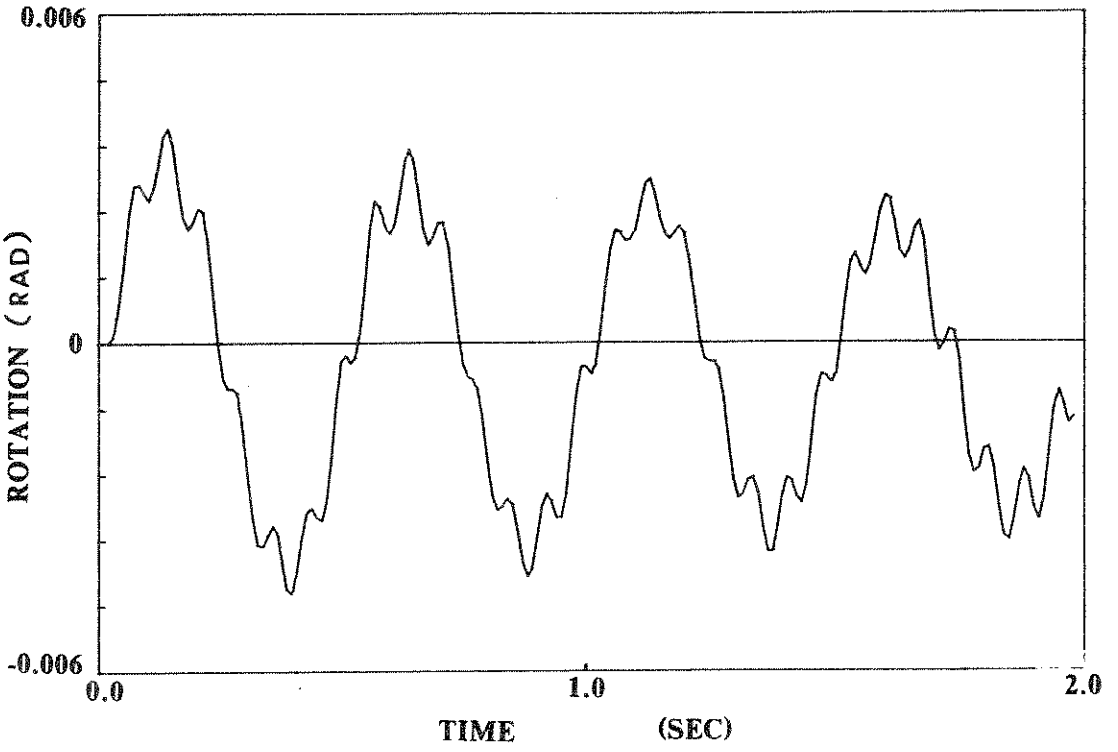

(a) Pseudodynamic Test

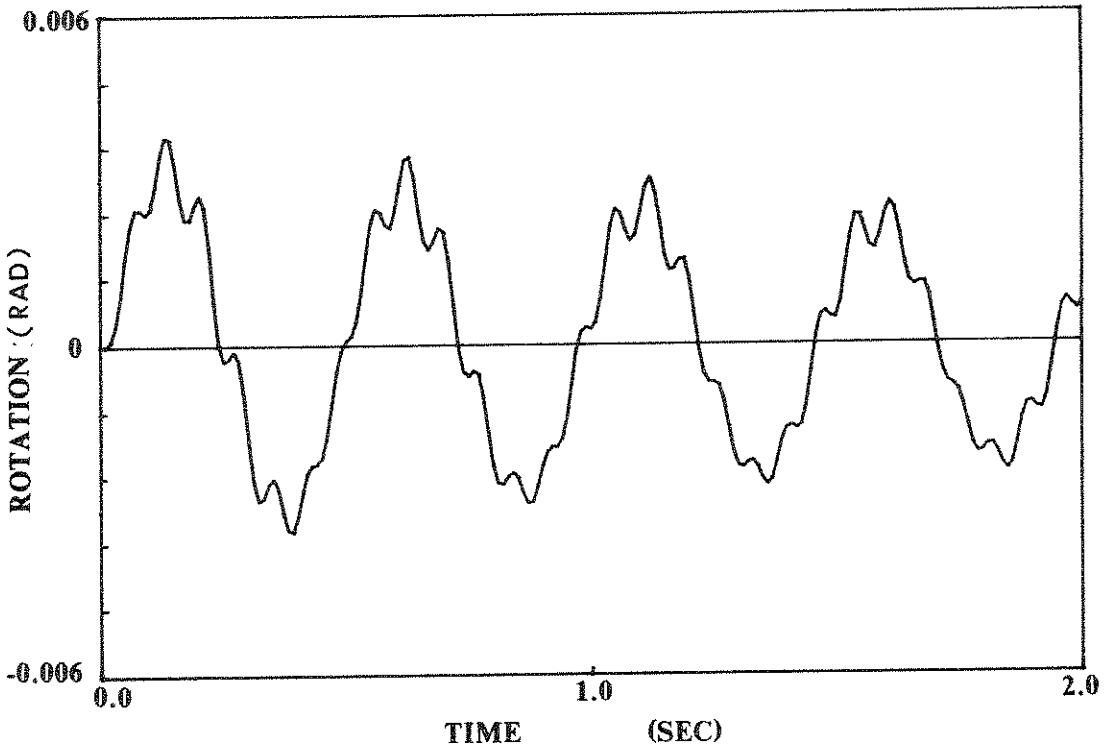

(b) Analytical Simulation

Fig. 5.7 Time History of Rotation of First Level
(Free Vibration Test)

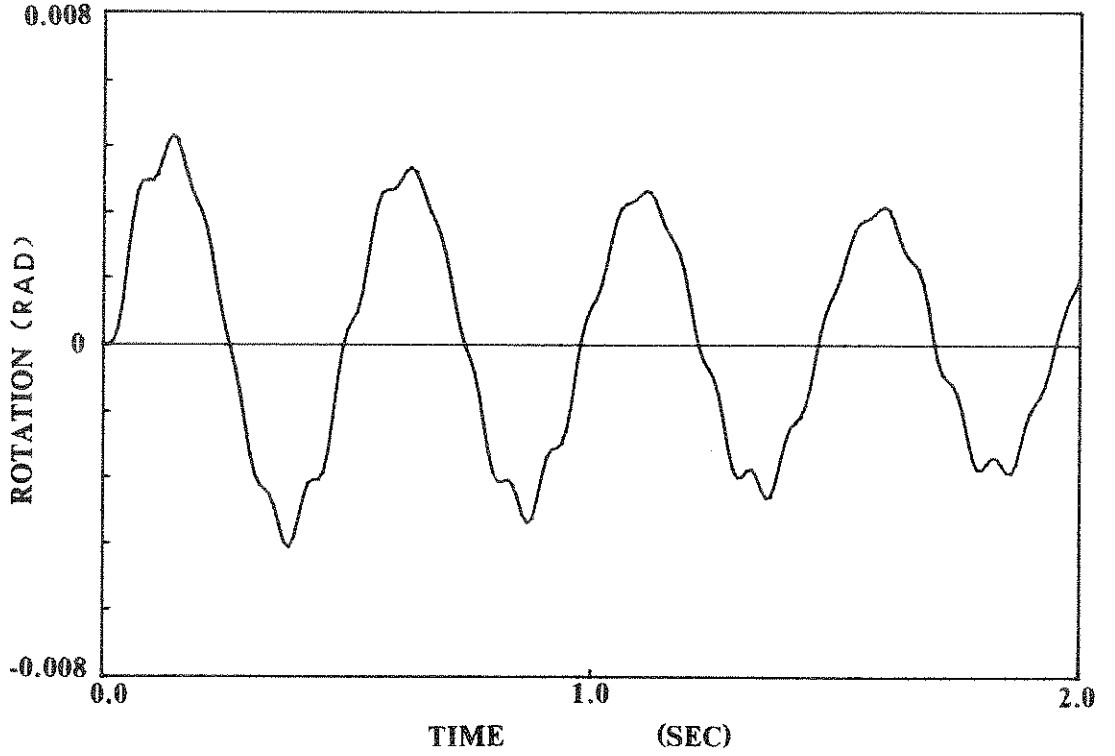

(a) Pseudodynamic Test

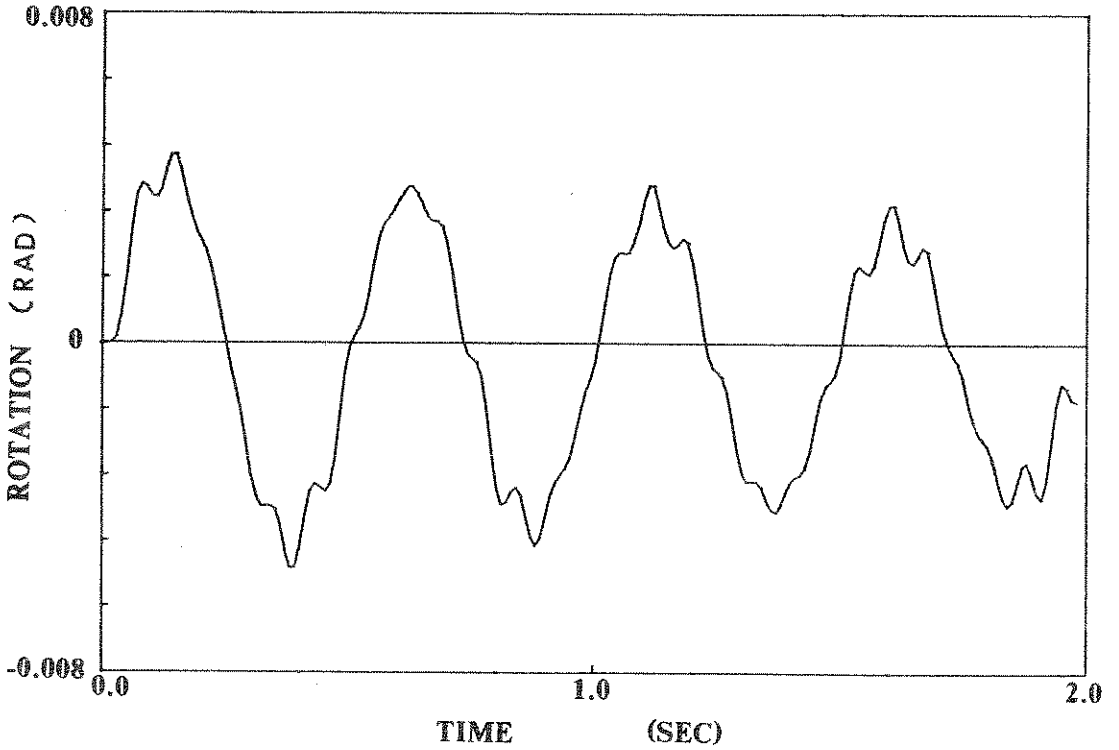

(b) Analytical Simulation

Fig. 5.8 Time History of Rotation of Second Level
(Free Vibration Test)

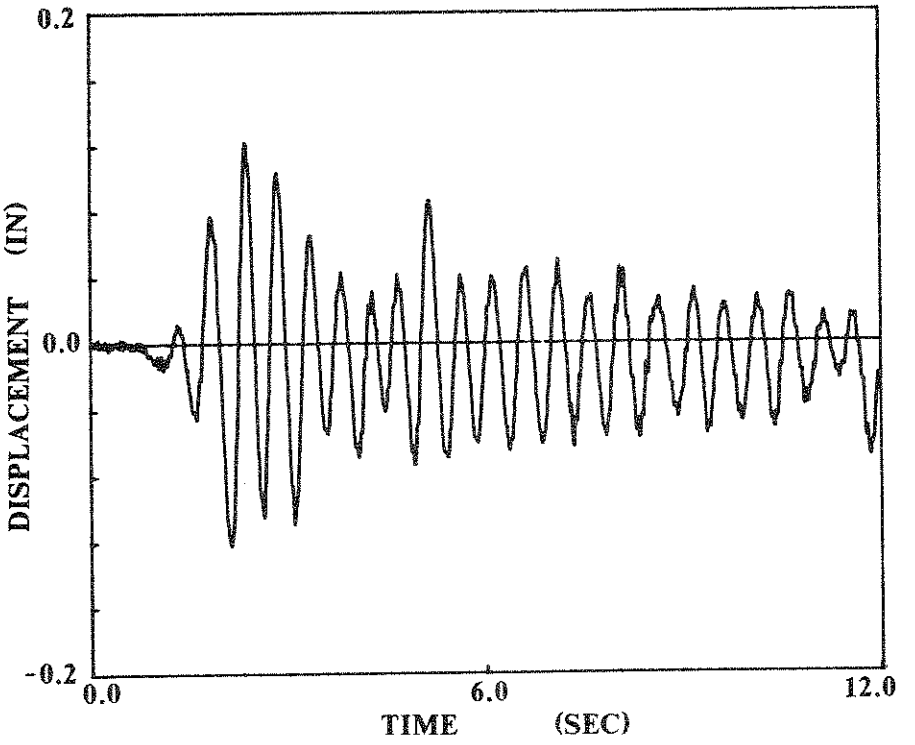

(a) Pseudodynamic Test

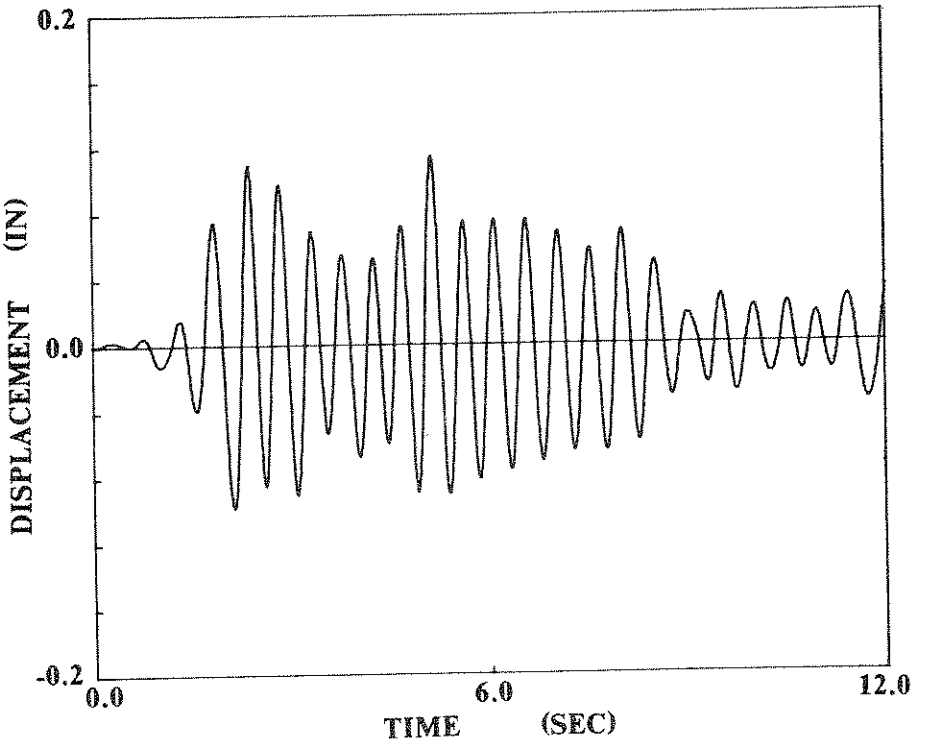

(b) Analytical Simulation

Fig. 5.9 Displacement Time History of First Level
(El Centro 0.05g Ground Motion)

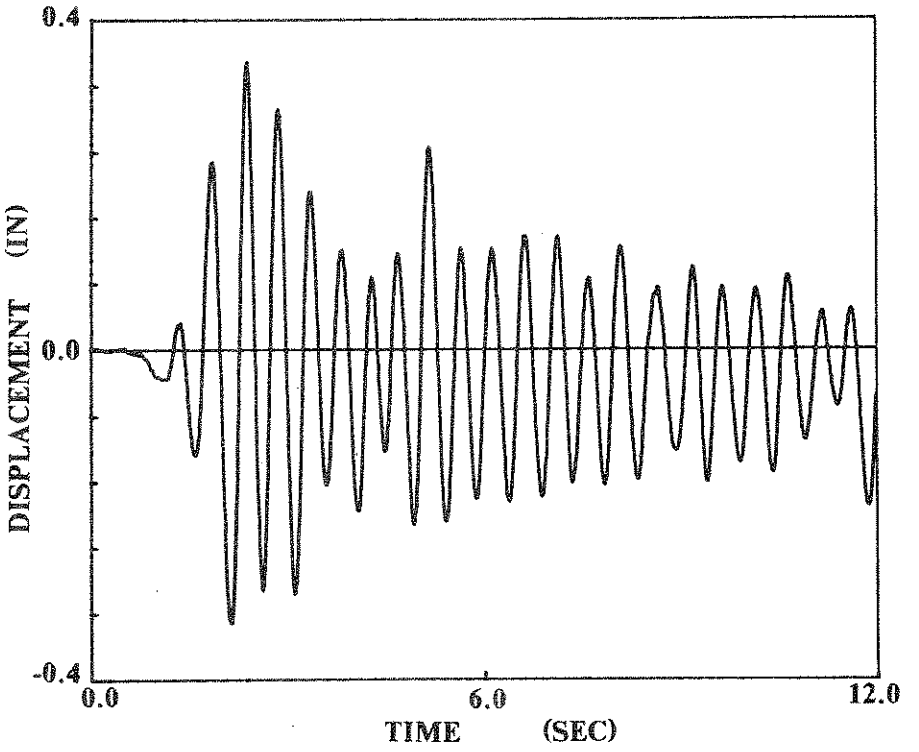

(a) Pseudodynamic Test

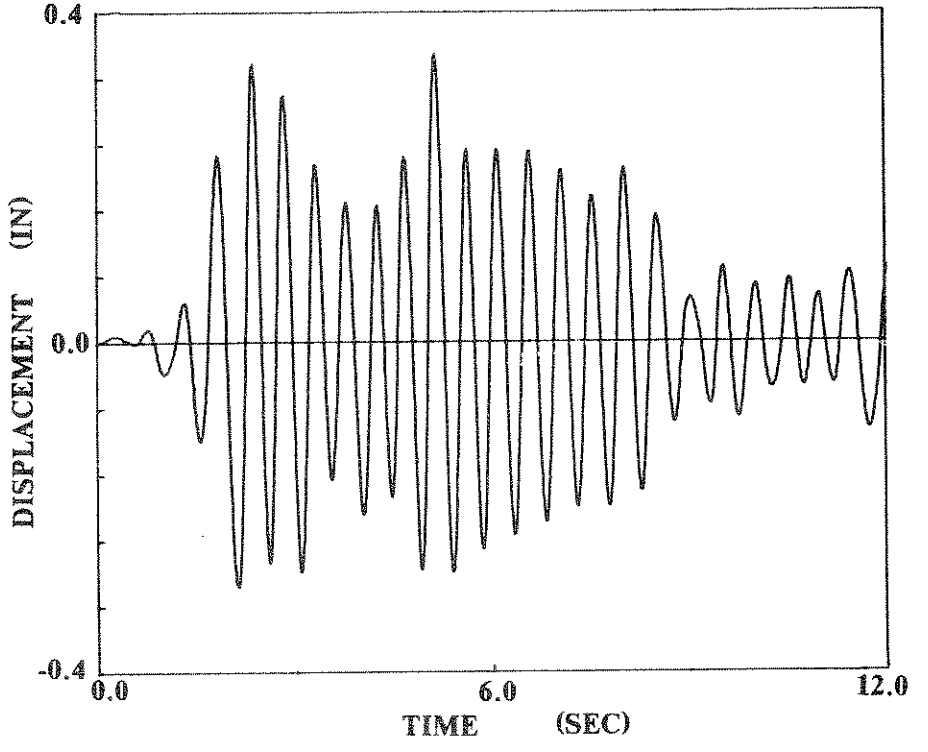

(b) Analytical Simulation

Fig. 5.10 Displacement Time History of Second Level
(El Centro 0.05g Ground Motion)

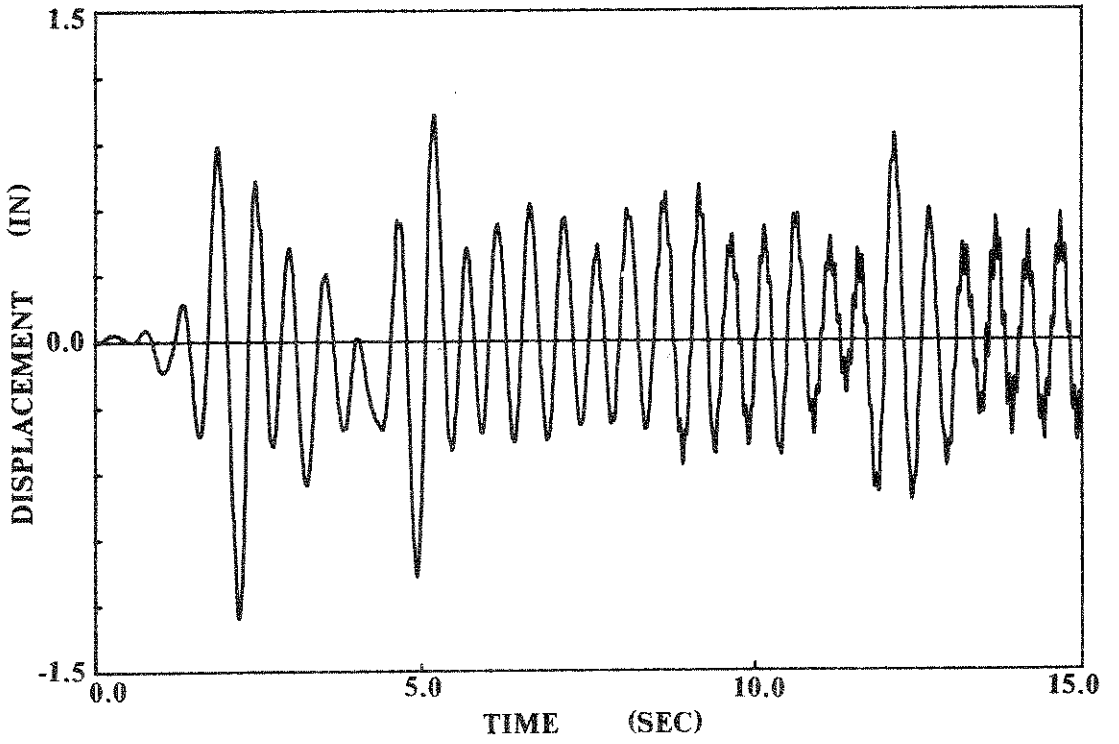

(a) Pseudodynamic Test

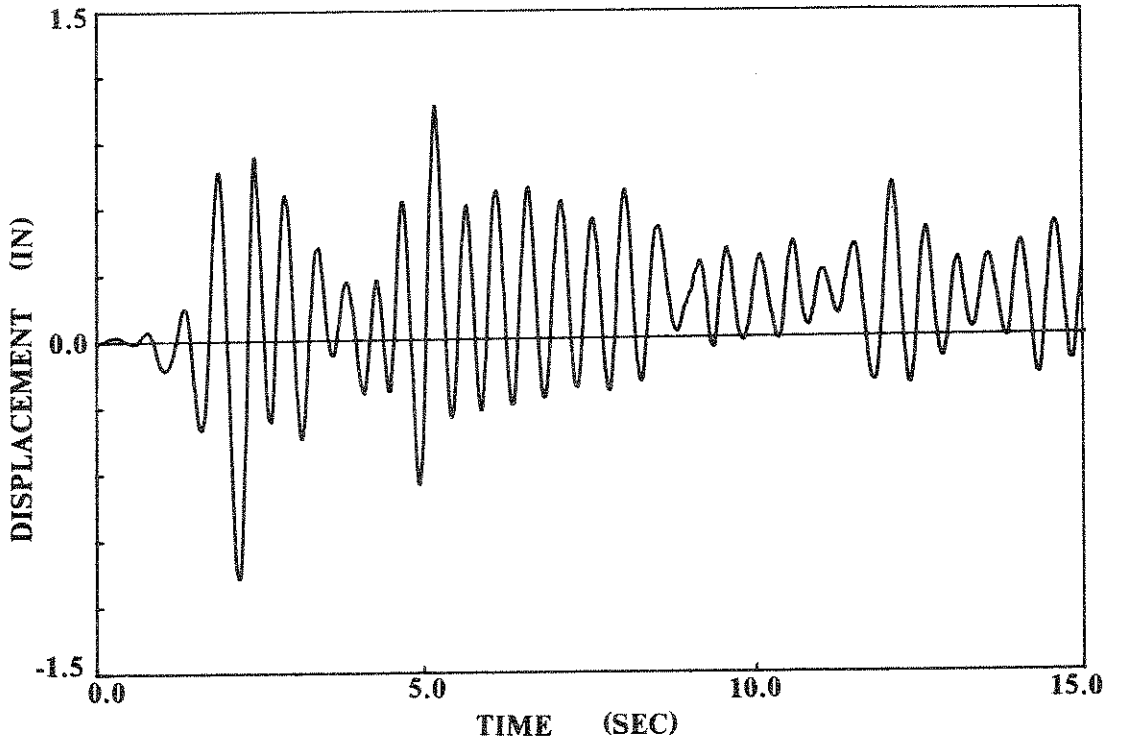

(b) Analytical Simulation

Fig. 5.11 Displacement Time History of First Level
(El Centro 0.5g Ground Motion)

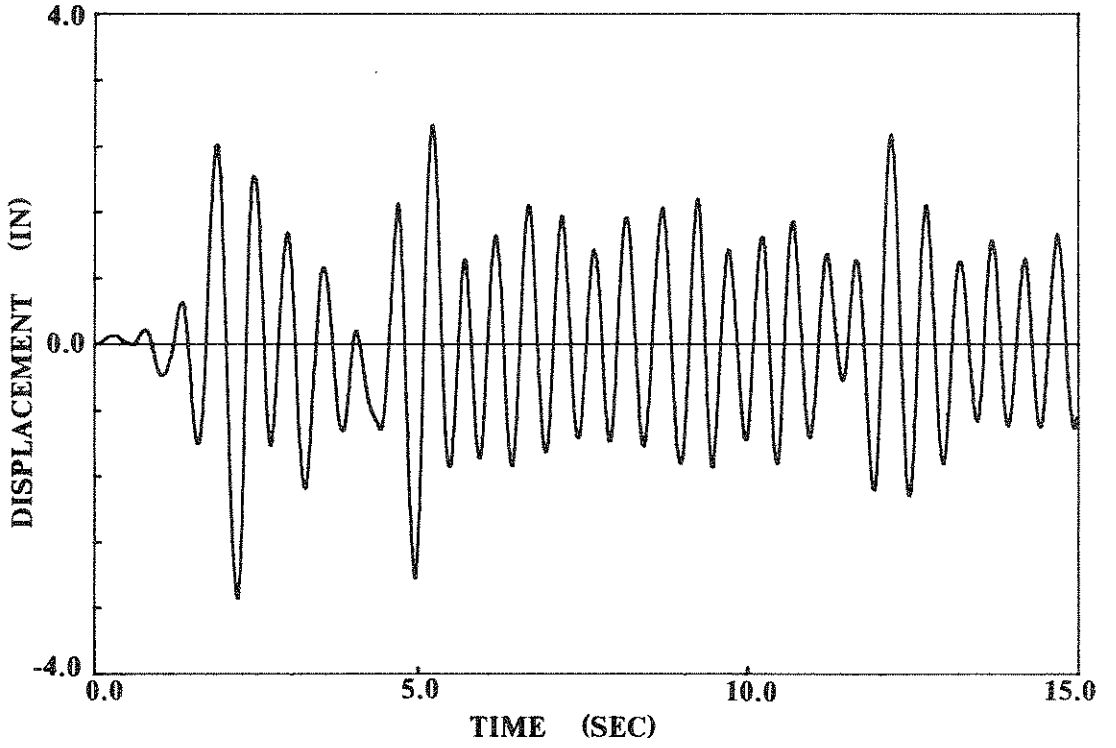

(a) Pseudodynamic Test

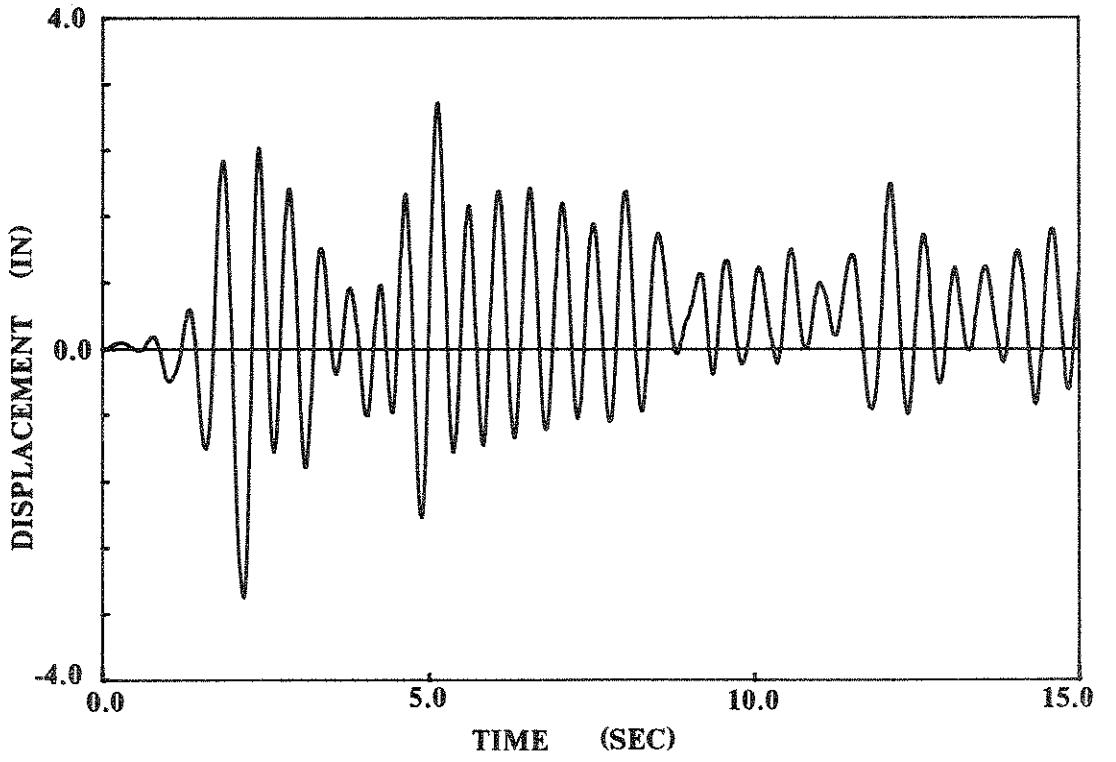

(b) Analytical Simulation

Fig. 5.12 Displacement Time History of Second Level
(El Centro 0.5g Ground Motion)

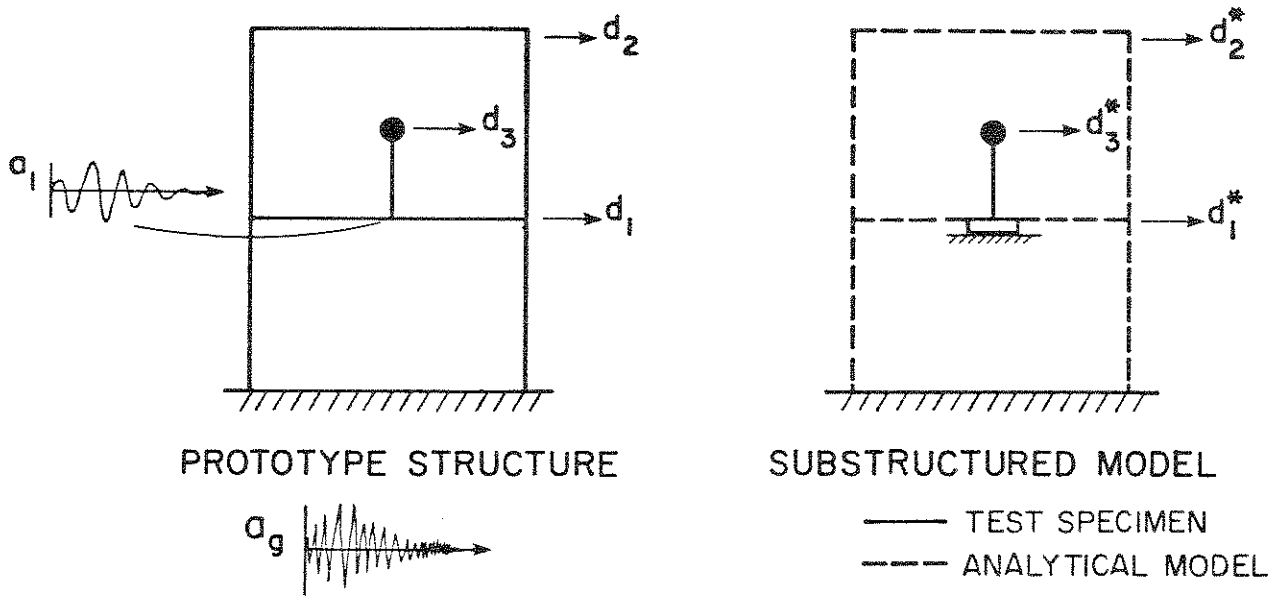

Fig. 6.1 Pseudodynamic Testing of Equipment
Using Substructuring Methods

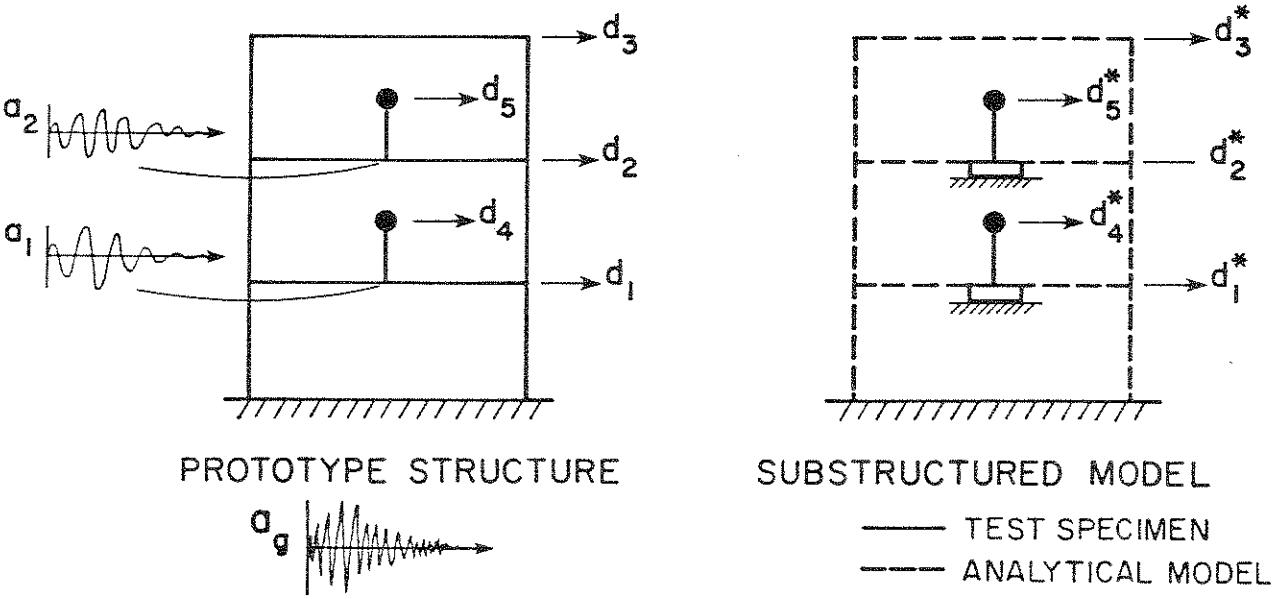

Fig. 6.2 Pseudodynamic Testing of Multiple Equipment
Mounted on a Structure

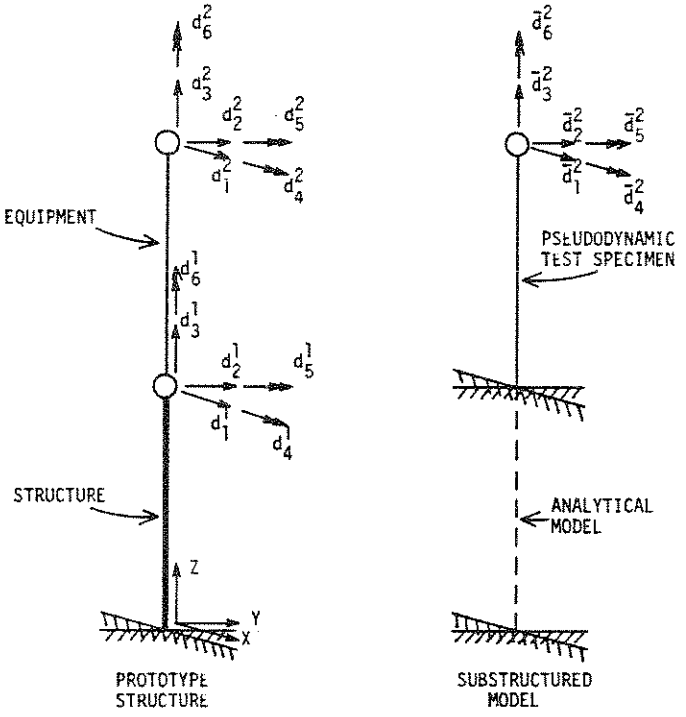

Fig. 6.3 Example of One-Story/One-Piece Equipment Structure System

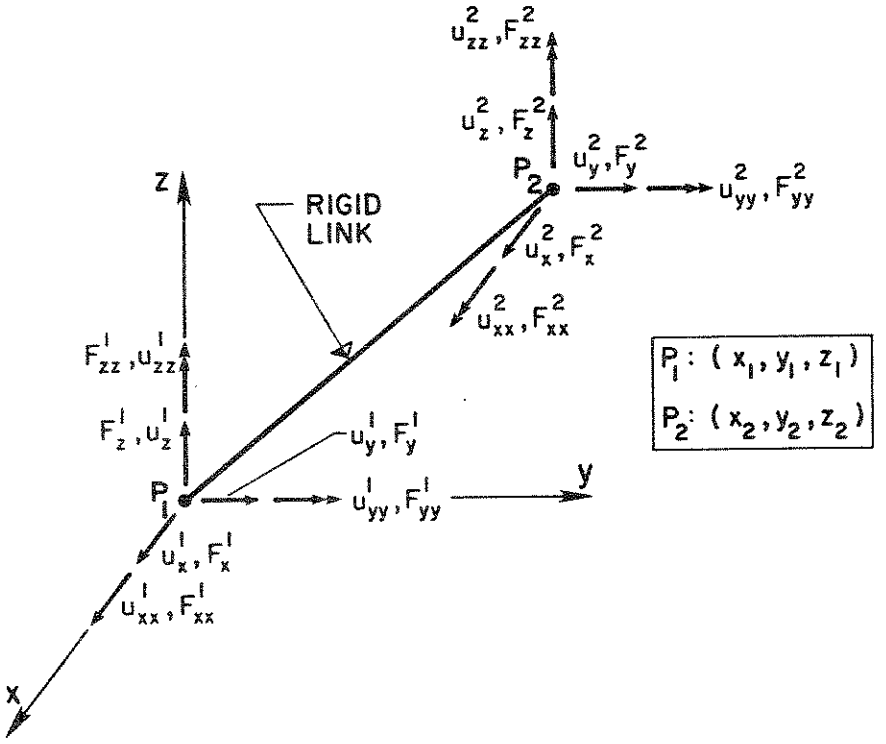

Fig. 6.4 Determination of the Transformation Matrix for Displacements

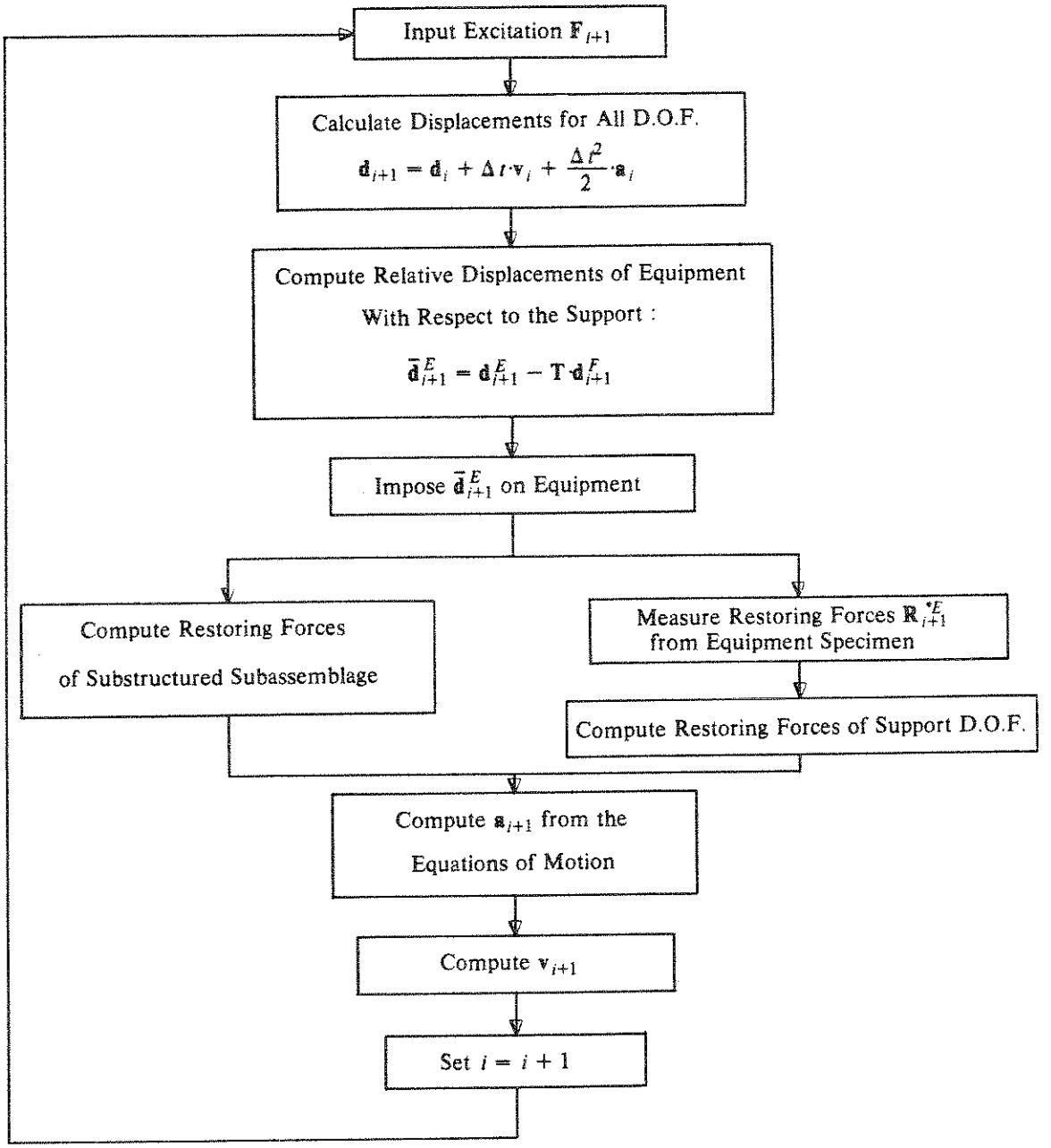

Fig. 6.5 Numerical Algorithm for Pseudodynamic Substructuring Equipment-Structure Tests Using Newmark Explicit Integration Method.

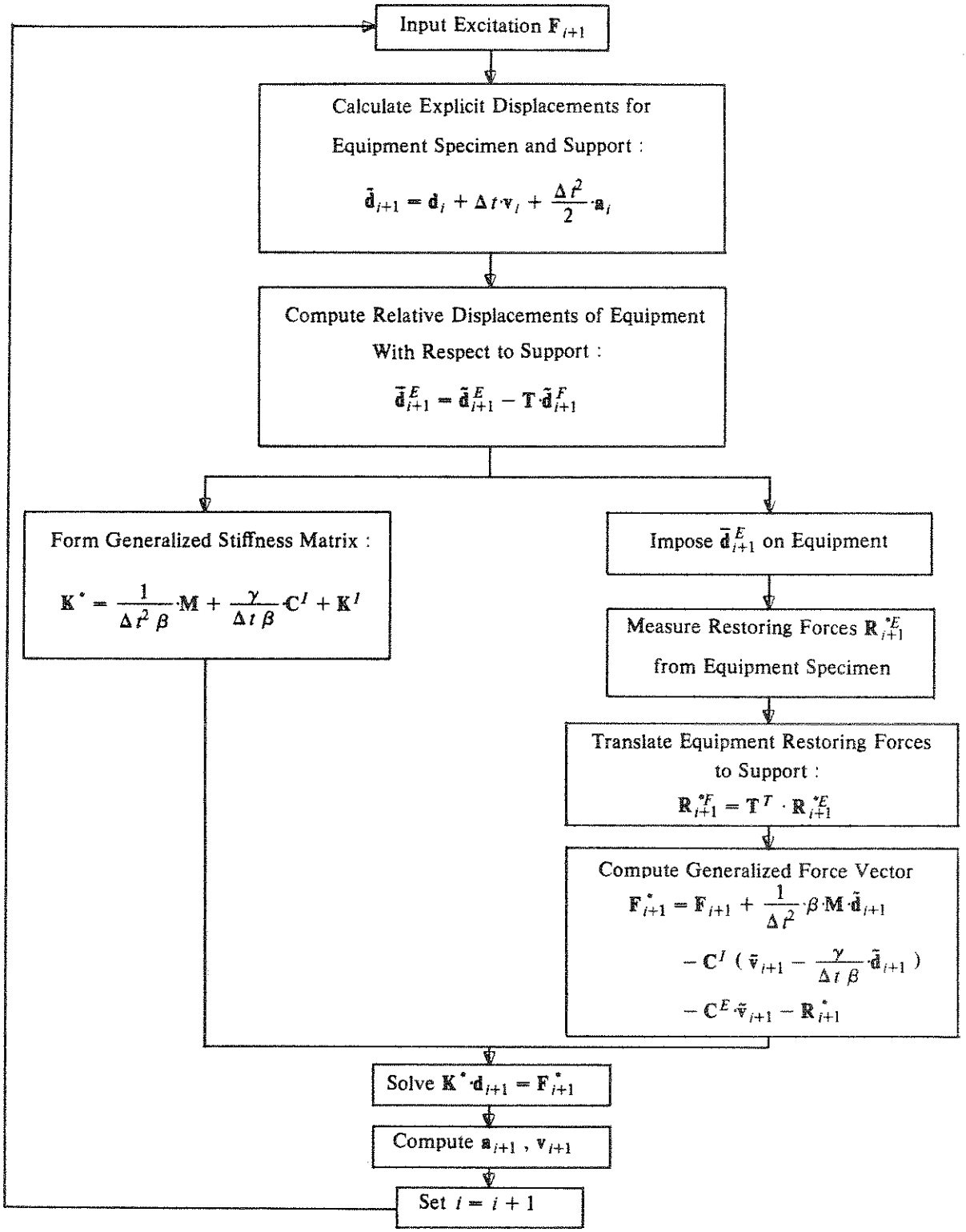

Fig. 6.6 Numerical Algorithm for Pseudodynamic Substructuring Equipment-Structure Tests Using the Implicit-Explicit Integration Method (Elastic Structure)

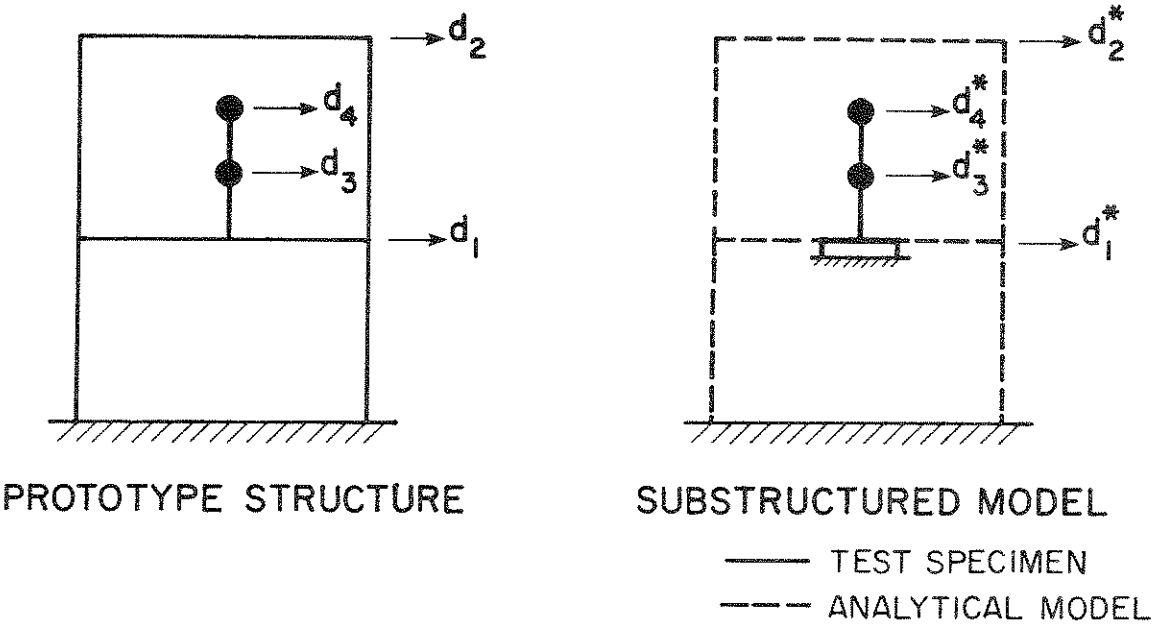

Fig. 6.7 Pseudodynamic Testing of Equipment with Two Nodes Using Substructuring for the Containing Structure

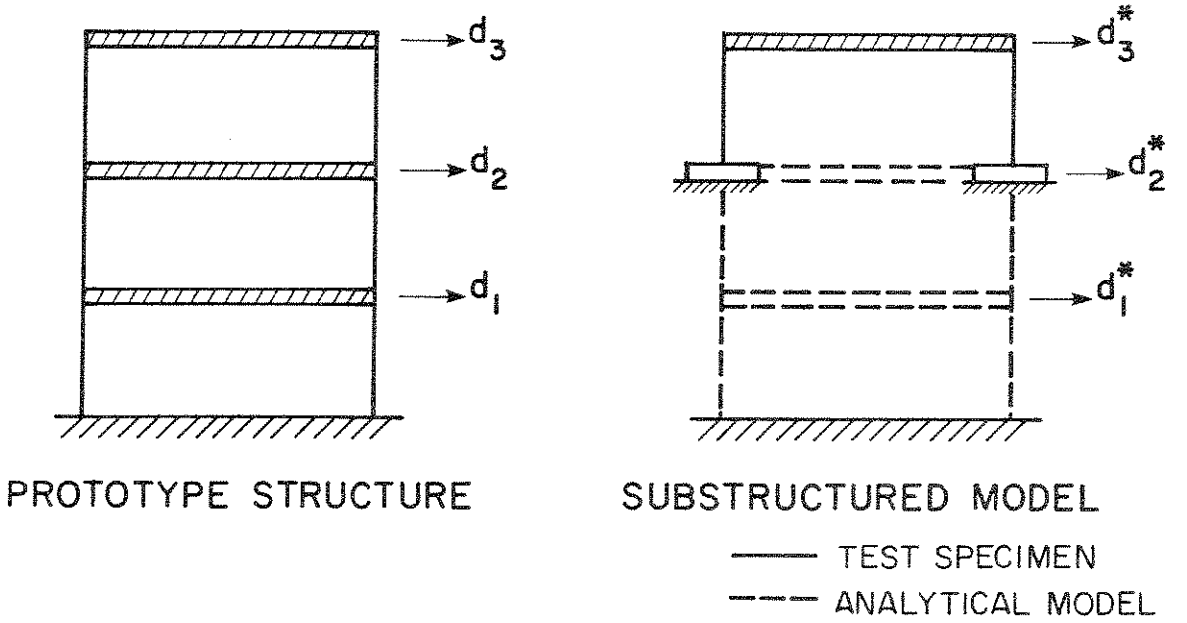

Fig. 6.8 Pseudodynamic Testing of the Upper Story of a Shear Building Using Substructuring

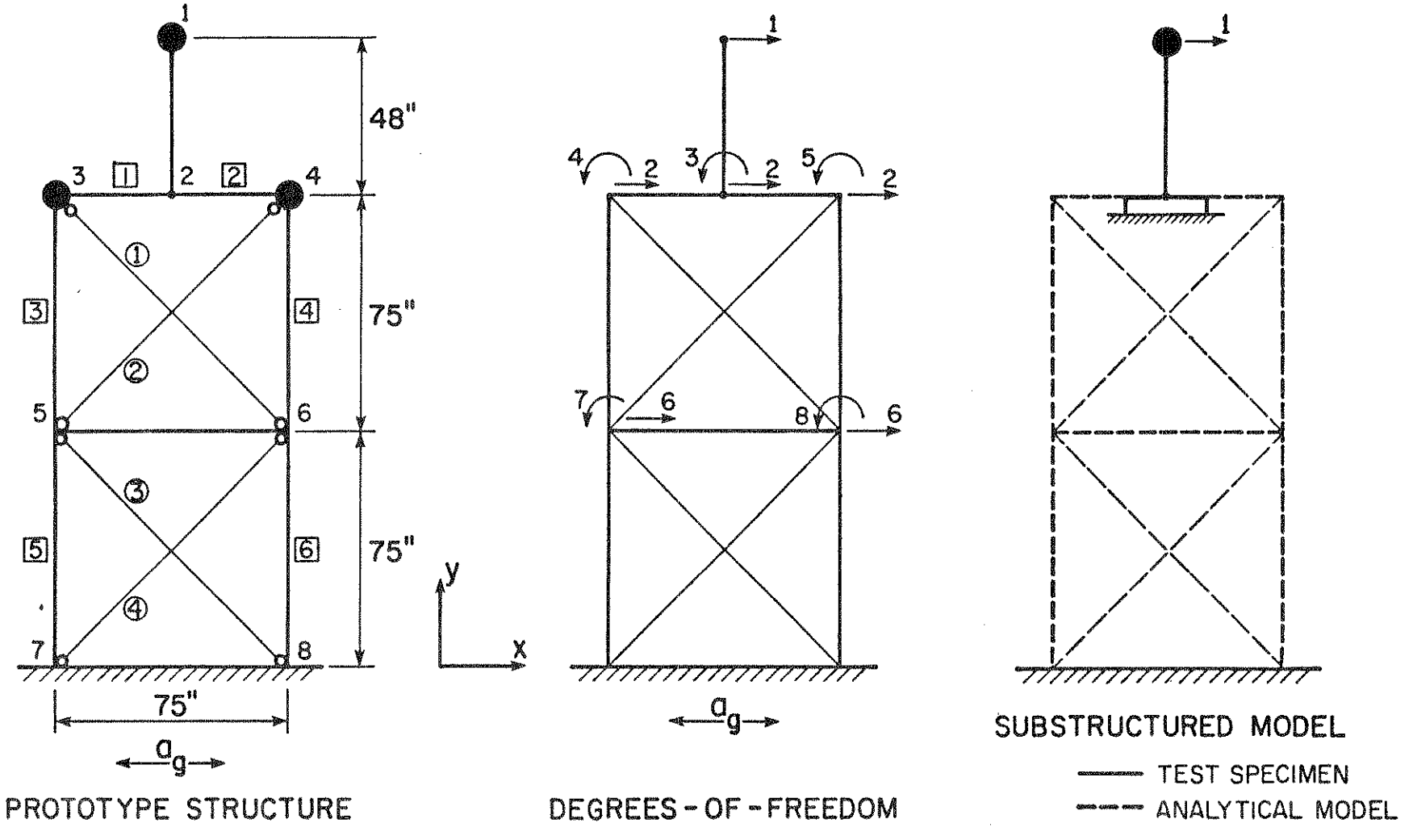

(a) Prototype Structure

(b) Degrees-of-Freedom Considered

(c) Substructured Model

Fig. 6.9 Equipment-Structure System

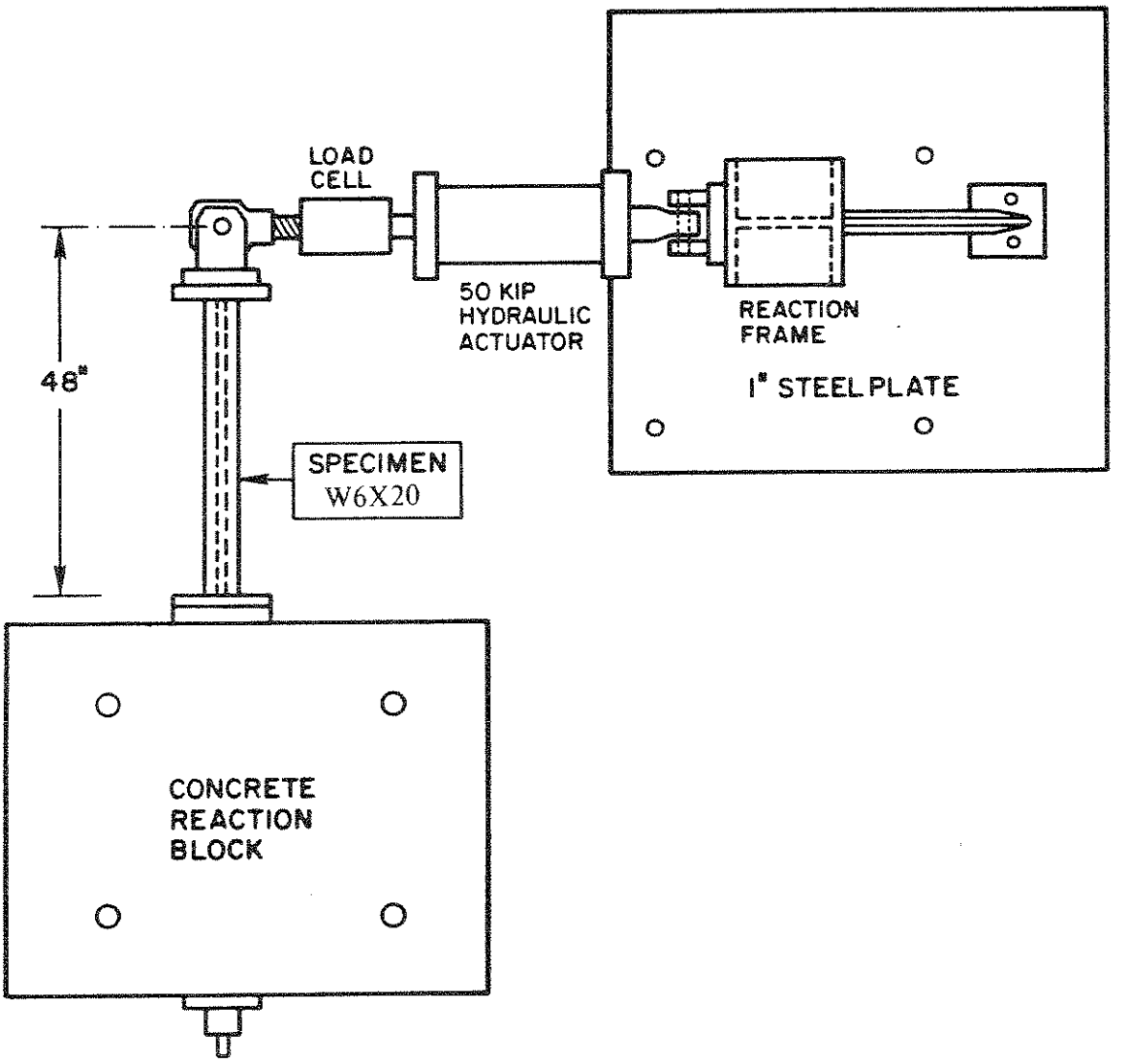

Fig. 6.10 Layout of Pseudodynamic Test

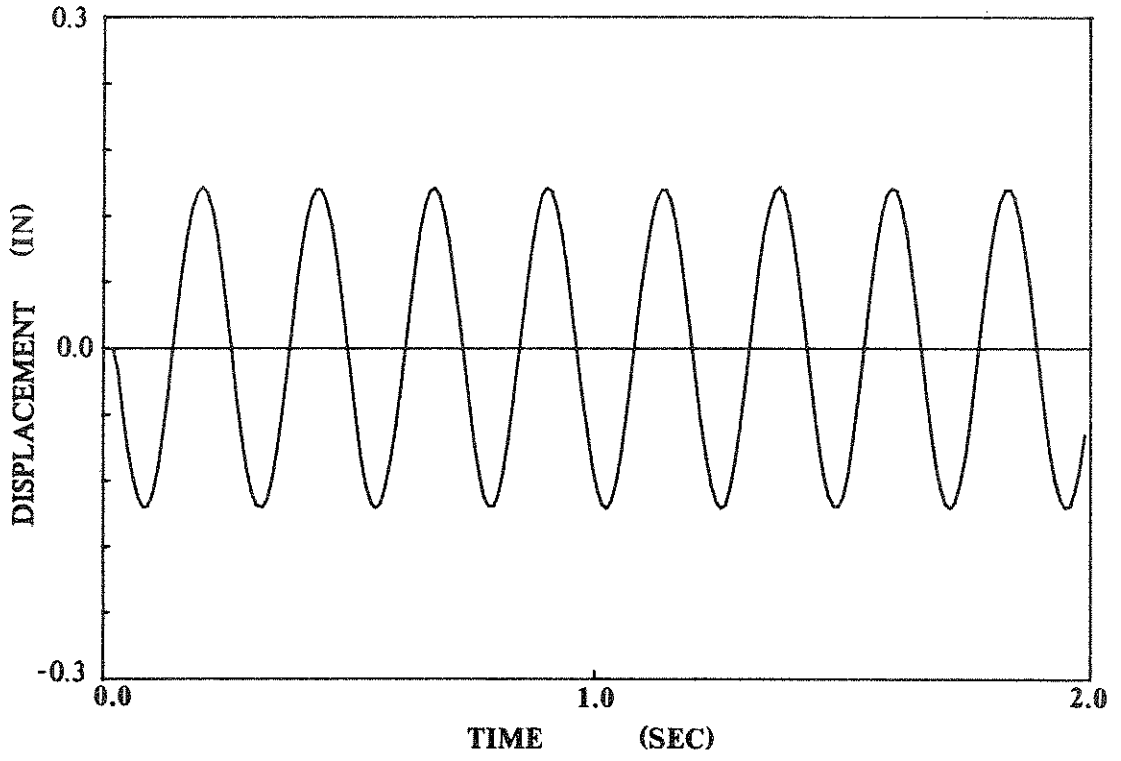

(a) Experiment

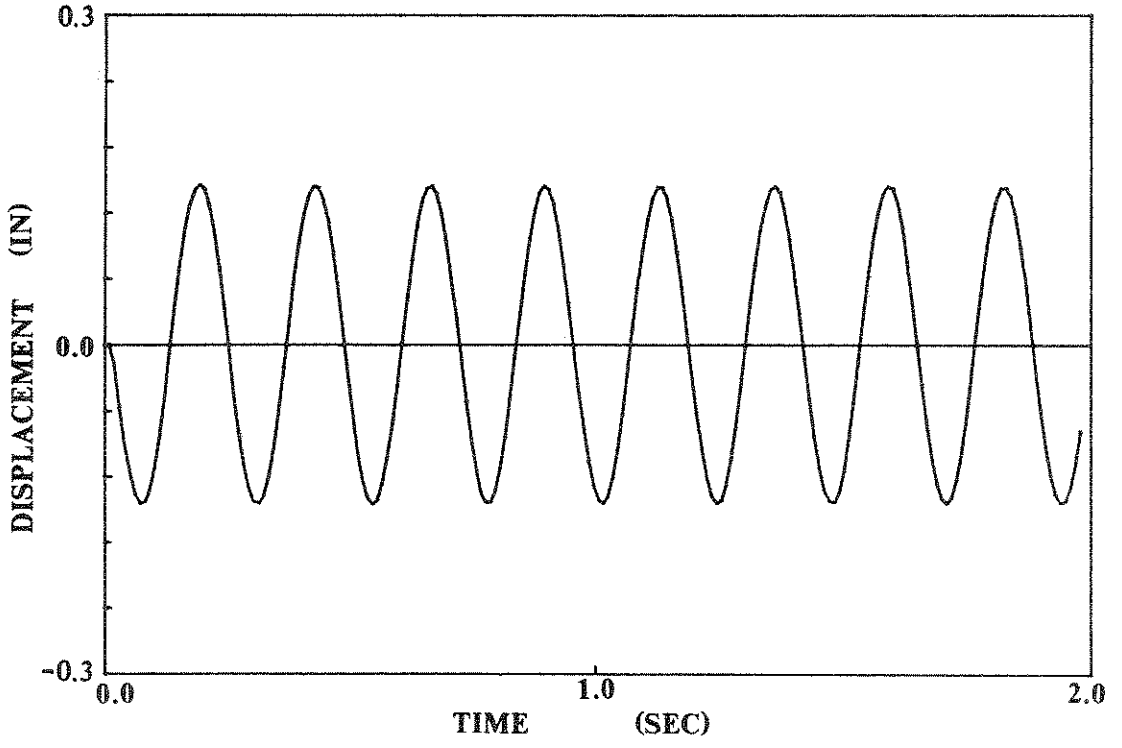

(b) Analytical Simulation

Fig. 6.11 Displacement Time History of Top Level (Free Vibration)

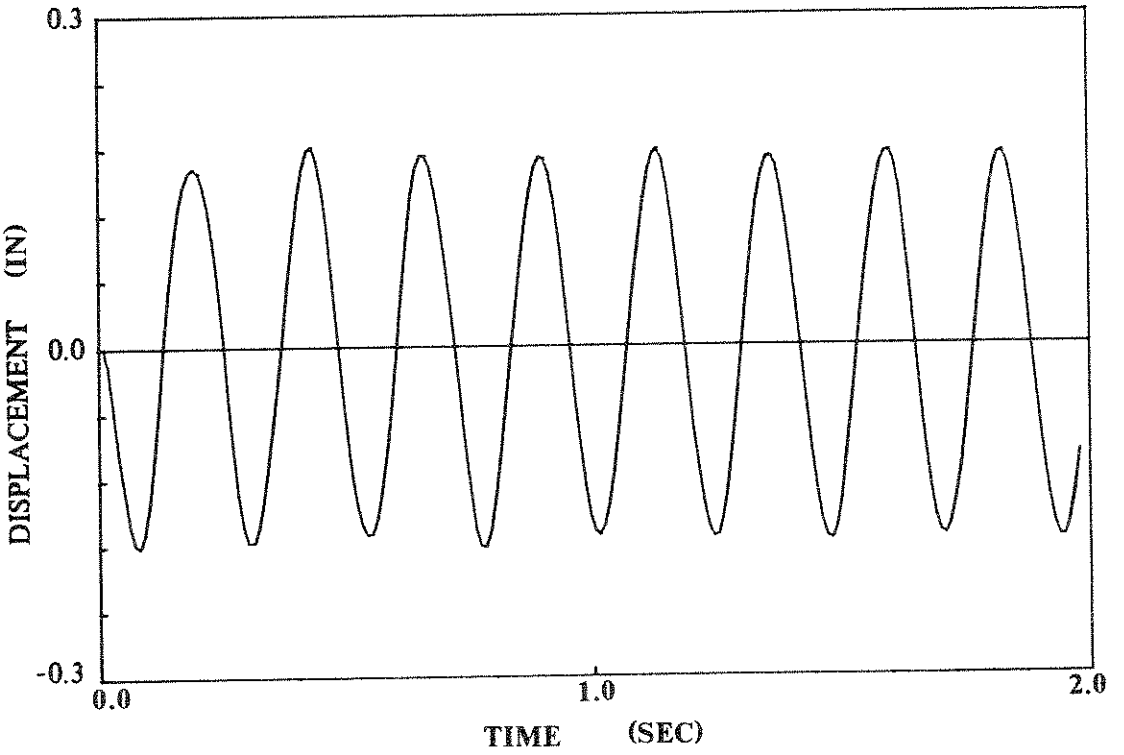

(a) Experiment

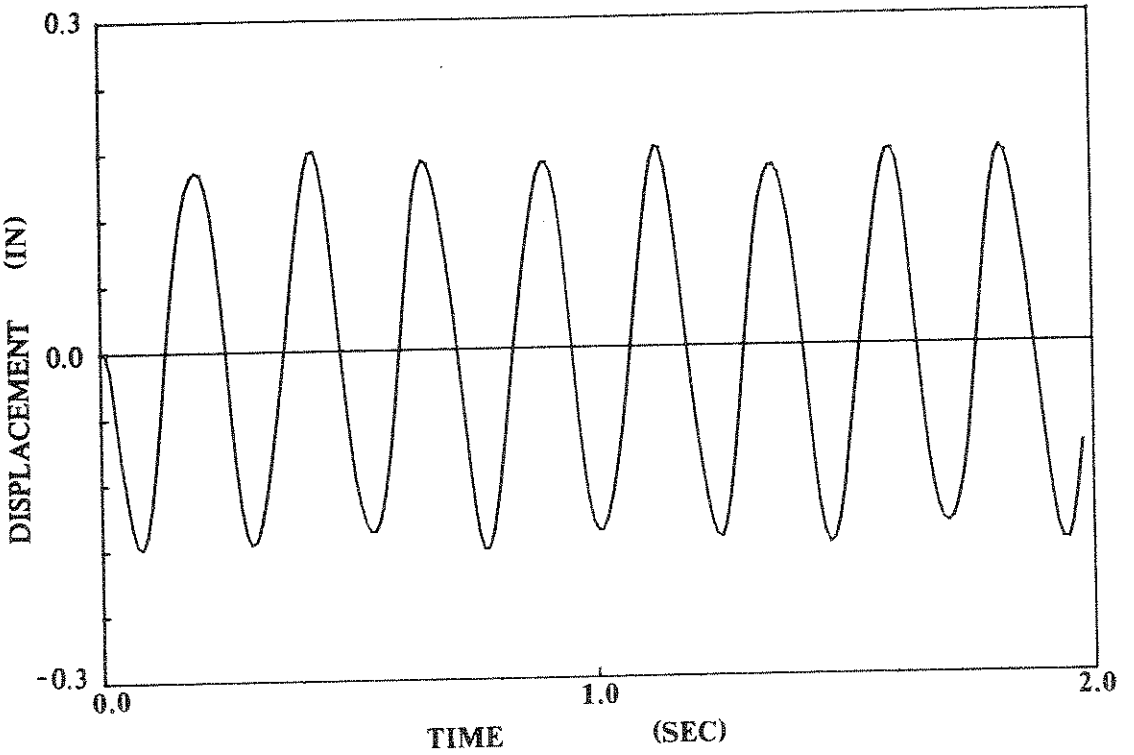

(b) Analytical Simulation

Fig. 6.12 Time History of Relative Displacement of Equipment With Respect to Ground (Free Vibration)

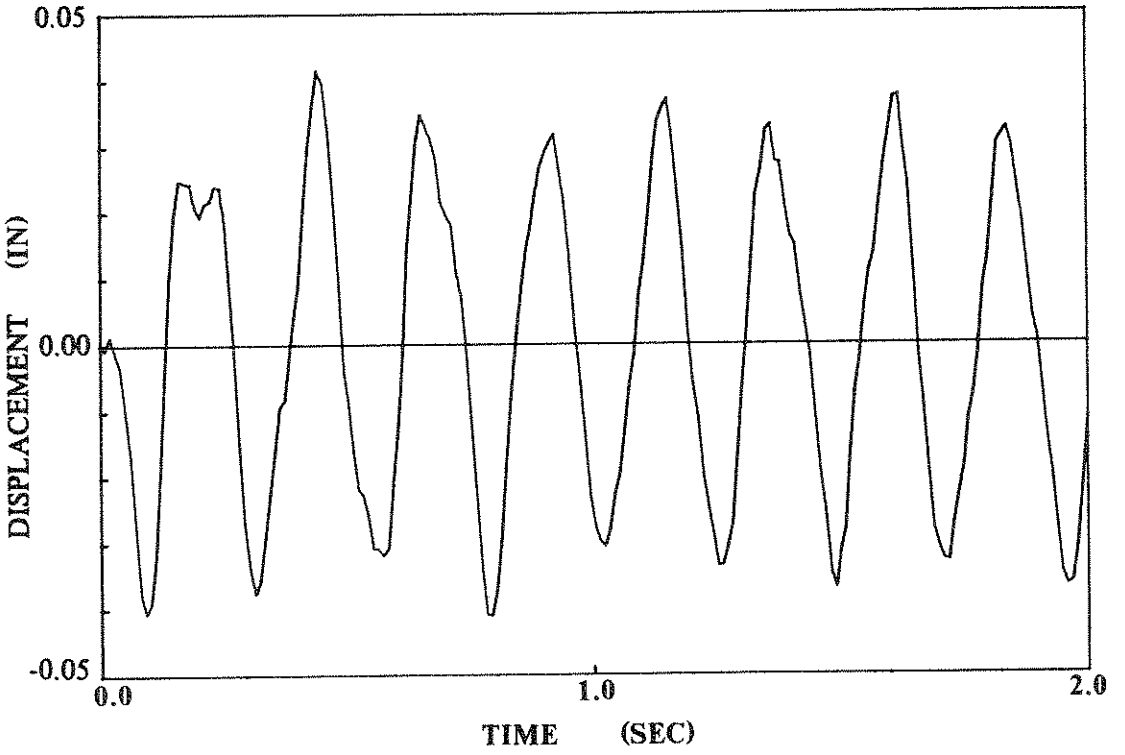

(a) Experiment

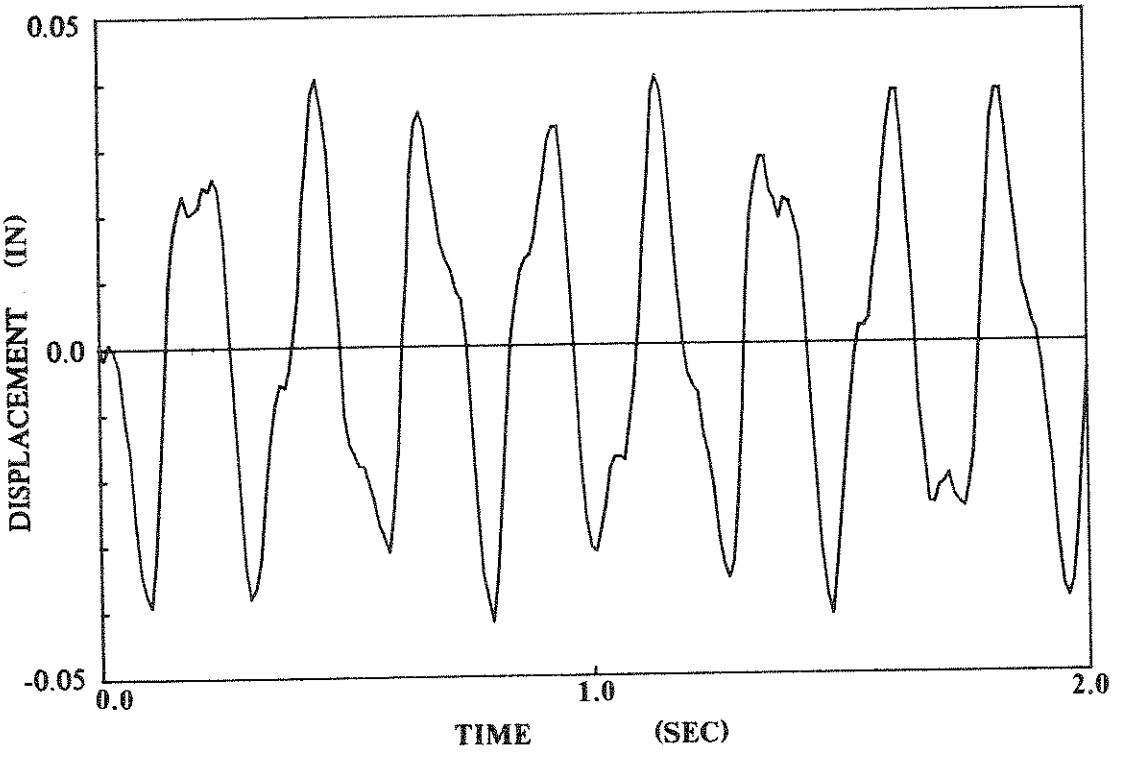

(b) Analytical Simulation

Fig. 6.13 Time History of Relative Displacement of Equipment With Respect to Top (Free Vibration)

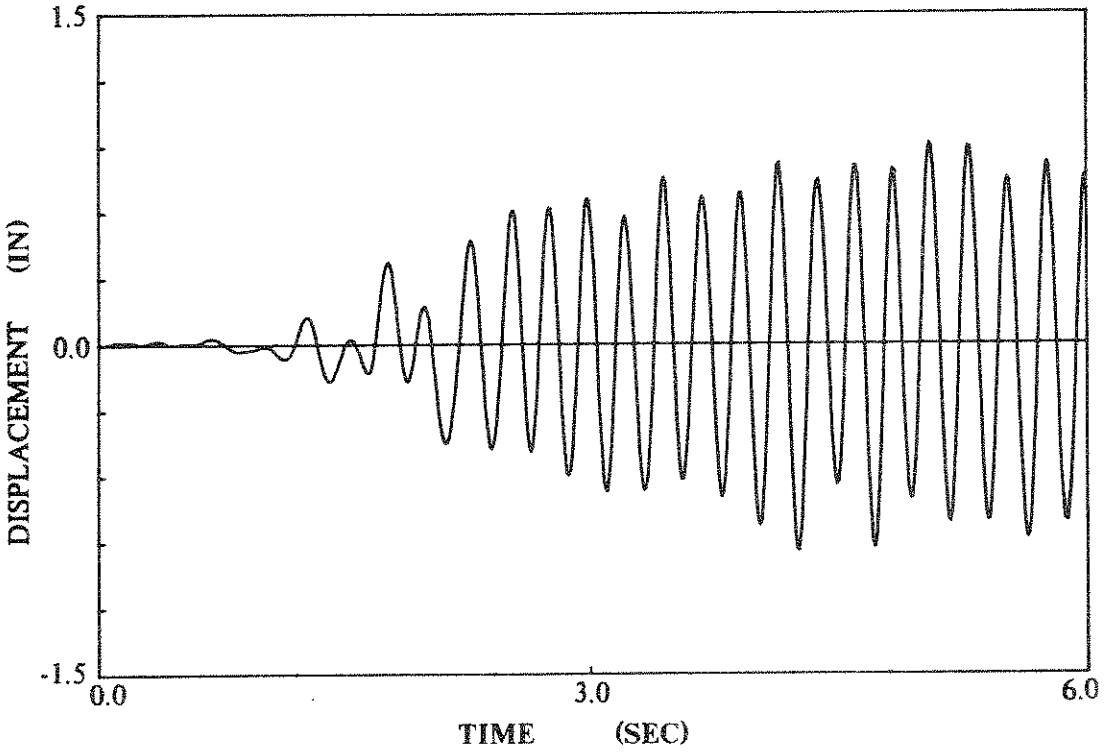

(a) Experiment

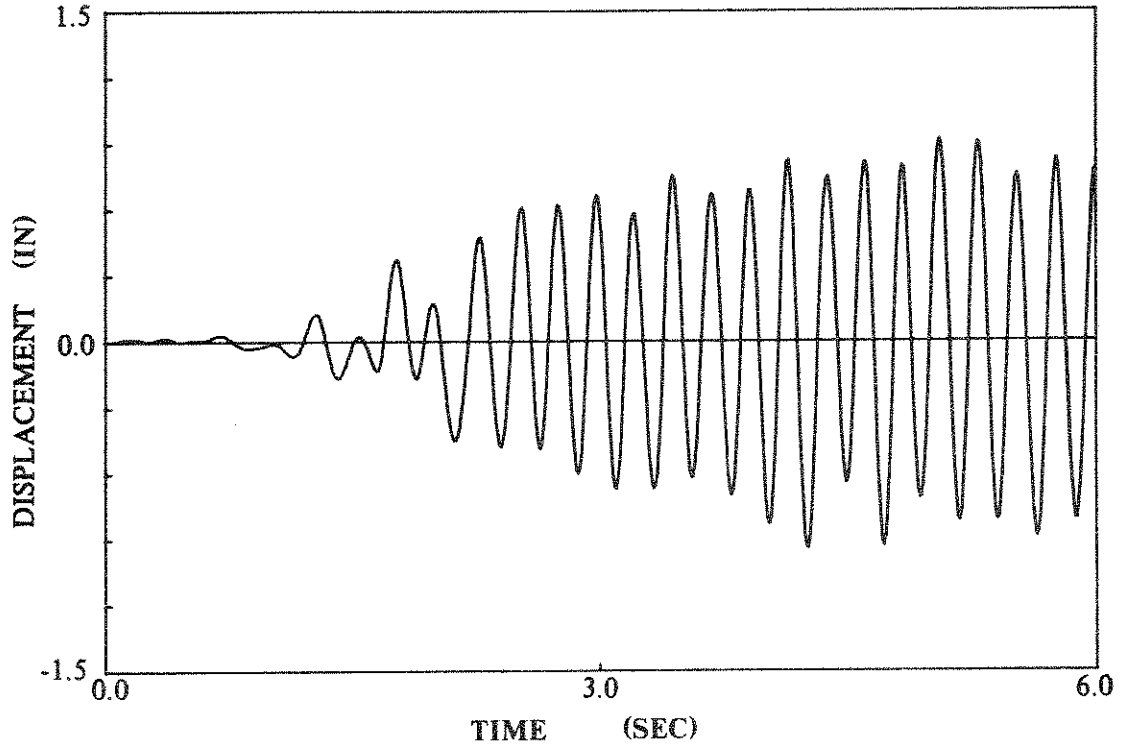

(b) Analytical Simulation

Fig. 6.14 Displacement Time History of Top Level
(El Centro 0.4g Ground Motion)

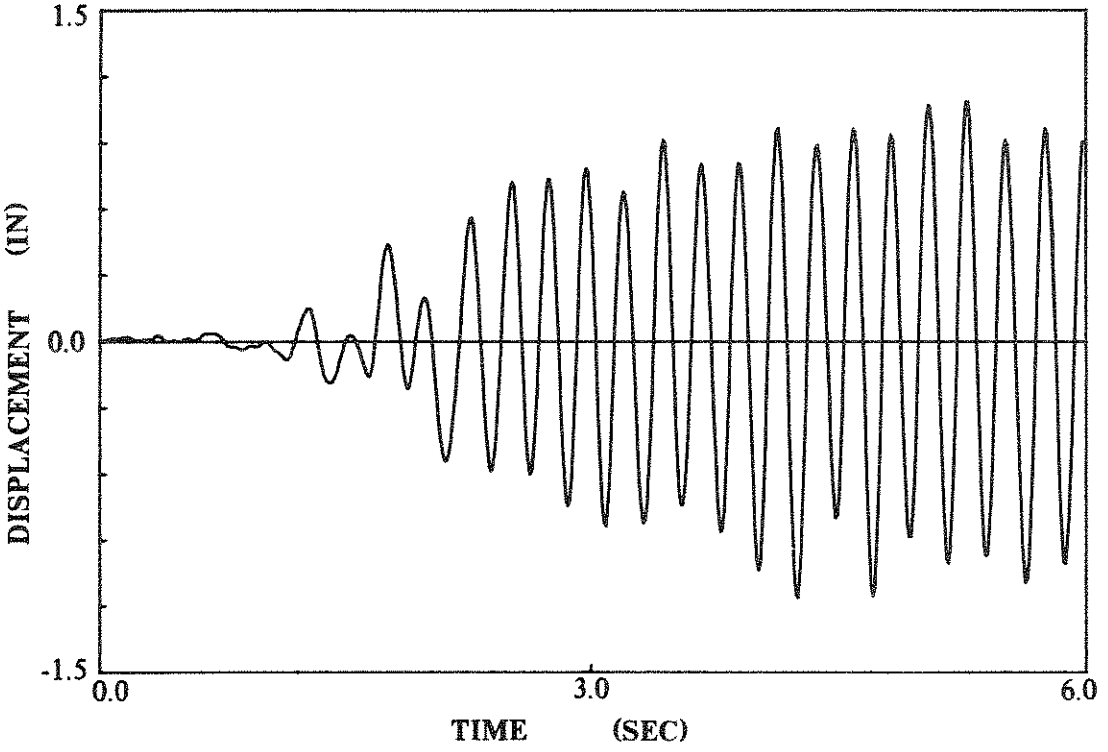

(a) Experiment

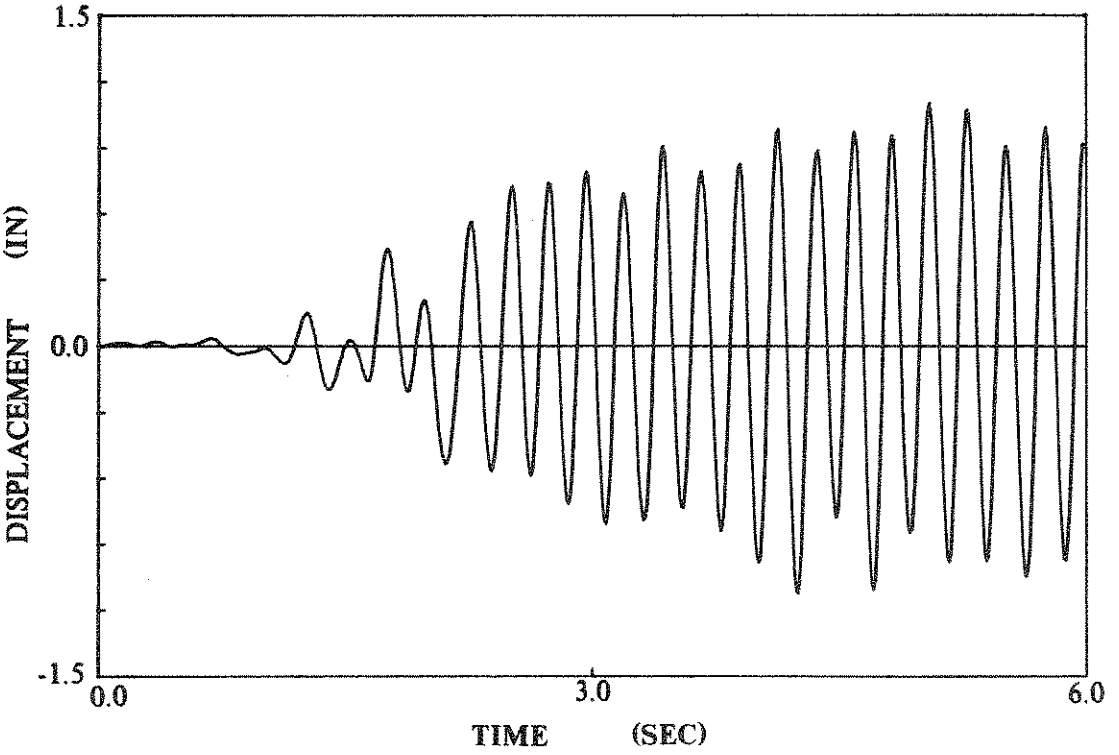

(b) Analytical Simulation

Fig. 6.15 Time History of Relative Displacement of Equipment With Respect to Ground (El Centro 0.4g Ground Motion)

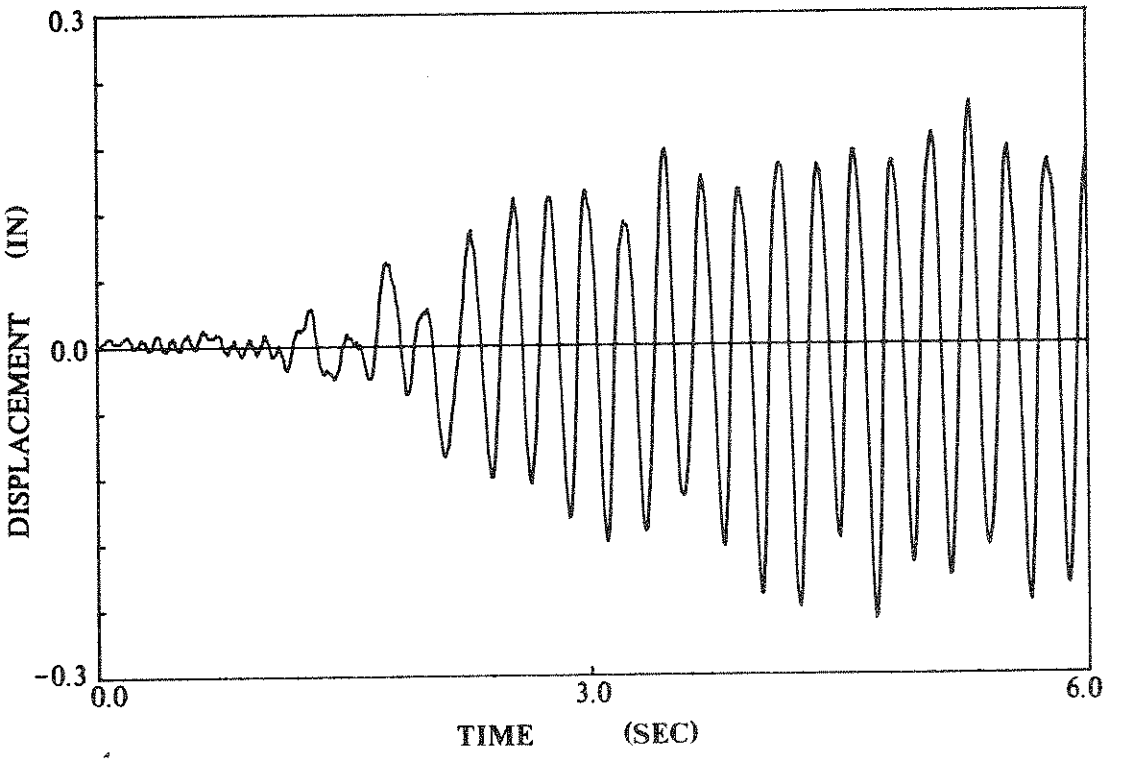

(a) Experiment

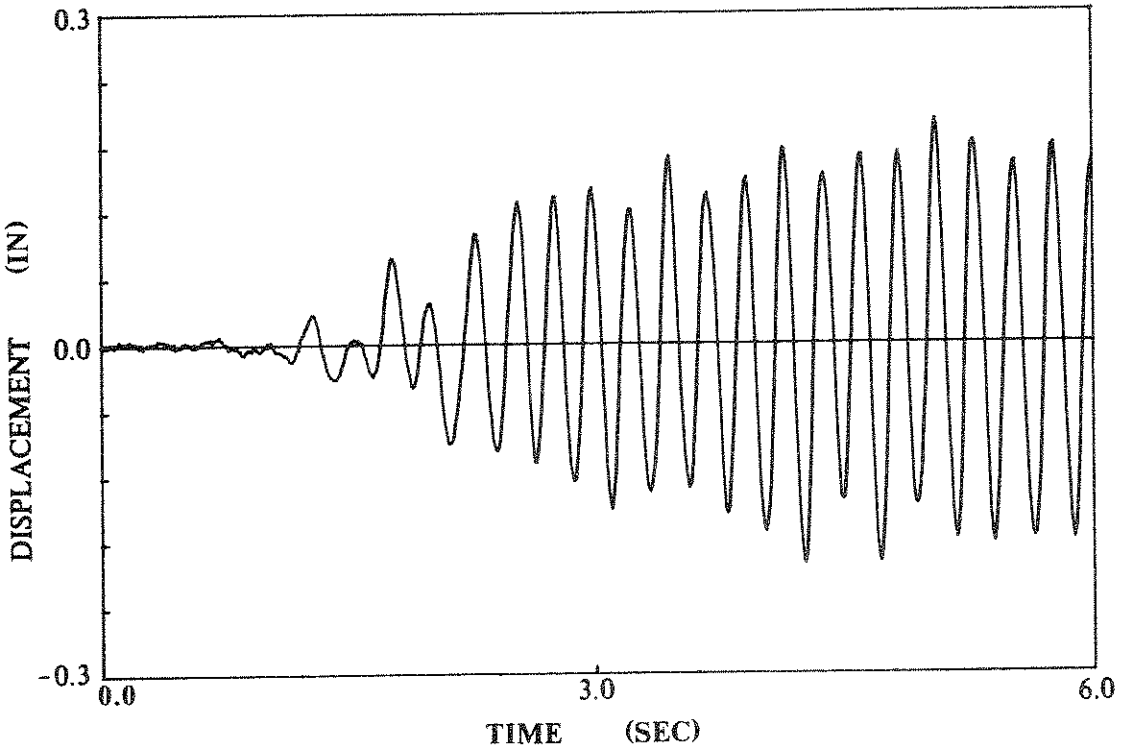

(b) Analytical Simulation

Fig. 6.16 Time History of Relative Displacement of Equipment With Respect to Top (El Centro 0.4g Ground Motion)

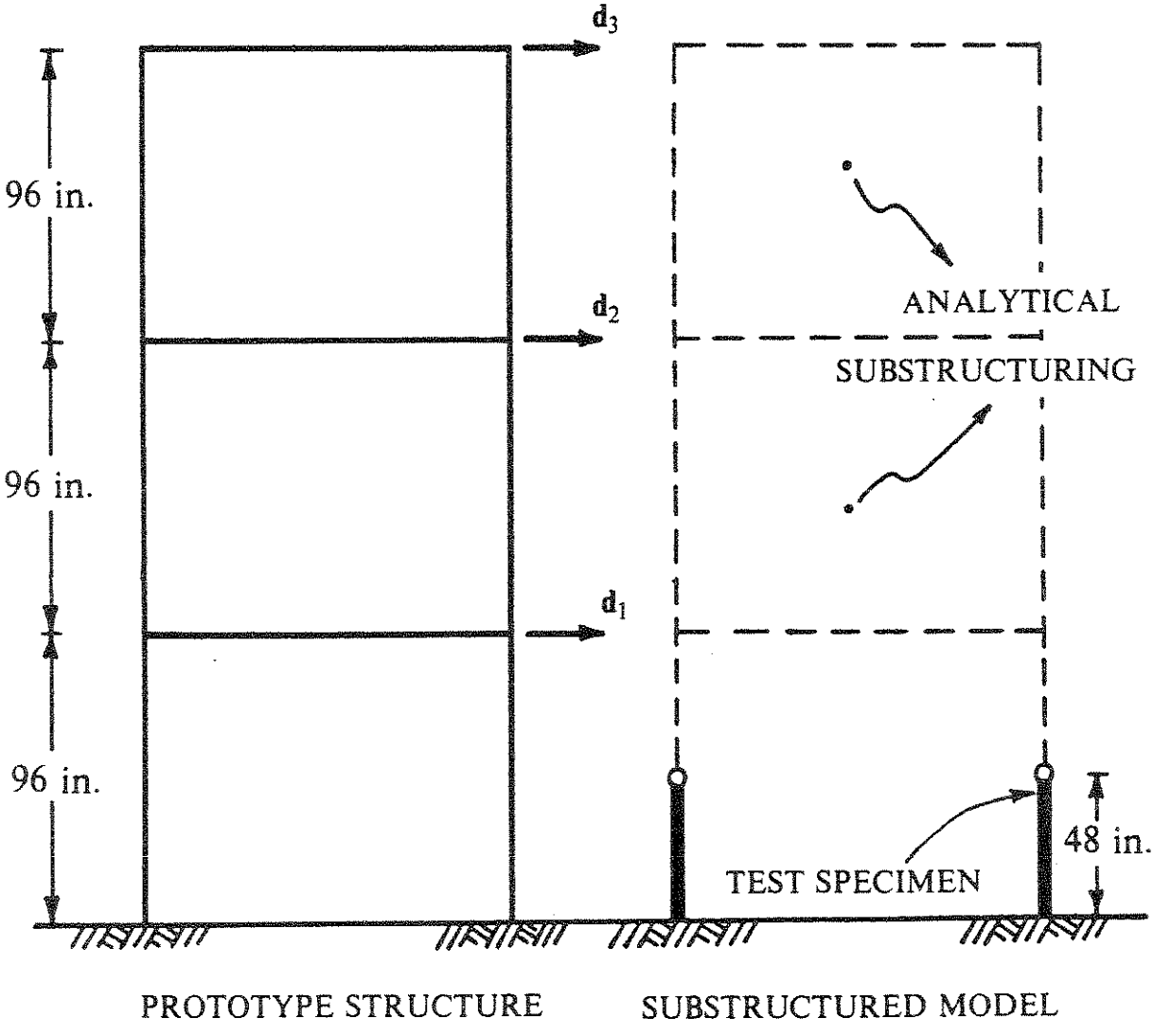

Fig. 7.1 Three-Story Test System

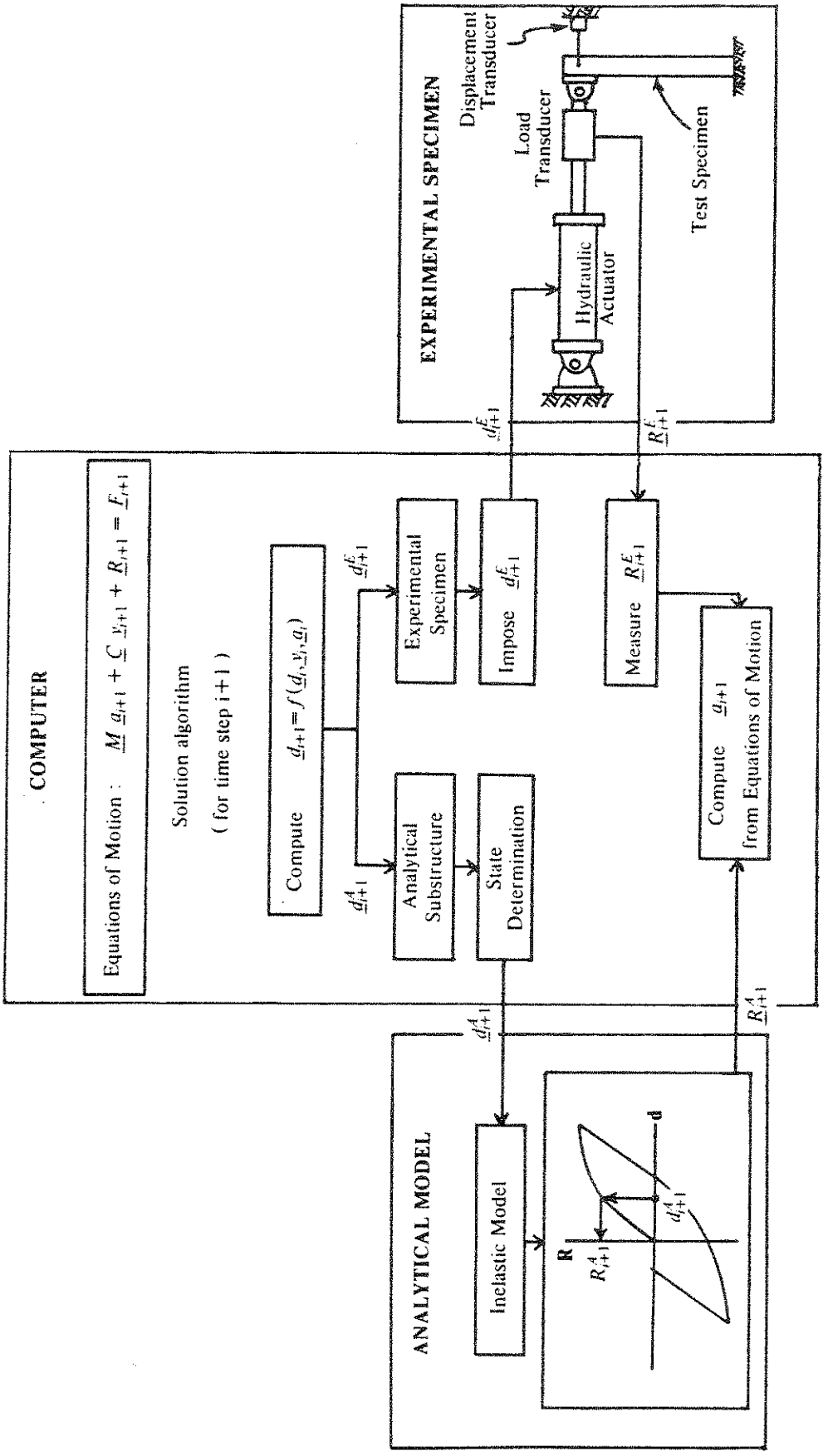

Fig. 7.2 Nonlinear Substructuring Algorithm Using Explicit Integration

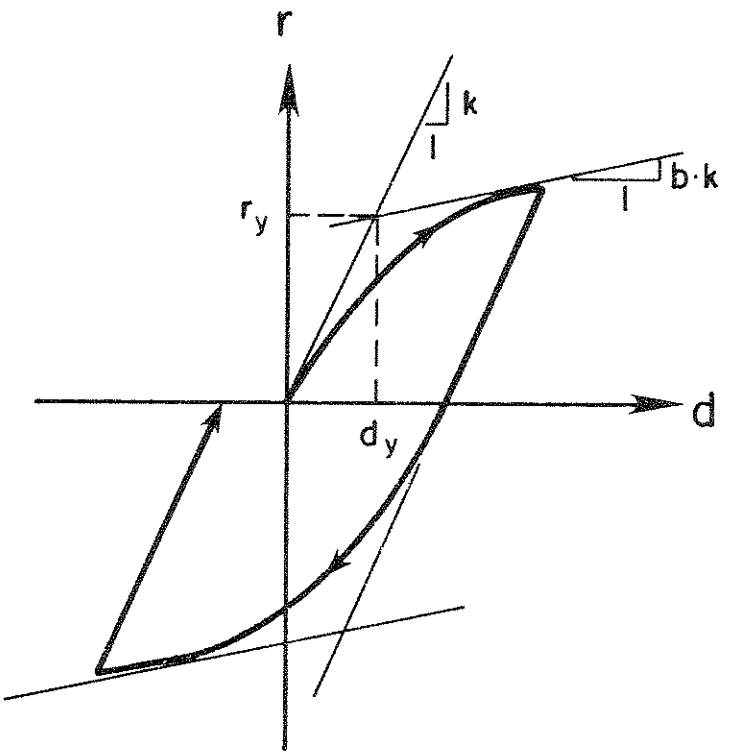

Menegotto-Pinto Model
(for Nonlinear Simulations)

$$\bar{r} = b\,\bar{d} + \frac{(1-b)\,\bar{d}}{(1+\bar{d}^R)^{1/R}}$$

$$\bar{r} = r/r_y$$
$$\bar{d} = d/d_y$$
$$k = r_y/d_y$$

Fig. 7.3 Menegotto-Pinto Model

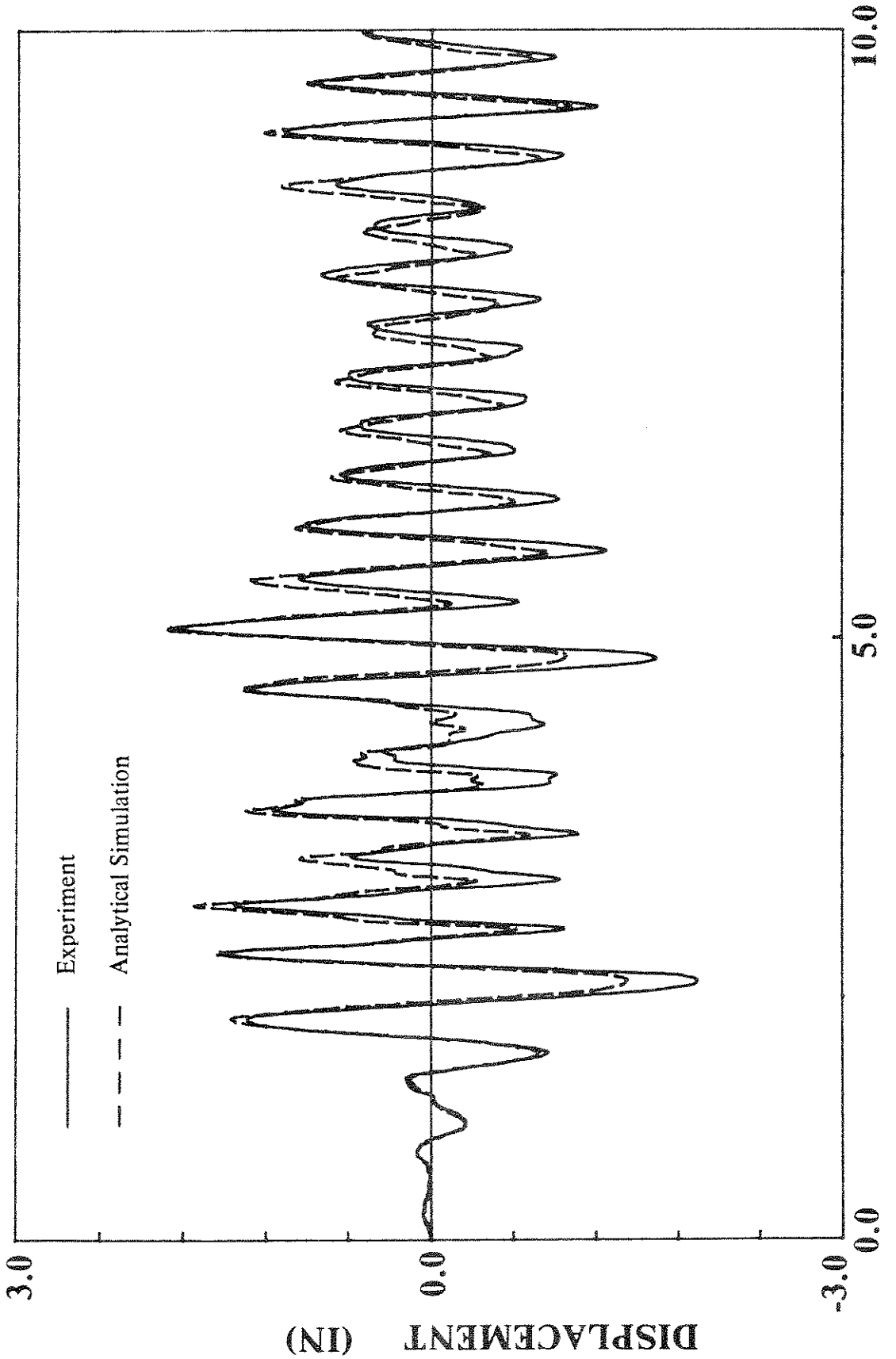

Fig. 7.4 Displacement Time History of First Level

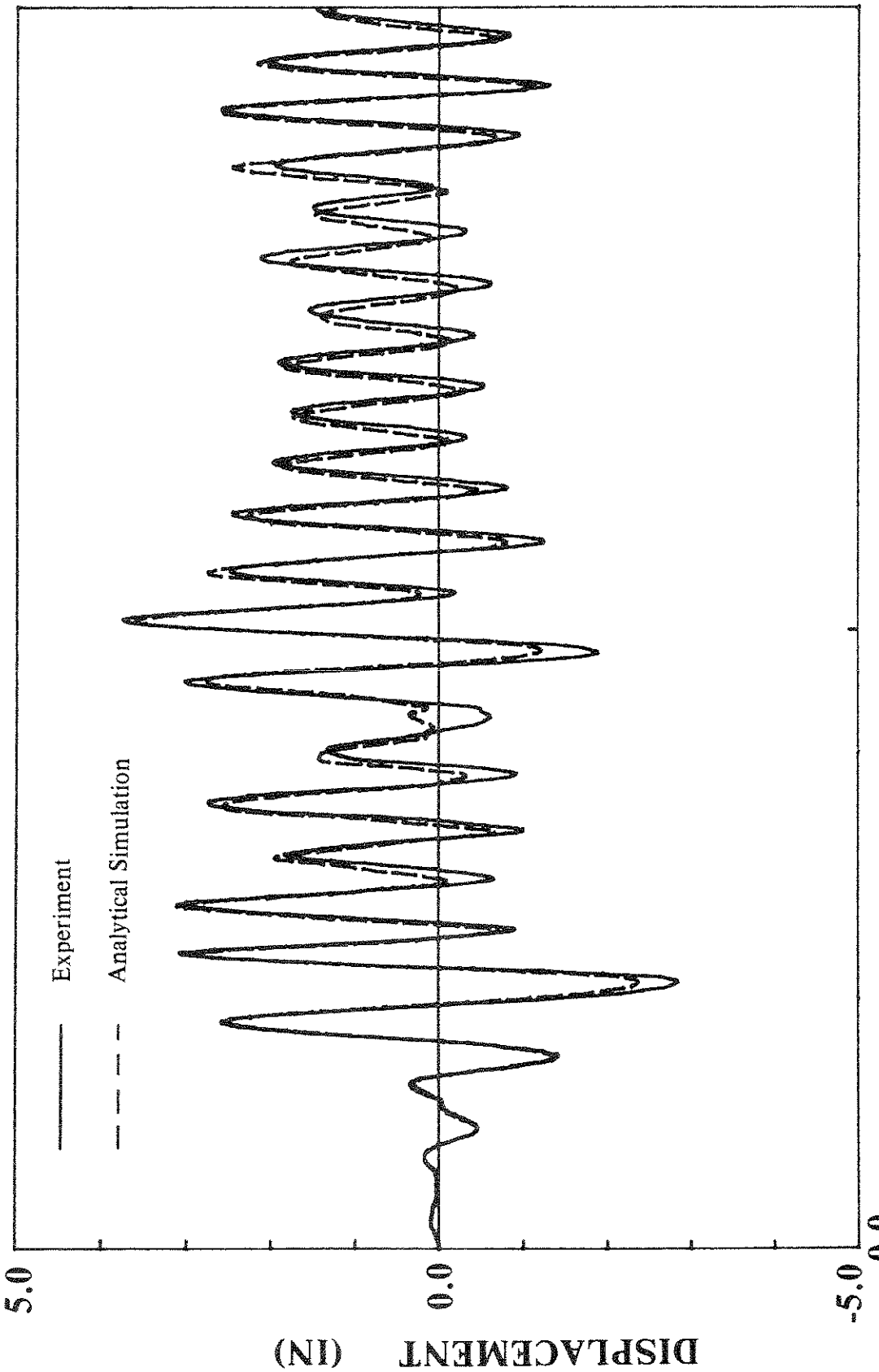

Fig. 7.5 Displacement Time History of Second Level

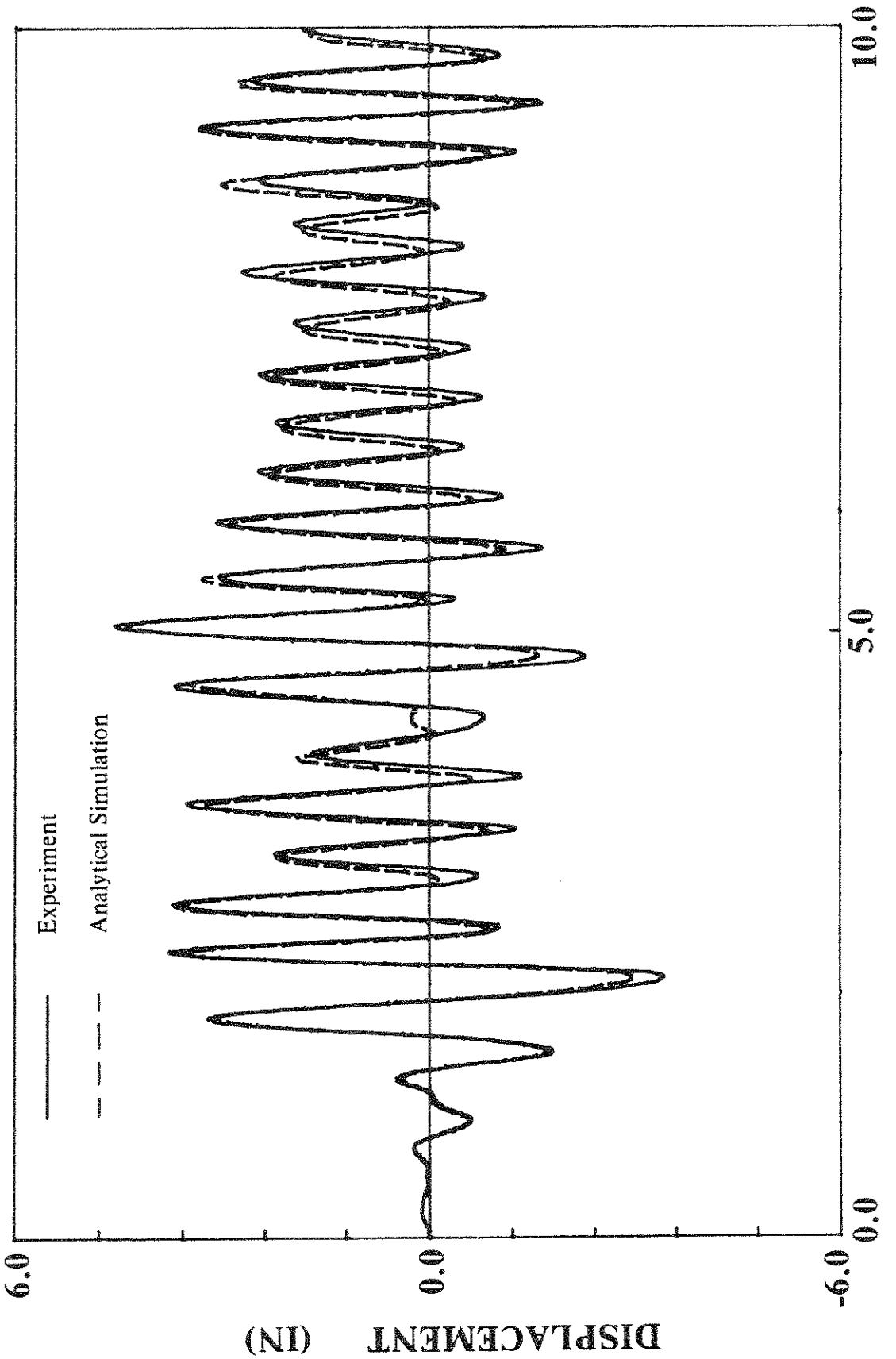

Fig. 7.6 Displacement Time History of Third Level

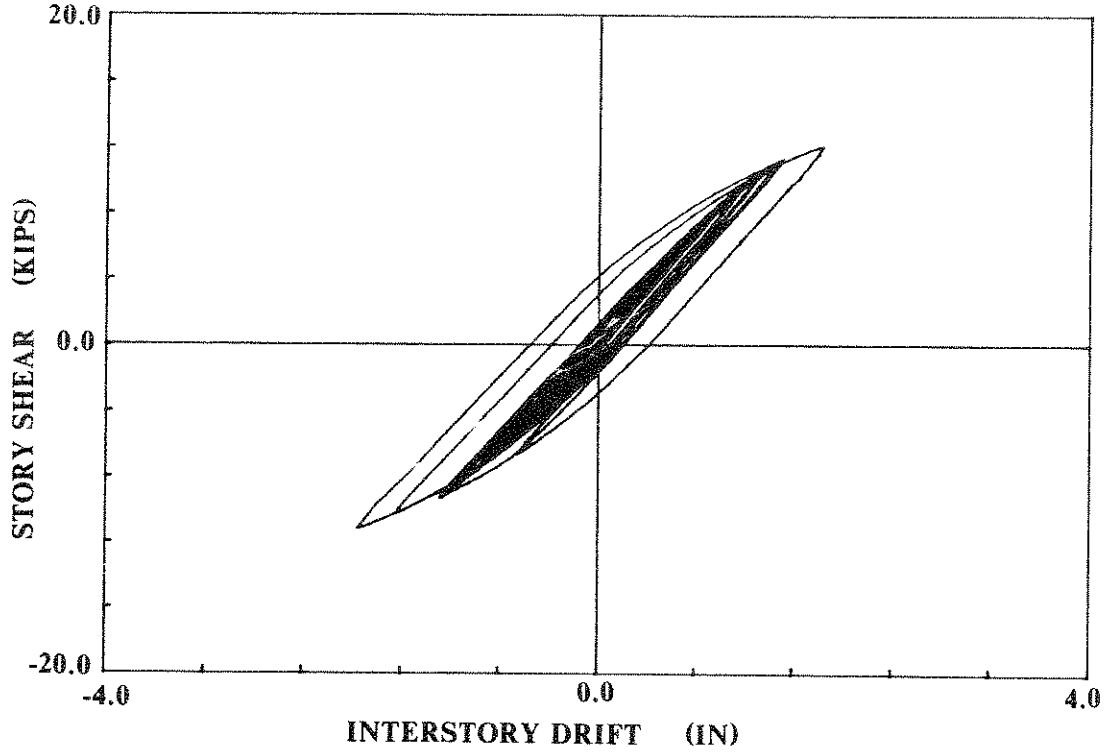

(a) Experiment

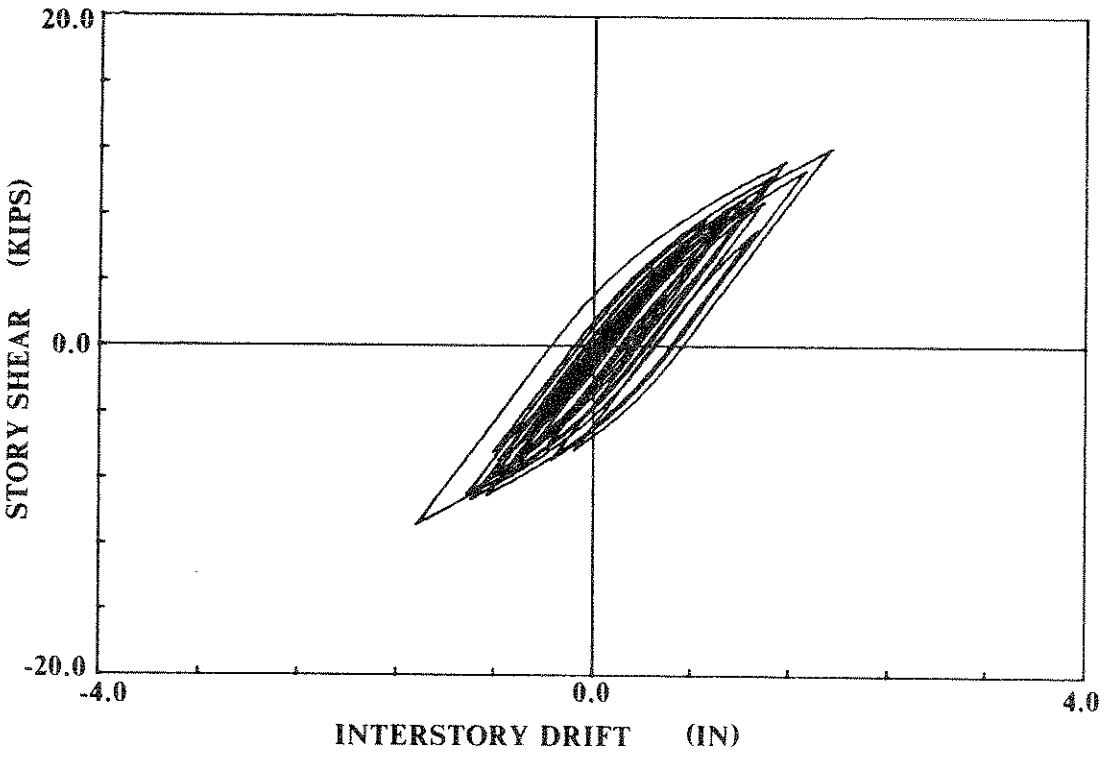

(b) Analytical Simulation

Fig. 7.7 Hysteretic Loop of First Story

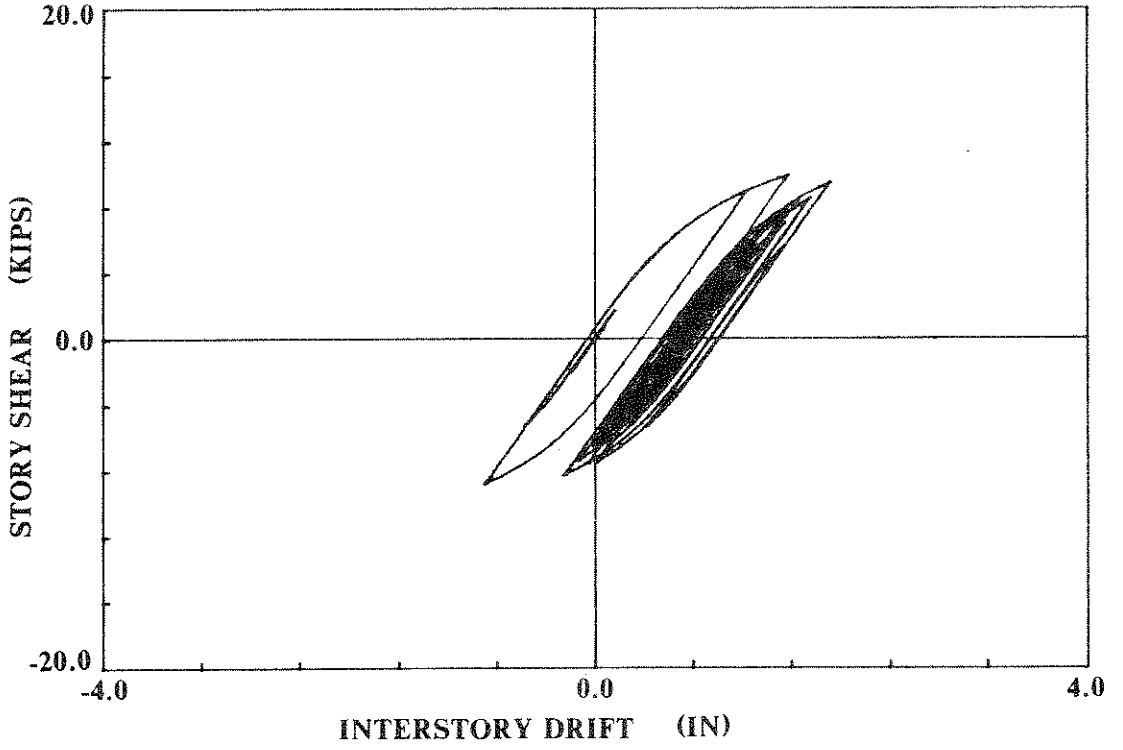

(a) Experiment

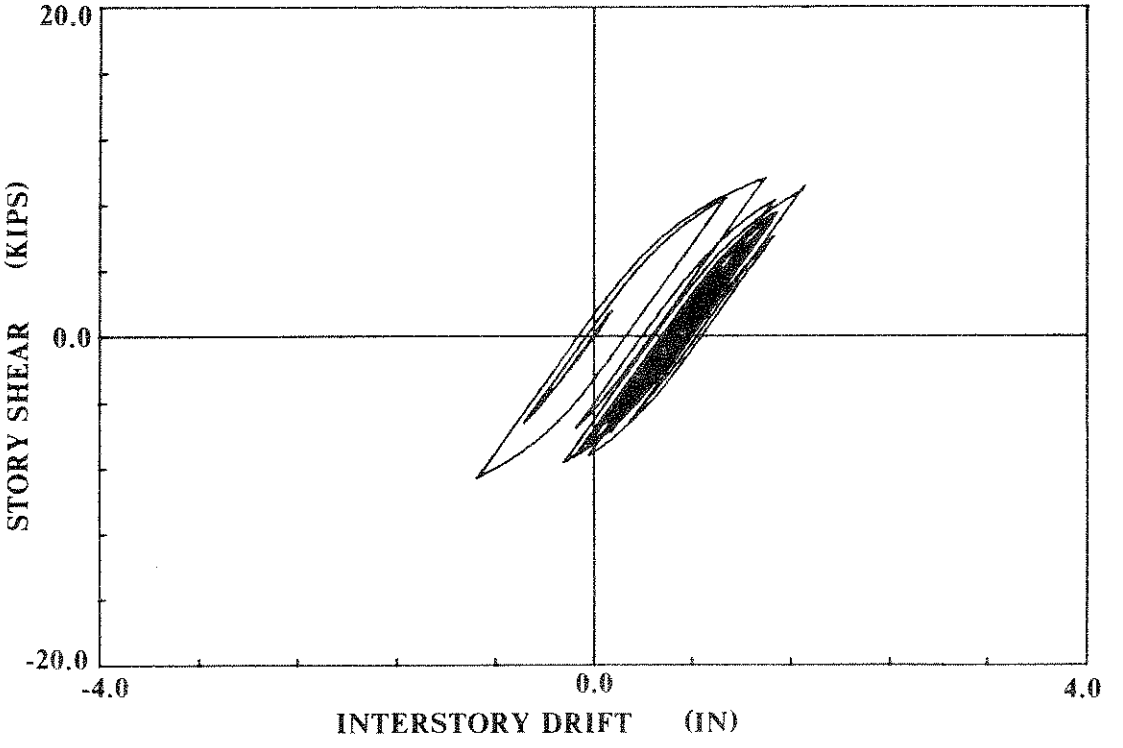

(b) Analytical Simulation

Fig. 7.8 Hysteretic Loop of Second Story

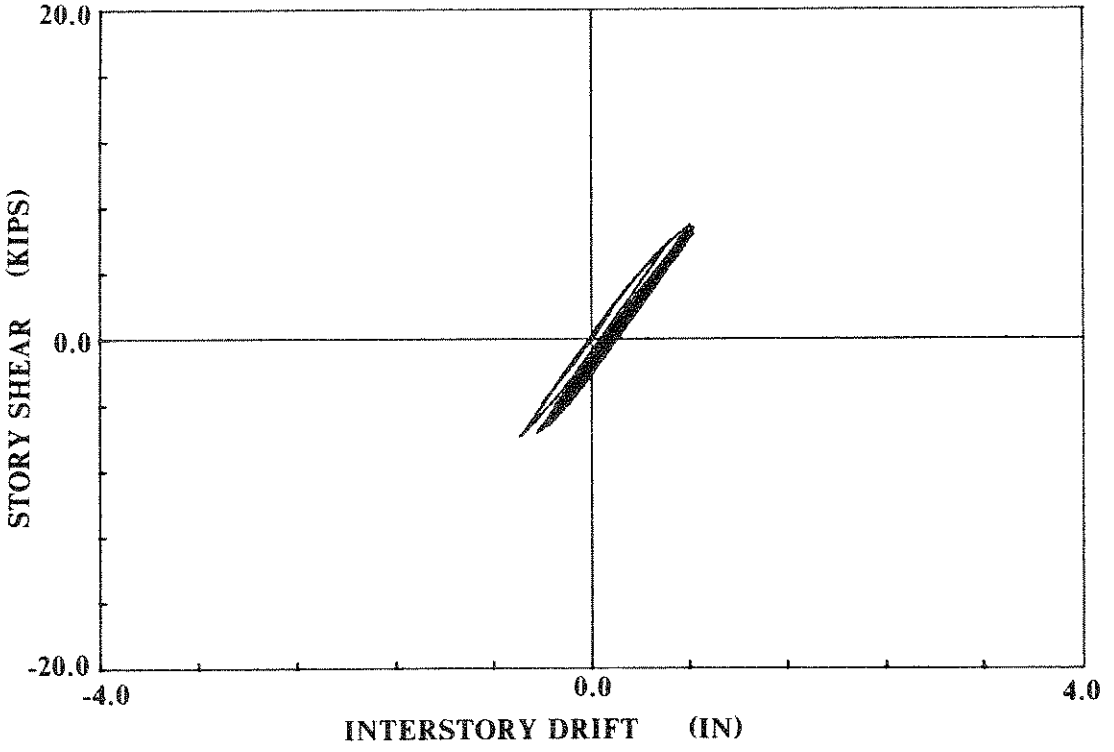

(a) Experiment

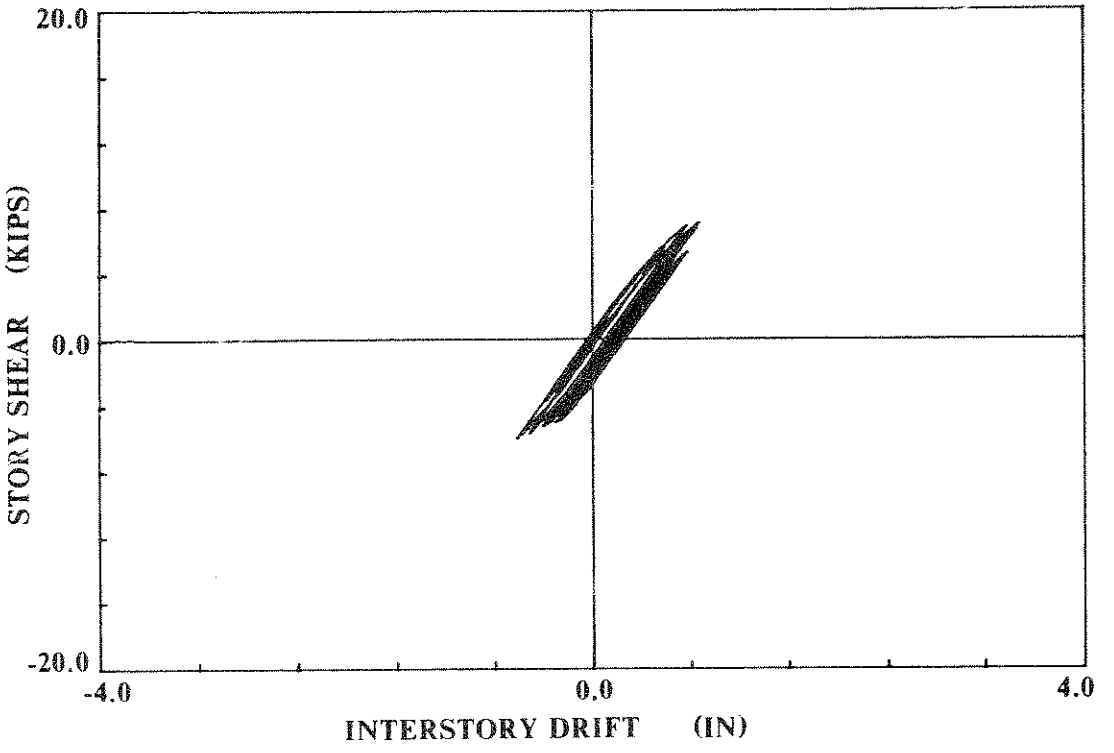

(b) Analytical Simulation

Fig. 7.9 Hysteretic Loop of Third Story

APPENDIX A

Description of the Berkeley Pseudodynamic Test System

A1.1 Testing Facilities

A pseudodynamic test system, which is capable of controlling six degrees of freedom simultaneously, has been installed at the University of California, Berkeley. (Fig. A.1). The system uses standard controllers and double acting electro-hydraulic actuators to impose displacements calculated by the computer (Fig. A.2). Ramp generators are programmable 12-bit digital-to-analog (D/A) converters which transform digital displacement commands from the computer to analog voltage signals. The voltage signals are transmitted to actuator controllers. The displacements are monitored by displacement transducers of the types shown in Fig. A.3 . The structural restoring forces are measured by load transducers mounted on the pistons of the hydraulic actuators (Fig. A.4) . Additionally, a high speed data acquisition unit is used to scan a maximum of 128 data channels in 6.4 milliseconds (Fig. A.5) .

Two digital interactive plotters are also provided to plot individual or combined data channels (Fig. A.6) . Plotting is possible during a test (for a more detailed observation of the response of the test structure) as well as after a test (for data reduction purposes).

A1.2 Software

Computer software have been developed to support a pseudodynamic test which can be performed with the apparatus described in the previous section. The software consists of two major parts :

(i) The Main Control Program and (ii) The Substructuring Program

Each part is assembled by a number of modules which are interrelated by a common data base. The main features of each major part are described in the following.

1. MAIN CONTROL PROGRAM

The pseudodynamic control program consists of two parts : (i) the operation mode and (ii) the test mode. Each mode includes the following functions :

1.1 *Operation Mode*

The operation mode performs the following :

(i) Calibration of measurement instruments.

(ii) Initialization of test parameters :

(a) Number of structural degrees-of-freedom considered

(b) Coefficients of mass and damping matrices

(c) Parameters for the integration algorithm

(d) Ramp speed

(iii) Measurement of the stiffness of the test structure.

(iv) Entering the test mode.

(v) Unloading of the test specimen.

(vi) Reduction and plotting of acquired test data.

1.2 *Test Mode*

The test mode performs the following tasks :

(i) Integration of the equations of motion

(ii) Control of structural deformations

(iii) Recording of experimental data at each step

2. SUBSTRUCTURING PROGRAM

The substructuring program is used for the specification of the dynamic characteristics of the analytical substructures. It consists of three parts : (i) the input module, (ii) the assembly module and (iii) the inelastic element module. The three modules are described below :

2.1 *Input Module*

The input module is used for the specification of necessary information associated with the analytically substructured subassemblages. This information consists of the following :

(i) Nodal coordinates of the entire test system

(ii) Boundary conditions of the analytical subassemblages

(iii) Specification of nodes with identical dispacements

(iv) Specification of elastic elements :

The elastic element data are given in groups of the same type of elements. Two groups are currently available : (a) beam-column members and (b) truss members. For each group the following data are entered by the user :

(a) Number of different types of stiffnesses

(b) Individual stiffness properties

(c) Element generation

(v) Specification of inelastic element stiffness data.

(Currently, parameters for the Menegotto-Pinto model can only be given)

(vi) Lumped mass data for all the degrees-of-freedom carrying inertial masses

(vii) Stiffness proportional and mass proportional damping coefficients

(viii) Specification of nodal pairs for computing relative displacements

(in case of equipment-structure or similar types of tests)

2.2 *Assembly Module*

The assembly module reads the data entered by the input module and sets up the necessary arrays to be processed by the test mode of the Main Control Program. In more detail, the assembly module performs the following :

(i) Computation of influence coefficients for each degree-of-freedom

(ii) Assembly of mass matrix

(iii) Computation of damping matrix (in case mass proportional and/or stiffness proportional damping is desired)

(iv) Assembly of global stiffness matrix of the elastic substructured subassemblages

2.3 *Inelastic Element Modules*

These modules are called by the test mode of the Main Control Program to provide the restoring forces of the inelastic elements which are incorporated in the analytical substructure. At present, only one module has been programmed which includes the Menegotto-Pinto model.

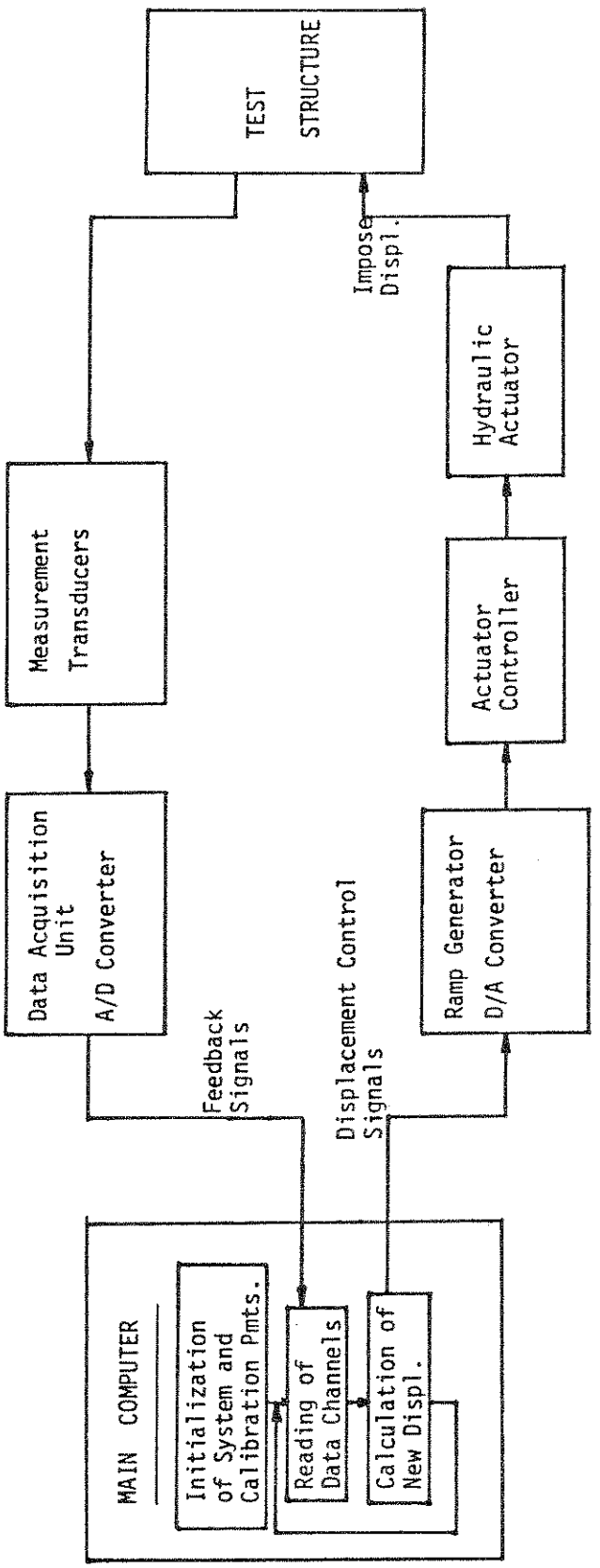

Fig. A.1 Pseudodynamic Test System at Berkeley

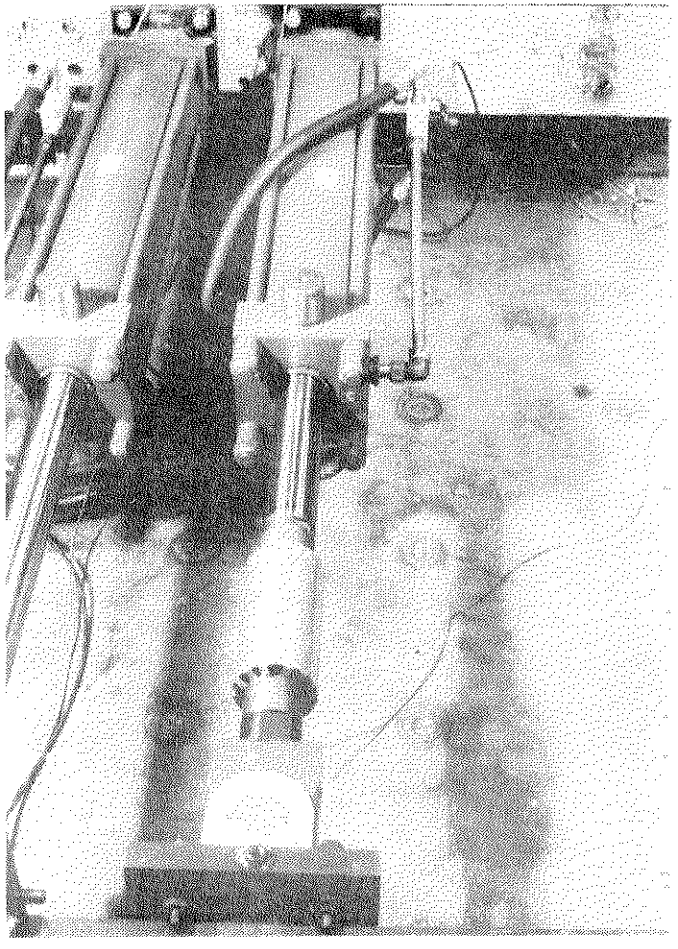

(a) Electro-Hydraulic Actuator

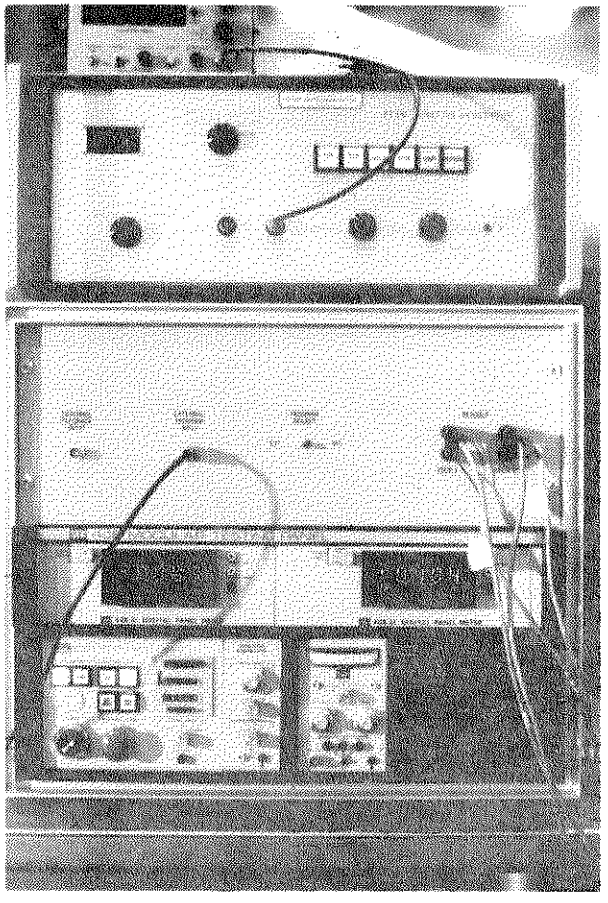

(b) Actuator Controller

Fig. A.2 Electro-Hydraulic Actuator System

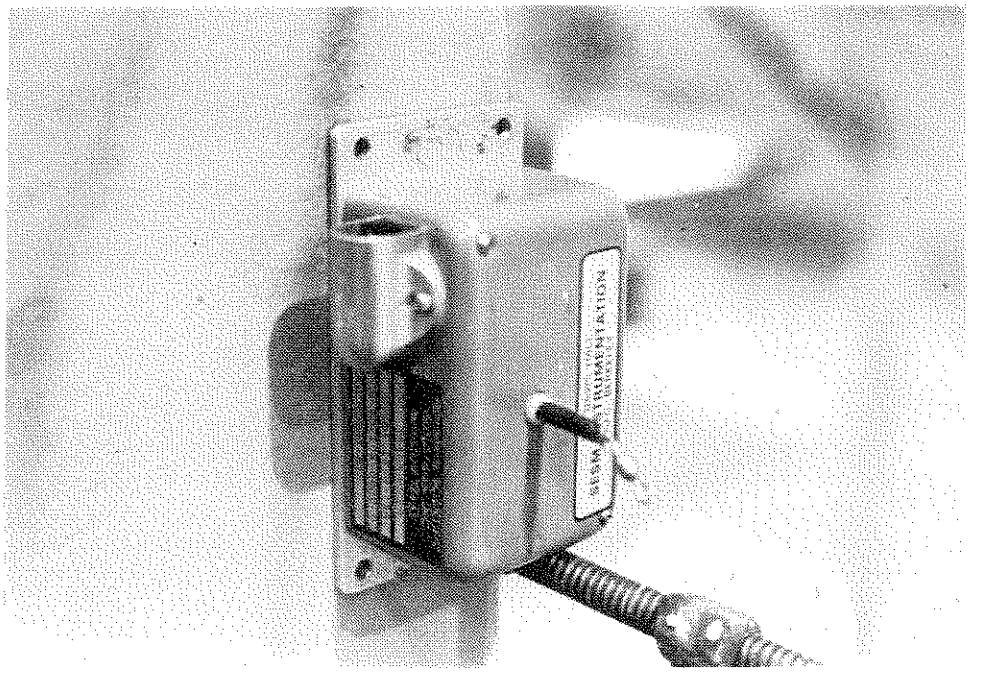

(a) Position Transducer

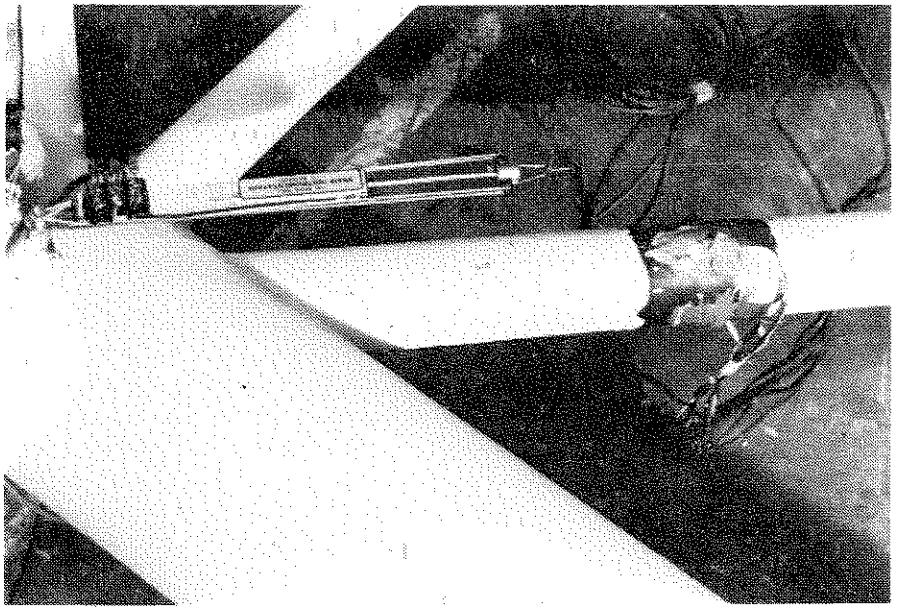

(b) Linear Potentiometer

Fig. A.3 Displacement Transducers

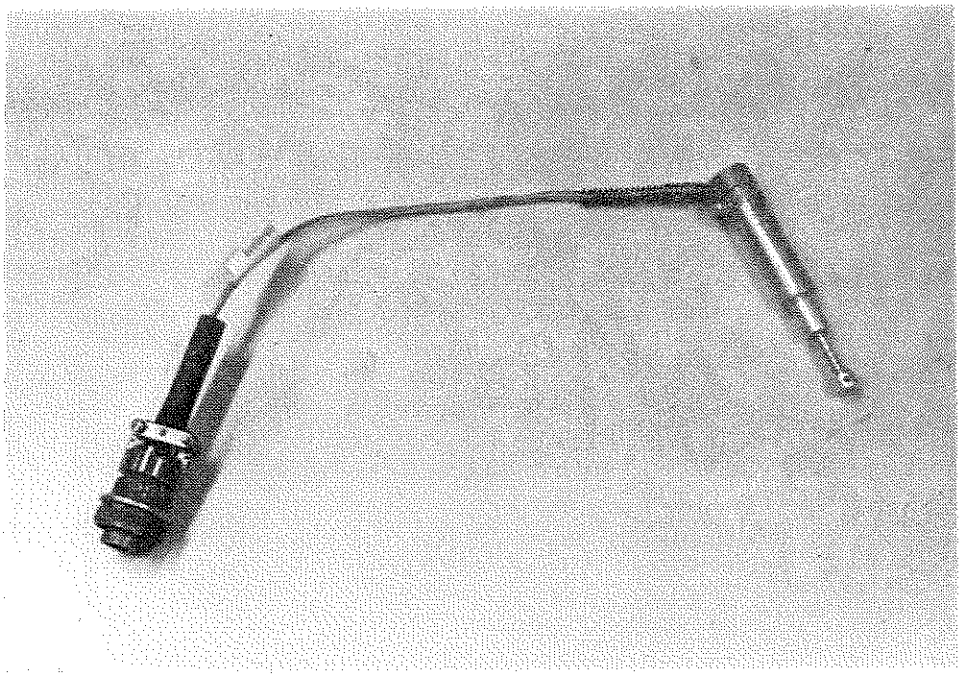

(c) Linearly Variable Displacement Transducer (LVDT)

Fig. A.3 Continued Displacement Transducers

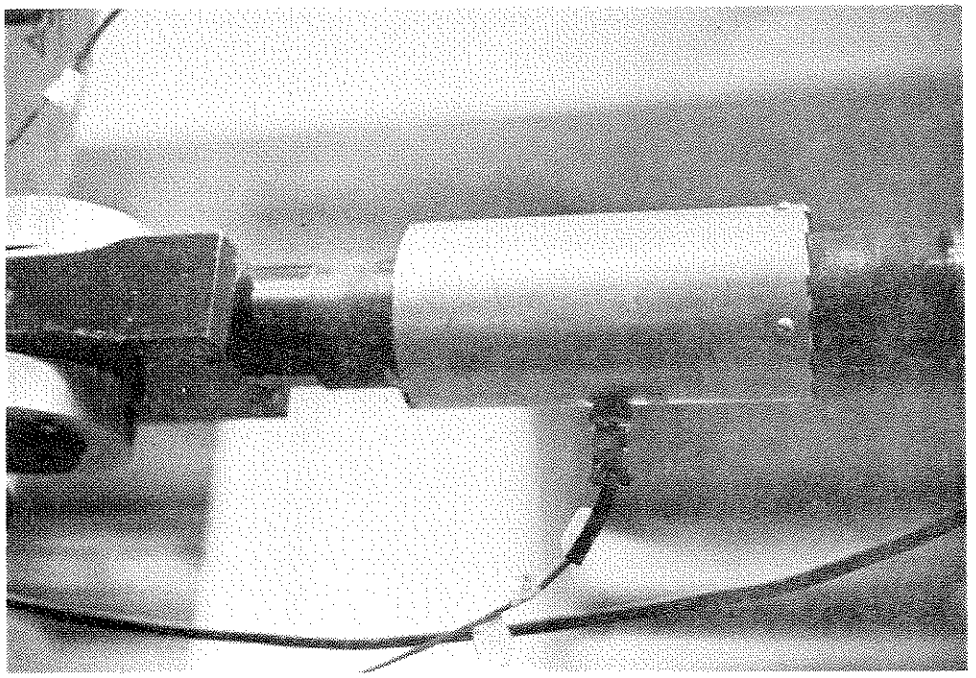

Fig. A.4 Load Transducer

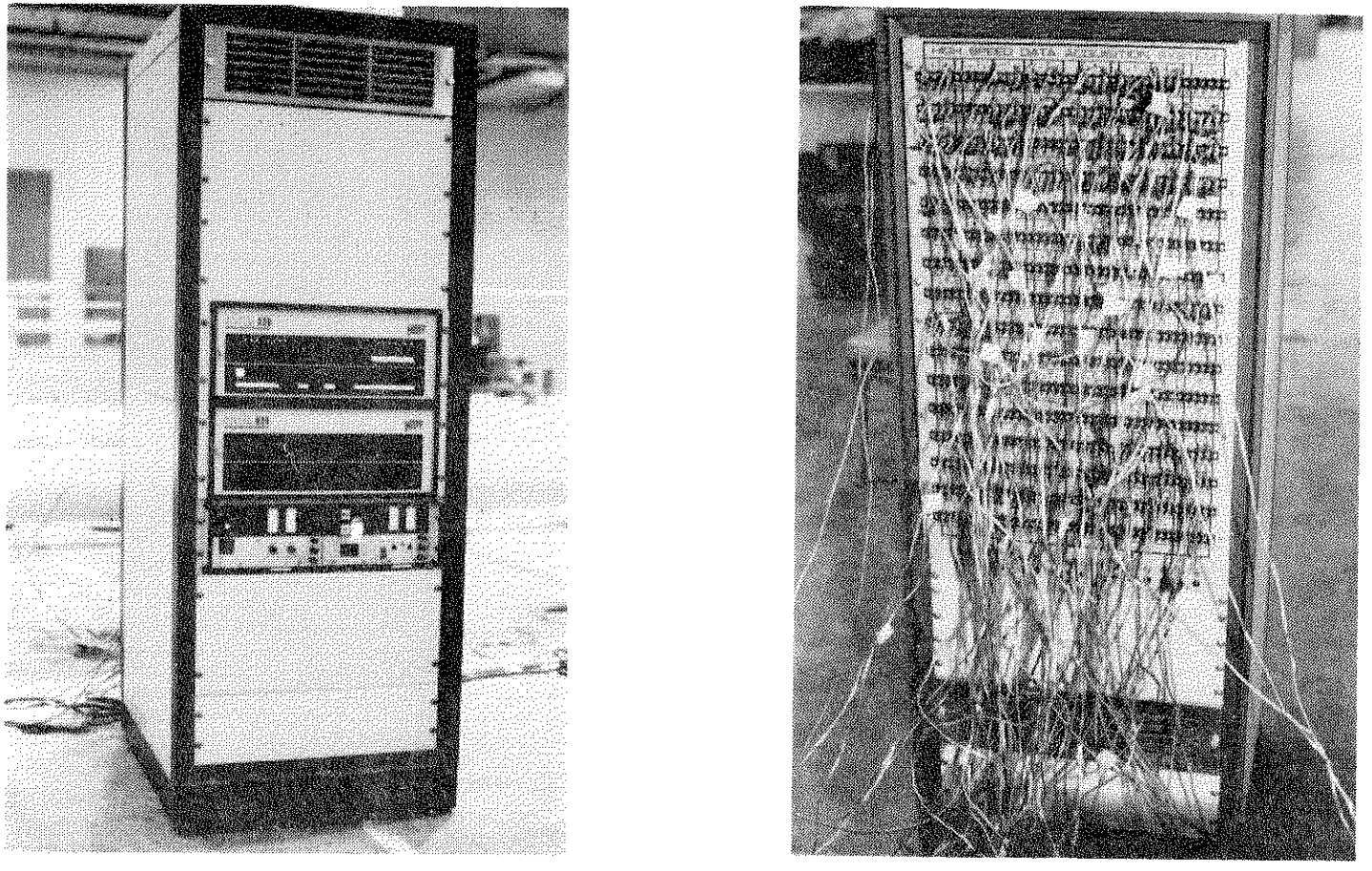

Fig. A.5 High-Speed Data Acquisition System

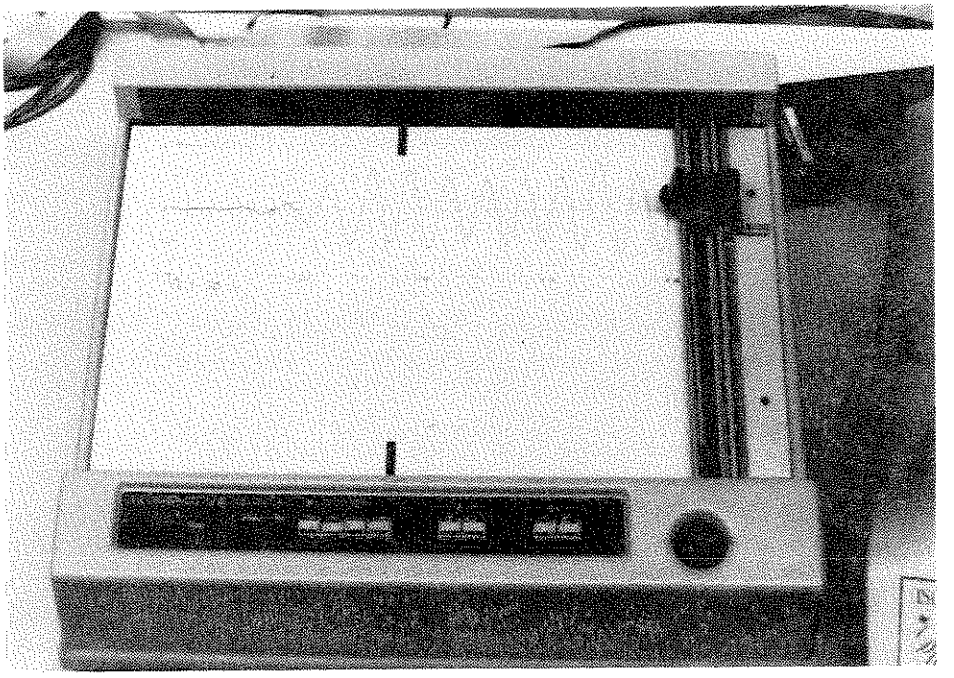

Fig. A.6 Digital Interactive Plotter